



Budapest University of Technology and Economics
Faculty of Mechanical Engineering
Department of Polymer Engineering

**Modeling of
Braided Fiber Reinforced Composites
Crosslinked by Electron Beam**

PhD THESIS

by

Balázs ZSIGMOND

Supervisor
Prof. Tibor CZVIKOVSKY

Budapest, 2005



BUDAPESTI MŰSZAKI ÉS GAZDASÁGTUDOMÁNYI EGYETEM
GÉPÉSZMÉRNÖKI KAR

Szerző neve: *Zsigmond Balázs*

Értekezés címe: *Modeling of Braided Fiber Reinforced Composites Crosslinked by Electron Beam (Fonatolt, szélerősítésű, elektronkezeléssel térhálósított kompozitok modellezése)*

Témavezető neve (ha volt): *Dr. Czvikovszky Tibor*

Értekezés benyújtásának helye (Tanszék, Intézet): *BME Polimertechnika Tanszék*

Dátum: *Budapest, 2005. március 23.*

Bírálok:

Javaslat:

1. bíráló neve:

Nyilvános vitára igen/nem

2. bíráló neve:

Nyilvános vitára igen/nem

3. bíráló neve (ha van):

Nyilvános vitára igen/nem

A bíráló bizottság javaslata:

Dátum:

(név, aláírás)
a bíráló bizottság elnöke

NYILATKOZAT

Alulírott Zsigmond Balázs kijelentem, hogy ezt a doktori értekezést magam készítettem, és abban csak a megadott forrásokat használtam fel. Minden olyan részt, amelyet szó szerint, vagy azonos tartalomban, de átfogalmazva más forrásból átvettem, egyértelműen, a forrás megadásával megjelöltem.

Budapest, 2005. március 23.

Zsigmond Balázs

*A doktori disszertáció bírálatai és a védésről készült jegyzőkönyv
a Budapesti Műszaki és Gazdaságtudományi Egyetem Gépészmérnöki Kar
Dékáni Hivatalában megtekinthetőek.*

In memory of my mother and grandparents.

Acknowledgements

I would like to express my thanks to my supervisor, Professor Tibor Czvikovszky for his attention and relentless support of my studies, and his guidance towards a deeper scientific way of thinking. I appreciate the valuable help and advice of László M. Vas, who introduced me into the secrets of fiber bundle cell modeling method and helped me apply it. I am grateful for my friends and the colleagues at the Department of Polymer Engineering lead by Tibor Czigány, for their help and the creative atmosphere prevailing there. I appreciate the support of Veronika Nagy who has not been only an excellent partner in PhD work but she was also my English lector, who helped a lot when I stroke a bad patch. I should like to express my thanks to Szalag- és Zsinórgyár Rt. (Ribbon and String Factory Co. Ltd., Budapest), where I made the braided structure for my feasibility study; as well as to Zoltek and Tenax Ltd. for supplying the carbon fiber rovings, to Budaplast Rt. for providing me with the vinylester resin suitable for electron treatment; to FE-MA Kft. Hungary, who let me use the LUE 8 type electron accelerator; to IVW Universität Kaiserslautern, Germany where I tested the braided structures in “falling weight” crash experiments; to Hodács Kft. where I impregnated the braids; to the Hungarian Science Research Fund (OTKA T 037733) for the financial support; to Kármán and Peregrinatio Funds for the financial support of my travels. And last but not least I would like to thank to my family for their continuous support in reaching my ambitious goals.

Budapest, 23rd March, 2005.

Balázs Zsigmond

Table of contents

List of symbols and abbreviations	iii
1. Introduction	1
2. Literature overview.....	3
2.1. Composites with special fiber architecture.....	3
2.2. Braiding in composite technology.....	8
2.2.1. The braiding process – general considerations.....	10
2.2.2. Dynamic stress behavior – crash test.....	15
2.3. Electron treatment in composite manufacturing, EB curable resins	18
2.3.1. EB curing in composite manufacturing.....	18
2.3.2. Current limitations to EB processing.....	20
2.3.3. Electron beam curable resins.....	21
2.3.4. Oxygen effect	23
2.4. Modeling of braided composites	24
2.4.1. Concept of fiber bundle	26
2.4.2. Fiber bundle cells method for modeling fibrous structures.....	27
2.4.2.1. Statistical single fiber model	28
2.4.2.2. Idealized fiber bundle cells.....	30
2.4.2.3. Modeling the structure of unidirectional fiber reinforced composites	35
2.5. Targets of the dissertation	36
3. Experimental materials, machines and methods.....	37
3.1. Experimental materials	37
3.1.1. Matrices and fibers	37
3.1.2. Production of specimens.....	38
3.2. Experimental machines and methods	39
3.2.1. Braiding machines	39
3.2.2. Electron accelerator	39
3.2.3. Instrumental falling weight impact-tester.....	40
3.2.4. Tensile and bending tests.....	41
3.2.5. Determination of contraction parameter.....	41
3.2.6. Determination of fiber content	41
3.2.7. Image processing system.....	41

4. Electron beam crosslinking of braided composite.....	45
4.1. EB crosslinking of epoxy-acrylates.....	45
4.2. Carbon fiber reinforced epoxy-acrylate composites.....	47
4.3. Crash test of EB treated braided CFR composites	49
5. Modeling of the tensile process of braided composite tubes.....	50
5.1. Examination of the tensile state of fibers in braided composite tubes	50
5.2. Modeling the tensile loading of braided circular cross-sectional composites.....	55
5.2.1. Application of non-pretensioned fiber bundles	58
5.2.2. Application of pretensioned fiber bundles	68
5.2.3. The effect of axial fiber introduction.....	69
5.3. Fiber bundle cell model of arbitrary braided structures	72
5.4. Evaluation of the model as compared to measured values.....	77
5.4.1. Braided composite tubes without axial fiber introduction.....	77
5.4.2. Braided composite tubes with axial fiber introduction.....	85
5.4.3. The improvement of the axial fiber introduction model of braided composite tubes – modeling with ETH-bundle.....	86
6. Discussion.....	90
6.1. Evaluation of mechanical behavior of braided profiles.....	90
6.2. Possibility of the continuous operation	93
6.3. Applicability of the braided composites.....	94
6.4. Tasks to be solved	95
Theses.....	96
Summary.....	98
References	I
Appendix	XI
Appendix A – Properties of applied fibers	XI
Appendix B – Properties of applied matrices.....	XVI
Appendix C – Properties of asymmetric composite profiles.....	XVII
Appendix D – Properties of composite tubes	XVIII

List of symbols and abbreviations

BPP	braiding pultrusion process
C	carbon fiber
CCA	composite cylinder assemblage method
CCD	charge coupled device
CFR	carbon fiber reinforced
EB	electron beam
E-bundle	well-ordered bundle cell
EH-bundle	preset (preloaded, pretensioned, prestretched, precrimped) bundle cell
ES-bundle	slipping bundle cell
ET-bundle	oblique bundle cell
ETH-bundle	ET- for braided and EH-bundle for axial tows
FBC	fiber bundle cell
FGM	fabric geometry model
GFRC	glass fiber reinforced composite
K	Kevlar fiber
PC	personal computer
PET	polyethylene terephthalate
PUR	polyurethane
RT	room temperature
RTM	resin transfer molding
SD	standard deviation
VARTM	vacuum assisted resin transfer molding

Arabic letters

a	exponent in Eqn. (46)
A_B	cross-section area of a bundle
A_C	cross-section area of a composite
$\overline{A_C}$	average cross-section area of composites
A_f	average cross-section area of all the fibers (perpendicular)
$A_{f,ij}$	cross-section area of the i-th fiber in the j-th bundle
$A_{f,j}$	average cross-section area of fibers in the j-th bundle

$A_{f,k}$	cross-section area correspondent to $\overline{F_{S,k}}$
A_{ij}	fiber cross-section area perpendicular to the direction of loading
A_M	cross-section area of matrix
$\overline{A_S}$	average cross-section area of fibers
b	contraction parameter
c	exponent in Eqn. (66)
\overline{d}	average diameter of elementary fibers
d_{ij}	fiber diameter perpendicular to the direction of loading
$D1$	width in direction 1
$D2$	width in direction 2
e_0	initial excentricity (obliquity) or skewness of a fiber
$e_{0,a}$	initial excentricity (obliquity) or skewness of an axial fiber introduction
$E_{init,b}$	initial bending modulus of the composite
EH	average value of precrimping
EL	average relative slippage length
E_M	tensile modulus of elasticity of the matrix
$\overline{E_M}$	average tensile modulus of elasticity of the matrix
ES	average slippage strain
$f(u)$	auxiliary function
$f_{\alpha_0-\overline{\alpha_0}}(x)$	density function of $(\alpha_0 - \overline{\alpha_0})$
$\overline{F1}$	tensile force of the whole fiber system referenced to one fiber
F_B	ultimate tensile force of an elementary fiber in Chapter 2.4.2 or tensile force of a bundle from Chapter 5
$\overline{F_B}$	average ultimate tensile force of elementary fibers in Chapter 2.4.2 or average tensile force of bundles from Chapter 5
F_B^{ETH}	tensile force of an ET and EH compound bundle
$\overline{F_B^{ETH}}$	average tensile force of ET and EH compound bundles
F_C	composite tensile force
F_{EH}	tensile force of an EH-bundle
$\overline{F_{EH}}$	average tensile force of EH-bundles
F_{ET}	tensile force of an ET-bundle

$\overline{F_{ET}}$	average tensile force of ET-bundles
F_{ET1}	tensile force of an ET-bundle in direction 1
F_{ET2}	tensile force of an ET-bundle in direction 2
F_{ij}	axial force of i-th fiber in the j-th bundle
$F_{f,ij}$	tensile force of i-th fiber in the j-th bundle
FH	normalized tensile force of a bundle
FH^*	utilization factor
F_M	tensile force of matrix
F_{max}	maximal measured tensile force
F_S	ultimate tensile force of an elementary fiber
$\overline{F_S}$	average ultimate tensile force of elementary fibers
$\overline{F_{S,j}}$	average ultimate force of fibers in the j-th bundle
$\overline{F_{S,k}}$	maximum average force of fibers
F_{SL}	limit force of slippage
$g(u)$	auxiliary function
h	thickness of a composite tube
h_0	initial thickness of a composite tube
h^*	average square of errors
$\overline{H^2}$	square of errors
k	normalized loaded radius
K	initial tensile stiffness of an elementary fiber
\overline{K}	average initial tensile stiffness of elementary fibers
K_i	tensile stiffness of the i-th fiber
k_0	normalized initial radius
l	loaded length of a fiber
L	loaded length of a bundle
ΔL	change of small length
l_0	unloaded length of a fiber
L_0	initial length of a bundle
l_s	length of slippage
m	number of components in an idealized parallel bundle cell

n	number of fibers
n_a	number of axial tows
N_B	weighted cardinality
N_i	number of elementary fibers in the defined direction
n_j	number of carriers of braider in the defined direction
N_j	number of elementary fibers in the j-th bundle
o	number of bundles in a braided structure
p_a	peak of axial tows
p_b	peak of bundles
$q_{\varepsilon_0}(x)$	probability density function of ε_0
$Q_x(y)$	normal distribution function of y function with x expected value
R	correlation coefficient
$R(u)$	loaded external radius of a composite tube
R_0	unloaded external radius of a composite tube
$R_k(u)$	loaded middle radius of a composite tube
R_{k0}	unloaded middle radius of a composite tube
s	running variable
Δs	small width of a cell
Δs_0	initial small width of a cell
t	time in Chapter 2.4.2 or number of measurements in Chapter 5.4
T_0	initial relative declination
u	bundle strain
u_S	strain limit of slippage
u_{SL}	relative slippage length
V	volume
V_0	initial volume
V_B	volume of bundle
V_C	volume of composite
VE	coefficient of variance of ultimate strain of fiber
VH	coefficient of variance of precrimping
V_M	volume of matrix
w	bundle shear deformation
W	contour width

w^*	wall thickness
w_i	weight of the i-th component in an idealized parallel bundle cell
Δx	small length of a cell
Δx_0	initial small length of a cell
y_i	measured value
Y_i	modeled value
z	normalized bundle strain
z_{max}	maximum value of the normalized strain
$ \cdot _+$	positive part of a function

Greek letters

α	braiding angle
α_0	initial braiding angle
$\overline{\alpha_0}$	average initial braiding angle
α_{01}	initial braiding angle in direction 1
α_{02}	initial braiding angle in direction 2
α_{ij}	angle of i-th fiber in the j-th bundle
α_j	average braiding angle of the j-th bundle
β_0	angle of the braiding cone
β_{0i}	i-th measured angle of the braiding cone
β_i	i-th measured angle
δ	ratio of thicknesses
ε	fiber strain
ε_0	initial strain of a fiber
$\varepsilon_{0,a}$	initial strain of an axial fiber introduction
$\varepsilon_a(u)$	strain of an axial fiber
$\varepsilon_a^*(u)$	strain of an axial fiber if $\varepsilon_{0,a} \neq 0$
ε_B	ultimate strain of an elementary fiber in Chapter 2.4.2
ε_i	strain of the i-th elementary fiber
$\overline{\varepsilon_M}$	average ultimate strain of matrix

$\varepsilon_{M \max}$	maximum value of ultimate strain of matrix
ε_S	strain of slippage in Chapter 2.4.2 or ultimate strain of a fiber from Chapter 5
$\overline{\varepsilon_S}$	average ultimate strain of elementary fibers
$\varepsilon_{S,i}$	ultimate strain of the i-th elementary fiber
$\varepsilon_{S \max}$	maximum value of ultimate strain of elementary fibers
κ	core function
μ	relative average square of errors
ξ	average proportionality factor
ρ	ratio of external radii
ρ_k	ratio of middle radii
ρ_{kA}	low bound function
σ_B	tensile stress of the bundle
$\overline{\sigma_B}$	average tensile stress of bundles
σ_{bd}	bending strength of the composite
σ_C	tensile stress of the composite
σ_M	tensile stress of the matrix
σ_S	ultimate tensile strength of a fiber
$\overline{\sigma_S}$	average ultimate tensile strength of fibers
σ_{α_0}	standard deviation of the initial braiding angle
σ_{ε_S}	standard deviation of the ultimate strain of fibers
τ	interlaminar shear strength
φ	fiber volume fraction
φ_B	fiber/bundle volume fraction
φ_M	matrix volume fraction
Φ_0	normalized initial thickness
$\chi(\cdot, \cdot)$	window function
ψ	average weighted function with whole cross-section area of fiber types of
	$\frac{1}{\cos(\alpha_j)}$

1. Introduction

The appearance of high performance polymer composites has widened the variety of structural materials since they have opened a new perspective in the realization of engineering structures tailored to loading. There are several definitions mentioned in the literature:

“Anyone who has never made a mistake has never tried anything new.”

Albert Einstein

“The composite principle is refreshed in the last century: a reinforcing phase is embedded in a matrix material, improving greatly the “ensemble”, the set of properties, offering the advantage of the built-in, pre-designed anisotropy, required in most engineering constructions.” – said Gay et al. in the most recent composite handbook [1]. At our Department Czvikovszky defined composites this way [2]: “Polymer composite is an engineering material, a multicomponent system consisting of a (high strength) reinforcing material, an embedding (high toughness) matrix material and an engineered interface in-between that assures good adhesion up to a reasonable level of repeated load for long time of service.”

Pre-designable anisotropy, the direction-dependence of mechanical properties, is the most advantageous characteristic of composite structures. Carbon fibers, for instance built in parallel to loading can increase the strength of the polyester structure by orders of magnitude, even to hundred fold of the original value.

Textile structures form not only a set of loose and independent fibers but are also interconnected systems of fiber bundles – such as a fabric prepared from carbon and glass fibers – hence they provide further benefits as composite reinforcements. My dissertation involves the examination of the reinforcing effect of a specially structured fabric, a braided textile hose, in theoretically infinite long composite rods, tubes and profiles of constant cross-section. Up-to-date braiding machines are capable of producing not only a two dimensionally connected shell (in order to reinforce the hose or profile in diagonal direction) but also a triaxial reinforcement, furthermore even a significant shell thickness can be achieved to form a three dimensional, multi-axial reinforcing structure. A versatile technical product-family of profile rods, tubes and beams can be manufactured this way from polymer composites for applications in the automotive industry, lightweight construction and a lot more branches of industry. This technique may open new applications for the Hungarian carbon fiber, the production of which started only a few years ago.

The advanced technique of crosslinking of polymers by accelerated electrons has been applied here for light composite structures. The electrons accelerated to a few million Volts serve the crosslinking of thermoplastic polymers in the cable industry, and single-use medical polymers are also sterilized in a similar way. More than 1,500 industrial electron accelerators are used all over the world for these purposes and two of them operate in Hungary. Those EB machines have been used in our experiments. The small energy (175 kV) electron treatment machine in our Department also served my measurement.

The abovementioned carbon fiber braiding technology, electron beam treatment and their favorable impact on the structure can be combined efficiently with the expected economic benefits in end-products like carbon fiber reinforced load bearing rods and profiles of infinite length. Owing to the excellent mechanical properties of these structures, they can be applied in most of the fields where metal profiles are used today, e.g. in the automotive industry, in structural engineering etc. The reliable application of this kind of braided composite profiles requires the exact and thorough knowledge of their mechanical load-bearing capability and failure behavior.

The fiber bundle theory elaborated in our Department has been applied on braided reinforced polymer composites for the sake of reliable engineering design.

2. Literature overview

In this Chapter the literature will be overviewed with regards to special fiber architectural composites, to braiding in composite technology, to electron beam treatment in composite manufacturing, to modeling braided composites and to the fiber bundle cell modeling method. Finally, the targets of the dissertation will be defined based on the literature.

2.1. Composites with special fiber architecture

This section will present a brief overview of the composites with special fiber architectures. Fabric can be designed to accommodate a variety of manipulative requirements in the construction of composites. The three general categories of requirements are absolute dimensional stability, subtle conformability and deep-drawing moldability / shapeability. Absolute dimensional stability is required in most pultruded, flat panel or flat laminar composites. Deep-drawn composites or tensioned / pressed / shaped / formed composites require considerable extensibility of the reinforcement material. The basic fabric structures which can be used to accommodate this variety of manipulative requirements are weaves, knits, braids and nonwovens (see Figure 1) [3].

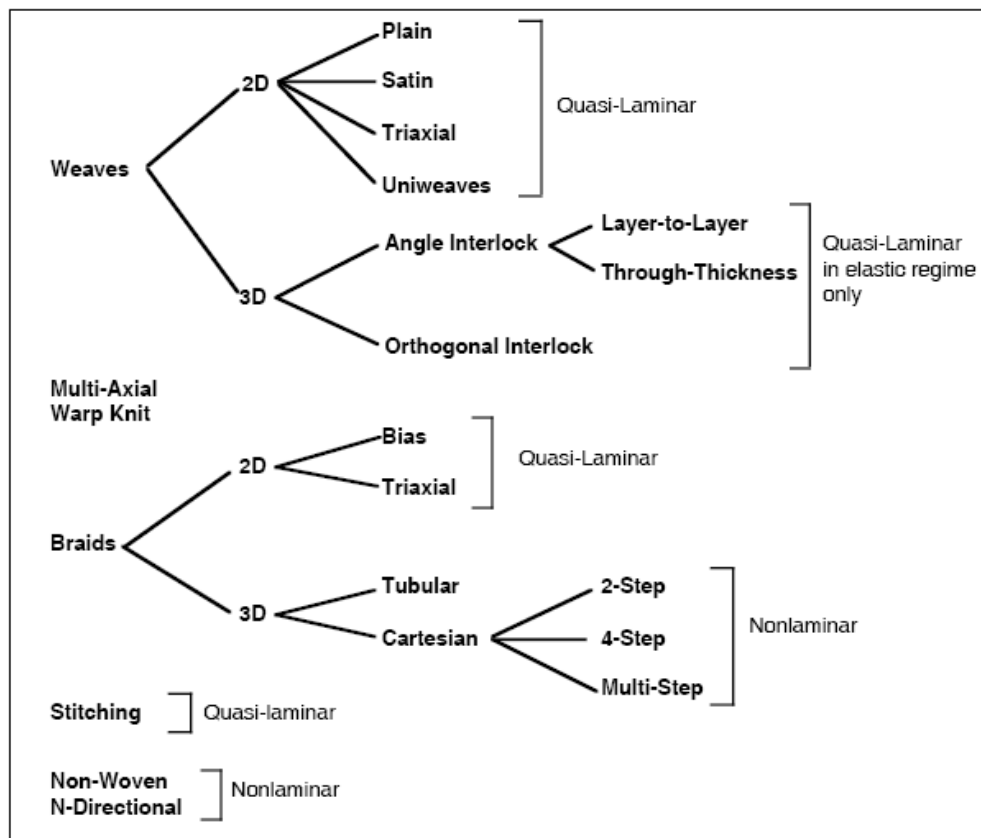


Figure 1 Some of the textile forms available for high performance composite structures [4]

Weaves

Made by interlacing two or more yarn systems at 90° angle weaves exhibit good stability in the warp and weft directions and offer the highest cover or yarn packing density in relation to fabric stiffness. Currently, most simple and hybrid woven fabrics used in composites are simple constructions, such as plain, basket, twill and satin weaves. Wovens are available in narrow and broad widths, in tubular and flat forms, and in multiple warp and filling constructions (e.g. doublecloth, triplecloth etc.) with or without laid-in (noninterlacing) yarn systems [3-5].

The disadvantages of woven fabrics concerning the design of certain composite products are anisotropy, limited conformability, poor in-plane shear resistance, difficult handling of open constructions, and reduced yarn-to-fabric tensile translation efficiency due to yarn crimp and crimp exchange. Fortunately, special high modulus weaves can be used to avoid crimp in the load-bearing biaxial yarn systems. Furthermore, rather thick multiple warp / multiple filling fabrics can be woven containing a large proportion of yarns with little or no crimp. Triaxially woven fabrics, made from three systems of yarns which interlace at 60° angles, offer improved isotropy, higher in-plane shear rigidity, more uniform conformability and less problems when handling very open constructions. However, no woven fabric construction offers sufficient extensibility for deep-draw molding.

Knits

Made by interlooping one or more yarns, knit fabric constructions containing high modulus yarns offer a much wider range of form and behavior than wovens. For example, simple weft and warp knit constructions provide considerable extensibility in all directions and therefore are quite suitable for deep-draw molded composites. Weft and warp knits can be designed for specific directional extensibility and through the use of laid-in (nonknitting) yarn systems can be designed for stability in one direction and conformability in the other directions. With laid-in yarn systems in biaxial directions, special weft and warp knit constructions of maximum stability are quite possible [3-5].

Weft inserted warp knits are particularly suitable for several composite applications because of an unusual preservation of yarn properties and because of a flexibility designed for performance requirements from complete dimensional stability to engineered directional elongation. Moreover, weft inserted warp knits with laid-in warp systems offer higher yarn-to-fabric tensile translation efficiencies, greater in-plane shear resistance and better handling

in open constructions than the comparable weaves. While warp knits offer the possibility of greater fabric width and greater productivity, weft knits offer a choice of net-shape fabrics. The major disadvantages of knits for certain applications are fabric thickness (from 3 to 5 yarn diameters) and high yarn consumption relative to fabric cover.

Multiaxial stitch-through warp knits are similar to weft-inserted warp knits except that yarn systems are oriented bias as well as in the warp and weft directions before stitching. Multiaxial stitch-through fabrics are available in up to six plies of yarn systems oriented in the warp, weft and bias directions. Light nonwoven webs can be added as a ply, if desired, and fabric widths of 1 to 3 meter are possible. All of the laid-in yarns are linear, positioned in a specific ply plane and are continuous between fabric edges. Fabric constructions of various ply orientations can be made up to 5 mm thickness, approximately.

Braids

Braided fabrics offer stability or conformability according to the construction and the design of the intertwined yarn system. The braiding principle and the motion of carriers are seen in Figure 2 and Figure 3 Braids are available in a variety of forms including hollow tubular, stuffed tubular (laid-in, nonintertwined yarn system), flat, stuffed flat, solid square and irregularly shaped or fashioned solids. All of these braided forms can be made with a laid-in (nonbraiding) yarn system positioned within the intertwining yarns. Fashioned braids, a special form of batch braiding permit variation in the sequential entanglement of the yarn system and the fashioning or design of specific net shapes [3-5].

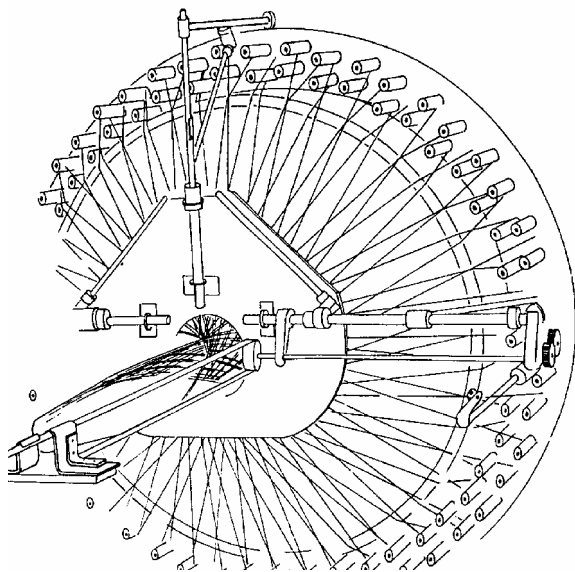


Figure 2 Tube-braiding principle [5]



Figure 3 Motion of carriers [6]

With laid-in or stuffer yarns or with jammed configurations, braids exhibit stability under tension in the yarn system direction. However, braids have poor stability under axial compression in the yarn system direction. Braids can be designed for multidirectional conformity within jamming limits and are essentially torque free in tubular or solid form. The major limitations in the design of machine-made braids are restricted width, diameter, thickness and shape selection. The major limitations of special or batch braids (3-D fashioned) are productivity and fabric length.

Nonwovens

Made from fibers and/or yarns, nonwovens which qualify for advanced composite applications include fiber mats, stitch bonded, 3-D and adhesively bonded fabrics. Needled or stitch bonded mats can be made with a controlled proportion of fiber segments in the X, Y and Z directions. Stitch bonded fabrics with nearly biaxial laid-in systems offer acceptable stability with slight conformability. The main problem with stitch bonded fabrics made from high modulus yarns is the lack of preservation of weft or bias yarn strength during stitching. The unusually thick XYZ interlaced three-dimensional fabric preforms are stable but can conform to shear deformation, if necessary. The major limitations of XYZ fabrics are high cost, low productivity and limited design or shapeability. Adhesively bonded laminar yarn systems oriented in biaxial or multiaxial directions can be made in 2-D or 3-D fabric form. While adhesively bonded laminar yarn systems offer economic advantages such as simplicity and speed of fabric manufacturing, the major vulnerability is delamination and splitting among the layers of yarns, similar to the problem with filament wound composites [3-5].

Alternative approaches to composite manufacturing

Given the general performance and design requirements, clear-cut specifications can be defined for textile structural composites for primary and secondary load-bearing applications. Material selection and textile structure must be matched with the composite construction and fabrication technique on a cost / performance / availability / processability / machineability / joinability / maintainability basis. With the variety of textile composite systems available, several alternative approaches should be considered for each application.

The shape of the braided cross-section is depending on the circular motion of the bobbins and some other mechanical elements of the machine. The simplest method is tube braiding, but even ribbons and belts can be produced as it can be seen in Figure 4.

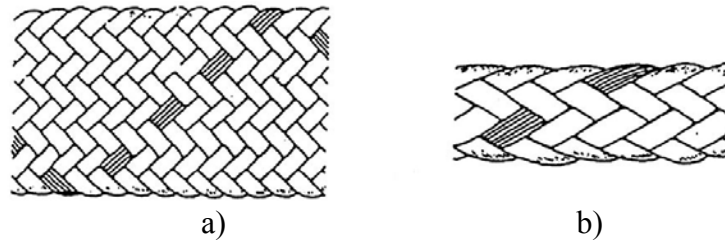


Figure 4 Simple-braided belt (a) and tube (b) [7]

Figure 5 shows the different profiles formed by tube braiding. Profiles far more complicated than a circular or square cross section can be produced this way such as H-beams, Δ -beams, channel beams, angle beams, ribbed and solid columns, tubes, plates etc. Choices can be applied to panels with reinforcing ribs and other secondary load-bearing structures as well. The final selection must satisfy all performance and design requirements and must be practical and economical also as well. For example, in case of the textile composite I-beam, the 3-D integrated fabric system may offer the best overall performance but the economic merits of a slightly inferior pultruded, concentrically laminated fabric system (e.g. tubular braids with incorporated straight laid yarns) may be far more attractive for certain applications.

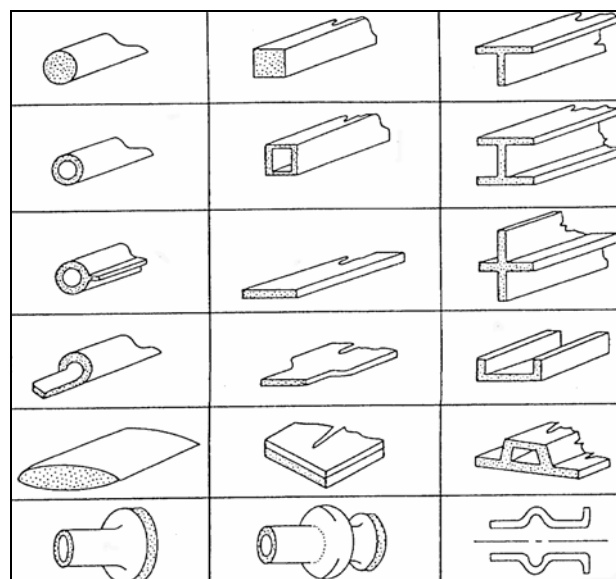


Figure 5 Braided profiles [3]

The braided product has a textile character; it has a woven structure owing to its diagonally woven fibers. This self-reinforcing feature would be the most important advantage in the production of fiber reinforced composites, as compared to filament winding and pultrusion.

2.2. Braiding in composite technology

Braiding is an ancient textile process that has been used historically to produce a wide variety of domestic and industrial products. Traditionally, these products have been designed to exploit the inherent flexibility of textile materials and are principally of two distinct types: axial load-bearing members for applications in which they are in direct competition with ropes and cables; or as reinforcement or protective covers for flexible pipes, cables and hoses. In both types of applications the relative simplicity and high productivity of braiding make it a cost-effective alternative to other manufacturing processes. In recent years, however, the same advantages have led to a serious evaluation of the braiding process for composite applications and there is a growing interest in the manufacture of composite products by this technique.

The examination of manufacturing techniques is a direct consequence of the growing maturity of the general field of composite technology. As the confidence in composites has grown and as design engineers have become more satisfied with these materials, manufacturers across the entire industrial spectrum have successfully incorporated composites into a variety of end-use applications. When the emphasis was on demonstrating the potential of composite materials, the main concern was the provision of high quality components without regard for the cost of producing them and hence slow and expensive hand lay-up techniques were acceptable. As the use of composites have become more widespread, this practice could not continue, and the focus of development effort has moved inevitably to the investigation of low-cost, reliable and reproducible manufacturing techniques that permit the exploitation of composites in all their potential applications.

Some characteristics of braided structures and of the braiding process itself make braiding an obvious candidate for the manufacture of composites. Much of the early development work focused on secondary structures for aerospace applications, particularly ducting, housings, good mechanical performance and low production costs have been demonstrated. More recently, the use of braided composites in load-bearing applications has received attention and the field is expanding rapidly [3].

Mouritz et al. [8] have shown that composite structures made with 3-D textile fabrics are potentially less expensive to manufacture and provide better through-thickness mechanical properties than composites made with the traditional 2-D fabrics. However, the application of 3-D composites to replace 2-D laminates in many structural applications has been unsuccessful. This situation was examined by reviewing present and future applications for

3-D textile composites made by weaving, braiding, stitching and knitting. The main factors were determined impeding the use of 3-D composites as well as the key technology issues that need to be resolved before the applications can be expanded were identify.

Kamiya et al. [9] have shown a review about the design of textile composites, which requires a systematic approach that integrates microstructural design, preform fabrication and composite processing to produce load-bearing structural components with desired fiber architectures and mechanical properties.

The braiding process is familiar to many fields of engineering as standard two dimensionally braided carbon and glass fabric has been used for a number of years in a variety of high technology items, such as: golf clubs, aircraft propellers, yacht masts, helicopter landing gears, blades and light weight bridge structures (see Figure 6 and Figure 7) [10].

Venkatappa et al. [11] have developed a simple machine at the Textile Technology Department of IIT Delhi that uses coir and jute yarns to manufacture 100% natural fiber drains to geotextiles. The machine employing braiding technology braids jute yarns to form the filter sheath and coir yarn as core.

De Oliveira Simões and Marques [12] have designed a hip prosthesis using braided composites.



Figure 6 Braided composite helicopter landing gear by Eurocarbon [13]



Figure 7 Joint of satellite truss made of braided composite by Muratec [14]

2.2.1. The braiding process – general considerations

The braiding process is extremely simple in essence. In its fundamental form, two sets of yarn package carriers are moved to follow intersecting undulating circular paths in opposite directions and the sequence of the crossovers is such that the two sets of yarns interlace to form a continuous tubular fabric (see Figure 4 and Figure 5). The detailed structure of the fabric can be changed by manipulation of the intersection sequence of the yarn packages just as the structure of a woven fabric can be modified by altering the shedding sequence of the warp yarns. The analogy with woven fabrics is exact since it is not possible to distinguish isolated sections of braided and woven fabrics of the same basic construction. The principal functional difference between a braided and a woven structure (both assumed to be orthogonal) is that the unit cell of the braided fabric is oriented at 45° to the direction of fabric production and is parallel to the direction of fabric production in the woven fabric (see Figure 8). If braided and woven tubes with nominally identical dimensions and fabric constructions are produced, the difference in the orientation of the unit cell leads to a braided assembly that is highly deformable, via the mechanism of fabric shear, in the axial and radial direction while the woven assembly is relatively undeformable in these modes, but is capable of considerable torsional deformation. The radial deformability of the braided tube is the key to the ability of the braiding process to produce a conformal fitting to surfaces and is in the center of many potential applications of braiding in composites.

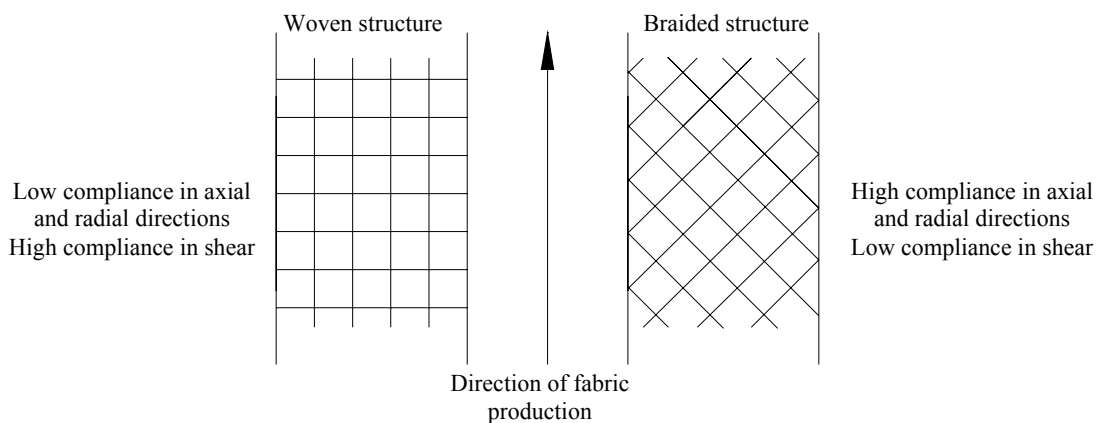


Figure 8 Comparison between woven and braided structures [3]

The process described above in which two identical sets of carriers intersect produces a bias braid. A simple modification that is of particular value in the production of tensile or compression members involves the incorporation of additional axially-oriented yarns into the braided structure. These yarns are supplied from a set of stationary package holders mounted parallel to and slightly behind the rotating package holder. These longitudinal yarns pass

through guide tubes located at the centers of the lobes of the undulating tracks that guide the bias yarn carriers and consequently this third set of yarns is trapped between the two sets of bias yarns (see Figure 9). The longitudinal yarns are not truly interwoven with the yarns from either of the bias sets, which are themselves mutually interwoven, but the array of longitudinal yarns is effectively located at the center plane of the resultant fabric and each individual yarn is unambiguously located within the plane of the fabric by the crossovers of the bias fabric structure.

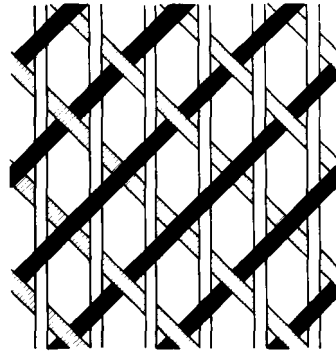


Figure 9 Structure of triaxially braided fabric [3]

The maximum versatility of the braiding process in composites is realized when the braided fabric is produced over a core or mandrel which is passed through the zone of fabric formation. Under these circumstances the final fabric configuration is set by the shape of the mandrel and the orientation of the bias yarns is set by the ratio of the rotational speed of the packages to the transverse speed through the machine. The mandrel can be of fixed or varying cross-sectional shape and if the perimeter of the section is not reentrant it is generally possible to obtain an automatic conformal fit to the mandrel shape. There are restrictions on the ratio of maximum and minimum diameters that can be accommodated, as well as restrictions on the absolute values of these diameters; these limitations are discussed in more detail in a subsequent section. Normally, braiders produce fabric in a single direction, but when braiding is used to produce a composite preform on an irregularly-shaped mandrel it is often advantageous to traverse the workpiece through the machine past the fabric formation point sequentially in each direction so as to lay up on the mandrel a series of layers of fabric in which the yarns are continuous throughout and there are no major discontinuities at the turnaround points. This adaptation requires the use of a reversing ring to avoid interference between the moving yarn packages and the paid-off yarns or for smaller diameter workpieces the use of dual formation rings in order to maintain the position of the fabric formation along the axis of the workpiece (Figure 10).

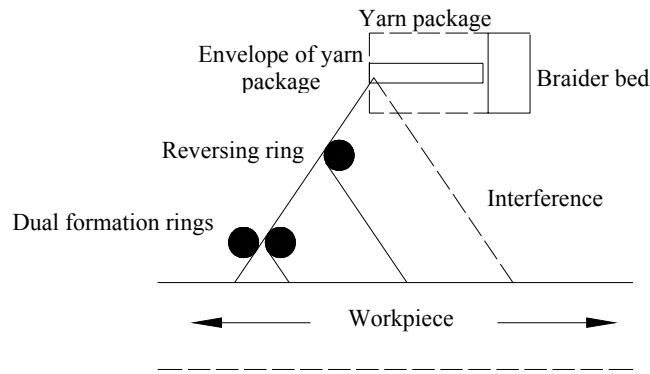


Figure 10 Use of reversing and formation rings [3]

The ability to manipulate three sets of yarns independently gives enhanced design capabilities. If the same yarn is used in all three directions and the sets are arranged to be oriented 60° apart, a fabric structure that is very close to being isotropic in its in-plane mechanical properties is produced. If there is only a small angle between the longitudinal yarns and the bias yarns, which requires a high ratio of transverse speed to rotational speed for the bias yarns, then in the limit the fabric structure approximates to that of a uniaxial tape; alternatively, as another limiting configuration, if the ratio of transverse speed to rotational speed is very low then the bias yarns are aligned at a high angle to the axial yarns and the fabric that is produced is similar mechanically to a conventional woven fabric. It is possible to make the change from one configuration to the other on the run so that a preform can be produced that has specific properties in various regions. In addition since bias and axial yarns are completely different materials and hence different mechanical properties can be supplied by the fixed and moving yarn carriers, the design potential becomes almost unlimited (Figure 11).

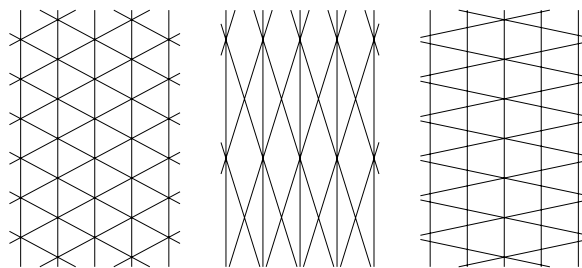


Figure 11 Limiting configurations of triaxial braided fabrics [3]

The high production rate of the braiding process is related to the number of yarn supply packages that are in action at any particular time. In a 96-carrier braider equipped with longitudinal yarn supply there are 144 packages in operation simultaneously and the amount of area coverage that can be achieved in unit time is quite large. Larger braiding machines, up

to 800 carriers [10 and 15], are now coming into commercial operation and this will allow braided fabric to be produced in larger diameters and at a faster throughput. The extent of coverage that can be achieved in a single pass through the braider is determined by several interrelated factors: the diameter of the workpiece; the rate of traverse and hence the helix angle of the carrier yarns; and the width of the individual yarns (rovings) as they lie on the workpiece subsequent to fabric formation. The latter parameter is controlled by both the linear density of the yarn and its twist: a low twist yarn is able to flatten out to give a cross-sectional aspect ratio of up to 10:1 which ensures high transverse coverage and low thickness; a yarn with high twist is not able to accept this type of cross-sectional distortion and a lower cover, thicker fabric is the result. In composite applications the flatter yarn sections are usually more desirable since the uniformity of the structure is improved and the number of voids in the structure is minimized. The maximum yarn linear density that can be accommodated by most unmodified braiders is set by the size of the carrier guides and pulleys, which limit the upper width of the flattened strands to approximately 5 mm: as an illustration of the scale of braided structures it is worth noting that a 96-carrier braider loaded with yarn of this size gives complete coverage in a single pass over a mandrel of 12 cm diameter with a braid angle of approximately 45°.

The braiding process was originally developed in conjunction with traditional textile materials, but it has also proved to be adaptable to handle metal yarns for sheathing applications. This background of adaptability to non-standard materials has been expanded and it is possible to braid in a semi-routine manner and on a production basis all of the modern high performance materials. Each material generally requires individual fine-tuning of the yarn tensions, let-off mechanism, package build and size in order to braid at maximum efficiency with minimum yarn damage: these adjustments are made on the basis of experience and know-how and their importance to the overall success of the braiding operation is enormous. In general, as might be expected on the basis of its mechanical properties, the carbon and other ceramic yarns require the most care and while they can be used as the axial yarn members with complete confidence they have proved to be difficult to handle on the moving carriers. Nevertheless, with sufficient care and attention it is possible to make, for example all-carbon braids for applications that demand the ultimate in stiffness though the rate of production is comparatively low.

Braided structures, which are intended to be the preforms for composites, require the addition of a suitable impregnating matrix material at some point during their production and the braiding process offers three major options for matrix incorporation. The first and most

common alternative involves the production of a dry preform from standard yarns with subsequent impregnation by resin transfer molding (RTM). The dry preform is braided to near-net-shape over a suitable mandrel often made from silicone rubber or closed cell foam which is capable of thermal expansion and which produces compaction of the composite during the thermal curing cycle. The form is then removed from the braiding machine and incorporated in a closed mold and sealed. The mold is evacuated and then resin is led into the mold cavity at low pressure. After the mold is completely filled the resin is cured and removed from the mold. This technique separates the braiding and impregnation steps which minimizes braider idle time and produces parts with excellent surface finish and dimensional tolerances with a minimum of void volume.

A modification of this technique involves a continuous, on-line impregnation system. This method produces an impregnated structure on the mandrel as the braiding is performed and is similar in principle to a wet-lay filament winding operation. The braider is fitted with an impregnation ring which is positioned between the reversing ring and the formation ring and holes or slots are provided in the impregnation ring which communicates with an internal annular resin manifold. Premixed resin is pumped through these holes at a predetermined rate and the yarns which are in continuous contact with the impregnation ring pick up resin as they pass down to the formation point. The wet-laid composite preform can be compacted and consolidated by a series of pressure rolls just downstream of the formation point and the finished article is commonly produced by vacuum bagging, autoclaving or electron beam (EB) curing. It has been developed as an integrated braiding technique which permits the fabrication of near-net-shaped preforms for 3D composite materials with reinforcing fibers oriented continuously by Hamada et al. [16] called braided pultrusion, which can be seen in Figure 12.

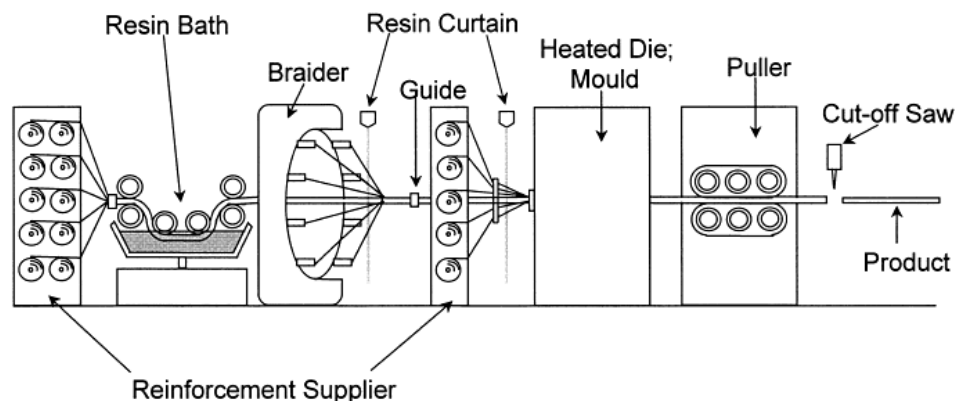


Figure 12 Schematic drawing of the braided pultrusion system [16]

The third major technique for incorporating the matrix material involves the use of prepreg yarns. These yarns are fully impregnated and partially cured and provide, in principle, an extremely convenient route to the manufacture of braided preforms. However, there are several features of the braiding process which make the use of prepreg yarns questionable. Prepreg yarns are inevitably stiffer than their unimpregnated counterparts and are much more difficult to handle in the eyes and guides of the package carrier system. The surface tackiness is another problem since this parameter affects critically the ability of the bias yarns to move over each other as they proceed toward the fabric formation point. High and variable interyarn friction can completely prevent good braid formation. Such yarns are now commercially available and the use of prepreg yarn can be expected to increase in braiding applications [3].

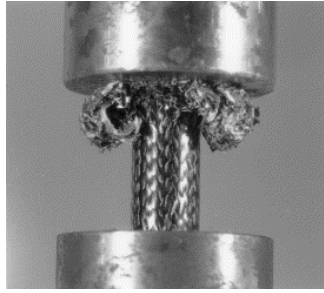
2.2.2. Dynamic stress behavior – crash test

This Chapter will present an overview of dynamic stress behavior of the braided composites. In the last two decades much research effort has focused on the energy-absorption characteristics and failure modes of laminated, woven and knitted composite tubes [17-24]. Farley [20] demonstrated that Kevlar/epoxy tubes were crashed by progressive folding with good post crash integrity. However, the Kevlar/epoxy tubes displayed lower energy absorption capability than the carbon/epoxy or glass/epoxy tubes. Mamlis et al. [22] studied the crash behavior of glass fiber reinforced composite (GFRC) tubes. They explored the mechanisms of crashing and crash growth and identified three distinct modes of collapse: end-crashing or delamination mode (Mode I), mid-length collapse mode (Mode II) and mixed mode of collapse (Mode III). The mode of collapse depends upon a number of factors related to the properties of the fibers and matrix and the arrangement of the fibers, as well as to the geometry of the shell of composite tubes [23 and 24]. Farley and Jones [25] concluded that the crashing response of composite tubes could be categorized into three basic modes: transverse shearing, lamina bending and local buckling. They pointed out that the mechanisms which control these different crashing modes are a function of the mechanical properties of the fiber materials. Hamada et al. [26] showed that the energy absorption and crashing mode could be tailored by controlling the fiber architecture. A hybrid of carbon and high-performance polyethylene fiber composite tube displayed higher energy absorption capability than tubes reinforced with high-performance polyethylene fibers only. Peijs and Vanklinken [27] suggested that hybrid composite tubes in which both high-performance polyethylene fibers and carbon fibers were used as reinforcement could obtain both post-crash integrity and reasonable energy absorption.

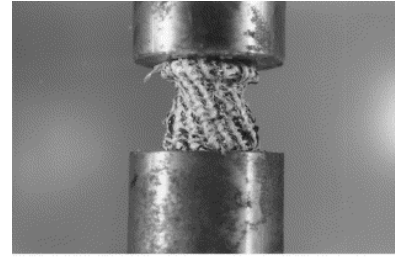
Apart from the aforementioned research on laminated, woven and knitted composite tubes, braided composite tubes have also drawn attention to the investigation of their crash energy absorption capability. Karbhari et al. [28] studied the effects of the fiber types, braid yield, type of braid pattern and number of layers on the energy absorption characteristics of 2-D hybrid braided composite tubes. They indicated that the braiding of preforms for crash energy absorbing structures is seen to be a very effective means of fabrication and the response is comparable to results obtained from specimens using conventional unidirectional prepreg based techniques. Chiu et al. [29] investigated the effects of braiding angle and axial yarn content on the crash energy absorption capability of 2-D triaxially braided composite circular tubes. They demonstrated that the tube with 20° braiding angle displayed the highest specific energy absorption among the tubes with various braiding angles. The tubes using 6-12k fiber (having 6,000 or 12,000 elementary fibers in each roving) tows as the axial yarn exhibited higher specific energy absorption among the tubes with various axial yarn contents. Chiu et al. [30] studied the crashing characteristics of 3-D braided composite square tubes. It is found that the failure modes of the crash tests of 3-D carbon/epoxy braided composite tubes included compressive shear failure, bending and local buckling of the axials, shear and tensile failure of the braiders. In their work the axial yarns are found to dominate the energy absorption, whereas the braiding yarns control the crashing failure mode. Chiu et al. [17] designed six different hybrid types of two-dimensional triaxially braided composite tubes containing Kevlar (K) and carbon (C) fiber to study their crash-failure modes and specific energy-absorption capabilities. Quasi-static axial compression was employed to investigate the effect of hybrid type on the crash-failure characteristics and energy-absorption mechanisms. Among those six different composite tubes braided with all carbon fibers exhibited the highest crash energy absorption. By contrast the structures braided with all Kevlar fibers showed the lowest crash energy absorption, but had the best post-crash integrity (see Figure 13).

Saito et al. [31] and Hamada et al. [16] have investigated the performance of braiding pultrusion process (BPP, see Figure 12) of circular composite rods and quantified their energy absorption capability, while analyzing the failure mechanisms.

Mouritz et al. [32] have assessed the Mode I interlaminar fracture toughness properties of vinyl-ester based composites reinforced with glass fiber manufactured by the advanced textile technologies of braiding, knitting, stitching and through-the-thickness weaving in comparison to a variety of traditional composites made from glass fiber such as unidirectional or woven rovings.



Photograph of a CCC braided composite tube under crash loading

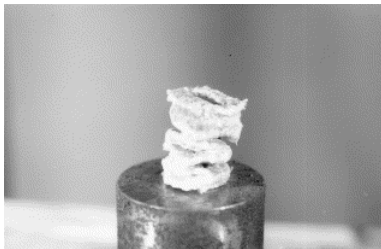


(a)

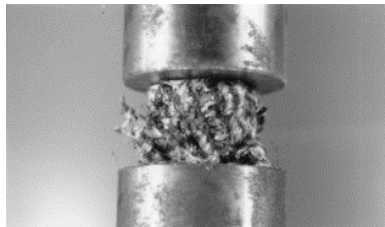


(b)

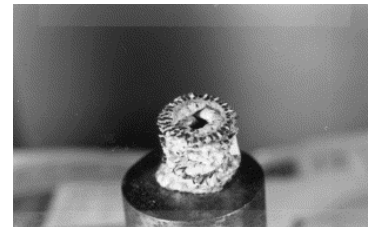
Photograph of type CKK braided composite tube under crash loading. (a) during crashing and (b) after crashing.



Photograph of a KKK braided composite tube after crash loading



Photograph of a KCC braided composite tube under crash loading



Photograph of a type KKC braided composite tube after crash loading.

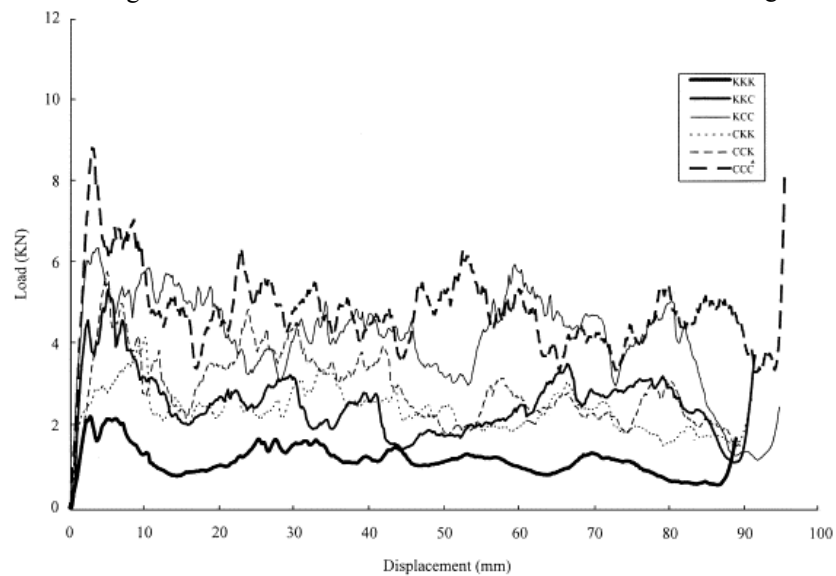


Figure 13 Typical photographs and crash load-displacement curves for CCC, KCC, KCC, CKK, CCK and KKK braided composite tubes [17]

Karbhari et al. [33] have investigated the effect of lateral-impact damage effects on the progressive crash response of hybrid-braided composite tubes. The lateral impact was intended to simulate prior damage to the composite structure at a point along its crashing zone.

Karbhari and Haller [34] have investigated the limited effects of a tenfold change in rate of loading on the progressive crash characteristics of hybrid braided composite tubes, enhancement of energy absorbing capabilities of composites through optimization of shape, tailoring of crash mechanisms and the use of appropriate hybrid forms of reinforcement construction.

Hamada et al. [35] have investigated the fracture behavior of progressive crashing braided I-beams by examining energy-absorption performance. Moreover, to clarify the crashing mechanism, the fracture process of the I-beam was observed by examining the crash zone of a partially crashed I-beam. The crashing mechanism of a braided I-beam was similar to that of a composite cylinder in which reinforcing fibers were oriented in axial and braid directions.

2.3. Electron treatment in composite manufacturing, EB curable resins

This Chapter will present an overview of electron treatment in composite manufacturing and of electron beam (EB) curable resins.

2.3.1. EB curing in composite manufacturing

Fabrication of fiber reinforced polymer matrix composites incorporates assembly and curing steps. Many different processes have been used for assembly such as hand lay-up, resin transfer molding (RTM), filament winding, braiding, automated tape placement etc. Although some resin matrices are designed to cure near room temperature most composites are processed at elevated temperature, while pressure is applied for consolidation [36 and 37].

Electron beam (EB) curing of fiber reinforced polymer composites is a promising new curing technology for fabricating aerospace and ground vehicle components. As a curing technology it must be combined with a method of compaction such as tape or tow placement, hand-layup with hot debulk, vacuum assisted resin transfer molding (VARTM) or pultrusion. The basic concepts of EB curing of composites and adhesives are shown in Figure 14 and Figure 15. The process reduces the time required to crosslink the polymer matrix compared to conventional heat curing. This potential for high throughput is especially important for automotive fabrication. For aerospace applications, the principal advantages of EB curing are the following [36 and 38]:

- Curing is done near room temperature, allowing the use of low cost, low temperature tooling such as wood, plaster or foam.
- Curing at low temperature can reduce residual thermal stresses.

- Co-bonding and co-curing operations with EB-curable adhesive allow fabrication of large integrated structure.
- EB-curable resins and adhesives have long shelf lives and can be stored at room temperature. They are typically one component and solvent-free.
- For large parts that are inconvenient or impossible to fit in an autoclave, EB processing may be the best low-temperature curing alternative. Using a portable EB system: one can bring the curing equipment to the part, rather than vice-versa.
- Recent cost comparisons of EB versus thermal fabrication have shown that EB processing can reduce costs by 10-40% for production of a variety of aerospace parts. Investment costs of EB curing systems (principally the electron accelerator and concrete radiation shielding) are similar to large autoclave costs.

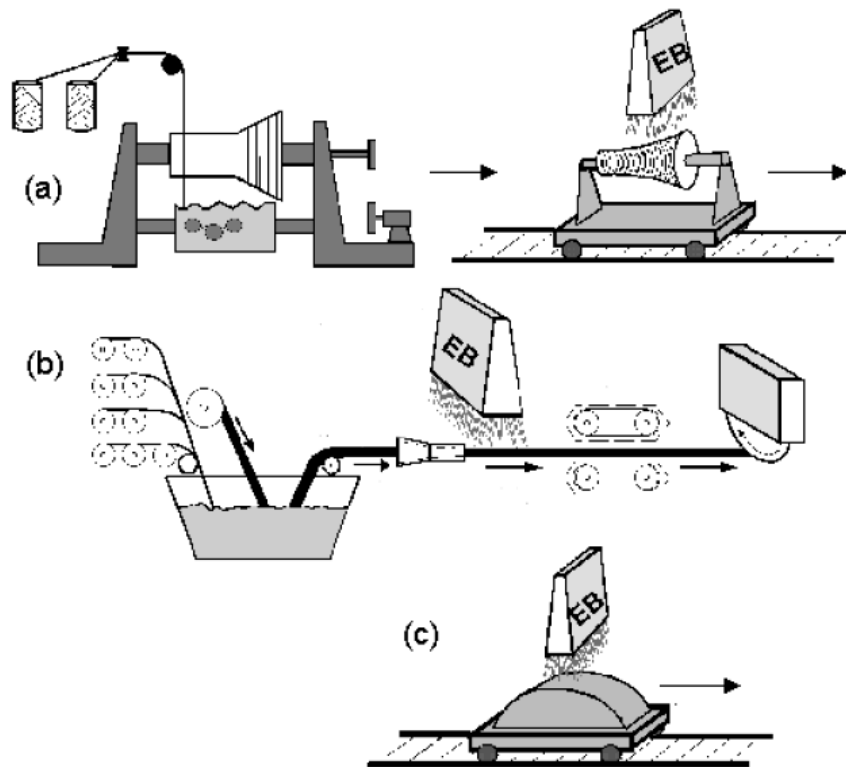


Figure 14 Composite manufacturing processes suitable for EB curing include (a) filament winding, (b) pultrusion and (c) prepreg layup with vacuum bag. Parts are transferred via cart or conveyor to be cured under an EB scan horn. In-line or in-situ curing processes are under development for pultrusion and automated tape placement [36].

Adhesive bonding coupled with autoclave curing is widely used in the aerospace or maritime industry to produce large composite parts with complex core structures. EB-curable adhesives have the potential to replace thermally cured aerospace adhesives in bonding large integrated structures in fewer steps at reduced cost and without autoclave processing [38-40].

The automotive industry uses adhesives to bond composite parts and structural assemblies. For ground vehicle fabrication EB bonding offers high throughput and “command-cure” bonding near room temperature. EB-curable adhesives can be used to bond composites to metals substructure. The process avoids debonding during the cool-down cycle that can occur due to differences in thermal expansion of the metal and composite [41-43].

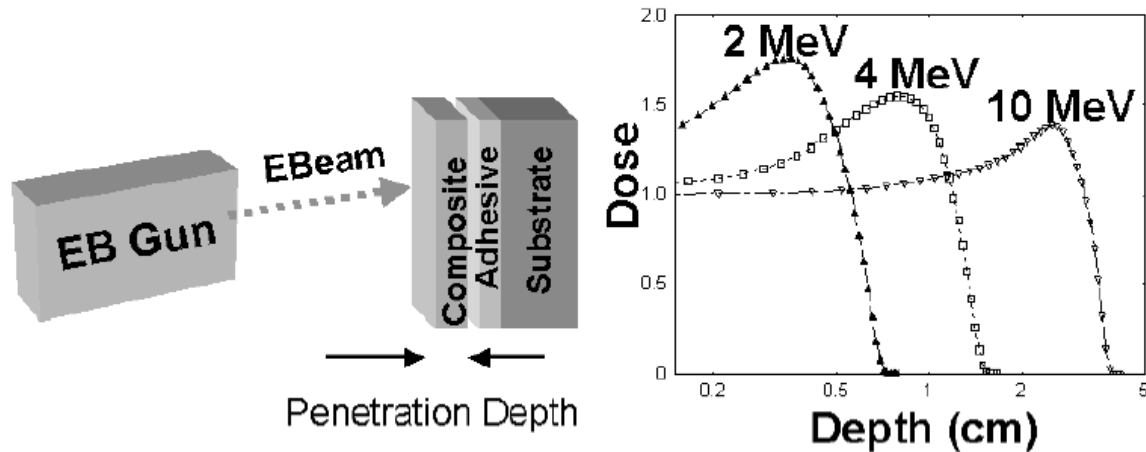


Figure 15 High energy electrons are produced in the accelerator (sometimes known as the EB gun), transport through the air and then penetrate deeply into materials. The depth of penetration is proportional to the energy, measured in millions of electron volts (MeV). The dose is a measure of deposited energy. Typical doses for curing composites or adhesives are in the range 50-200 kGy [36].

2.3.2. Current limitations to EB processing

Although electron beam curing and bonding of composites is an active area of research, the technology has not been widely adopted in industry yet. This is partially due to the conservative nature of the aerospace and automotive industries. On the other hand, this is because few new aircraft designs are planned, the design cycles are extremely long. In the automotive industry, work done by research groups on new technologies though promising, are not necessarily adopted for production. The reason that novel automotive concepts are not produced is often due to market forces, rather than to technical issues.

In addition to overcoming the resistance to change of the risk-sensitive automotive and aircraft industries EB researchers still faces significant technical challenges, especially to meet demanding aerospace requirements [36 and 38]. EB-cured composite properties have achieved those incorporating first generation heat curable resins, such as Cytec-Fiberite 3501-6 [36]. But composite properties, especially compressive properties that require good fracture toughness, are not yet as good as those containing toughened second-generation resins such as Hexcel 8552 [36]. Although preliminary material qualification has begun, the EB community does not have a reputation for “stable” materials with consistent properties.

Suppliers and users have not developed the processing specifications and acceptance standards that are the hallmarks of a mature technology.

EB-curable adhesives have made significant achievements in the last few years. Their properties meet the requirements of automotive applications. The strength of the best EB-curable paste adhesive is close to that of industry-standard aerospace systems. However these adhesives cannot be used in the hottest or coldest aerospace environments and are just at the beginning to be used in secondary structures. In some cases, aerospace companies find it more convenient to have their adhesive supplied as a film rather than as a paste. However, EB-curable film adhesives do not currently possess the strength needed for any aerospace application [44 and 47].

There are several reasons why properties of simple EB-curable composites and adhesives do not match those of the best high strength systems. One reason is that the resin chemistry of the cationically initiated epoxies produces different polymer structures than the EB-curable systems. Another oft-cited reason for reduced composite properties is reduced fiber-matrix interface strength due to the imperfections of the interface between EB-curable resins and fiber finish [48 and 49].

2.3.3. *Electron beam curable resins*

EB-curable epoxies constitute a unique class of polymers that can be rapidly cured to produce material properties that meet or exceed the properties of high-performance thermosetting epoxies. Hundreds of EB-curable resin systems, including toughened formulations, are now commercially available. Formulating EB-curable epoxies involves mixing a cationic initiator at a concentration of 1 to 3% with conventional epoxy resins. Cationic initiators react when subjected to irradiation from ultraviolet light, ionizing radiation (x-rays or gamma rays), or a beam of high-energy electrons. Most resins exhibit physical and mechanical properties that meet or exceed the properties of the analogous thermosetting epoxies. It appears that the outstanding properties of these resins are caused by efficient crosslinking of epoxy groups, resulting in similar or better properties than with thermoset resins. Table 1 summarizes the characteristics of the EB-curable resins currently available [38].

Features	EB - curable epoxy resins	Conventional epoxy resins
Mechanical properties	high-performance	high-performance
Manufacturing costs (overall)	moderate (25÷65% less than thermal)	High
Prepreg storage and handling	extended lifetime at 20°C	limited lifetime below 0°C
Environmental and health concerns	Low	moderate to high (hardeners)
Material shrinkage on curing (%)	2÷3	4÷6
Volatile emission (%)	<0.1	<1.0
Glass transition temperature (°C)	up to 400	up to 300
Residual stresses in the composite	Very low	moderate to high
Water absorption (%)	<2	<6
Production throughput	fast	Slow
Maximum dimension of composite part	50 mm (EB)	20 mm (thicker parts can be destroyed by exothermic reactions)
Thickness limit in a single cycle	200 mm (X-ray)	
	1mm (ultraviolet)	
Tooling material	metals, wood, ceramics, plastics, waxes, foams	metals, ceramics, graphite
Tooling cost	low-moderate	moderate-high
Cure time (10 mm thick part)	seconds - minutes	hours
Energy requirements	high	high to very high (autoclave)
Source material availability	resins and initiators available	resins and hardeners available
Material cost- complete resin (\$/kg)	4 - 10 (commercial)	4 – 8 (commercial)
System cost- complete resin (\$/kg)	16÷40 (high performance)	16÷40 (high performance)

Table 1 Features of EB-curable epoxy resins [38]

High energy electrons generate ionic species, free radicals and molecules in excited states capable of initiating and sustaining polymerization. Figure 16 summarizes the pathways for induction of polymerization by EB irradiation.

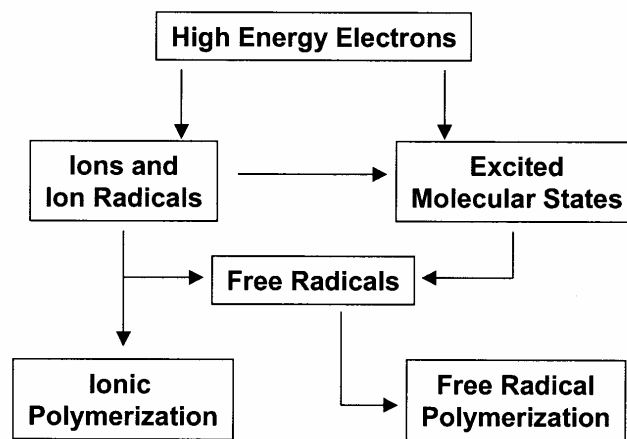


Figure 16 High energy electrons in EB-curable resins and adhesives generate ionic species, free radicals and molecules in excited states that initiate and sustain polymerization [36].

Depending on the chemistry of the resin system being irradiated, polymerization can occur by free radical as well as ionic mechanisms. The polymerization of acrylic/methacrylic systems, maleic and fumaric polyester resins, maleimides and thiol-ene systems proceeds via free-radical mechanisms without initiators. EB-induced polymerization of nitroethylene proceeds via anionic mechanisms and epoxies are polymerized cationically with the appropriate photoinitiator under EB irradiation. Of these systems, free-radical-cured systems

based on acrylate and methacrylate functionality and cationically cured epoxies catalyzed using diaryliodonium or triarylsulfonium salts have shown the most promise for composites applications [36, 44-47].

2.3.4. Oxygen effect

In the great majority of cases, radiation curing is a free-radical process and oxygen has a pronounced inhibiting effect. If curing is carried out in air, oxygen reacts with radicals in the surface layers of the coating, slowing polymerization and giving a sticky, easily damaged surface. The damaging effect of oxygen is increased by the ozone formed in the irradiation zone. A number of methods have been proposed in order to suppress the oxygen effect [50]:

1. Irradiation in an atmosphere of chemically inert gas (e.g. N₂, Ar, CO₂).
2. Covering the oligomer-monomer formulation with a polymer film (e.g. PE, PA, PET) before irradiation, and removing the film afterwards.
3. Successive irradiation with fast electron and then UV light. This is often described as the “dual-cure method”. The ultraviolet light dissociates peroxides formed on irradiation in air, and the radicals produced complete polymerization process. Since the photochemical step is slower than simple radiation curing, the coating may exhibit less shrinkage and improved adhesion to the substrate [51 and 52].
4. Use of additives to inhibit oxidation (e.g. amines) or sensitize curing (e.g. transition-metal salts) and of waxy compounds (e.g. paraffin wax) that are displaced during polymerization and form a protective layer on the surface of the coating.
5. Covering the coating formulation with a protective layer of water.
6. Through the use of special formulations containing oligomers modified with phthalic anhydride, dicyclopentadiene, styrene etc.
7. Irradiation at very high dose rates ($\sim 10^{11}$ Gy s⁻¹) using nanosecond pulses of electrons.
8. Polymerization via a cationic mechanism, since cationic reactions are not affected by oxygen. However, this type of curing is seldom encountered [53 and 54].

In practice only the first three methods are used, the first widely and the second and third more rarely. Nitrogen is generally used as the inert gas and should contain not more than 0.05-0.1% residual oxygen. The second method was chosen to eliminate the oxygen effect in

our experiments because this was the most cost-effective at a low number of production samples.

2.4. Modeling of braided composites

A composite material consists of two or more components and therefore has different phases. In the interior of composites, internal “boundaries” exist which are often referred to be “interfaces”. Hence, a composite can be treated as being a heterogeneous medium with internal structures [55–60]. There have been a number of models developed for the evaluation of the mechanical properties of various composites including textile fabrics [55, 61-63]. Kuo and Chen [64 and 65] have determined the elastic moduli, damage mechanisms and microgeometry in 3-D braided composite pultruded rods. Chen et al. [66] have studied the microstructure of 3-D braided preforms produced by the four-step 1 x 1 method. An analytical approach was employed in conjunction with experimental investigation to establish the relationship between the braid structure and the braiding parameters. Kuznetsov [67] has developed a comprehensive geometric analysis of a single lamina in a form suitable for subsequent geometric optimization of laminate layout. An optimized layout will avoid or minimize reinforcement excisions and darts, along with the resulting patches, splices and overlaps. Wang et al. [68] have studied yarn structures in 3-D braided preforms and have discussed the topological characteristics of fiber architecture in rectangular and tubular braided preforms. It should be pointed out that the model [69] has a disadvantage that the continuity of yarn on surfaces and in corners was not considered.

Basically, these models can be classified into two categories, namely, numerical predictions and analytical estimations. With the rapid development of computing technology, numerical models (finite element, unit cells etc.) exhibit advantages and are increasingly employed in practice [70-73]. Wang and Sun [74] have established the concept of a digital-element to simulate textile processes and determine the micro-geometry of textile fabrics. It modeled yarns by a pin-connected digital-rod-element chain. Zhou et al. [75] have continued the development using the multi-chain digital element analysis in textile mechanics. D’Amato [76] has investigated a methodology for the structural analysis of braided composites based on the use of standard finite element codes. This approach used the geometrical description at micro-structural level and can be applied when the size of the analyzable model was adequate to illustrate the global behavior of fabric which was applied in the aerospace industry. Tang and Postle [77 and 78] have demonstrated that the braiding angles and fiber volume fraction can be represented as functions of the normalized pitch

length introduced as a key parameter of 3-D braided reinforced composite materials. The models for the prediction of the tensile and shear moduli of three-dimensional braided composites were established by numerical simulation and mathematical modeling. 3-D braided preforms were produced from the material system comprising glass/polypropylene and their moduli are measured.

Nevertheless, analytical or semi-analytical techniques still play an important role in many aspects, particularly in pre-design of new textile composites, optimization of fiber architectures and estimation of structural properties etc.

Analytical techniques are primarily based on average or homogenization procedures evaluating the “effective” or the “overall” properties of composites the internal structures of which are identified. Typical techniques include the composite cylinder assemblage method [79-81] (CCA), the variation method [58], the generalized effective stiffness method [59 and 82], the self-consistent method [60] and the laminate plate theory [83] etc. For most practical composites, higher order spatial fluctuation effects (of stresses and strains) have to be omitted due to complexity of mathematics. Nevertheless, it is still quite difficult or even impractical to obtain 3-D analytical results for most composites without invoking further approximations except for a few ideally simplified cases. For textile fabrics, since their meso-structures are much more complex than those of laminated composites, researchers have to make efforts continuously to develop simplified but efficient models [84-87] to estimate their mechanical properties. Technically, those models for textile composites were still based on the concepts and methodologies previously developed for traditional composites with improvements being made. For example, for 2-D woven hybrid fabrics a classic study is the Mosaic Model [88], which is based on the concept of the classic laminate theory. Some other models in this aspect, such as the Bridge model [87], the 1-D fiber undulation [89] and the 2-D fiber crimp model [90-92] etc. are also based on the laminate theory but they are used locally when the Mosaic model is not applicable. For 3-D textile fabrics, some simplified models were also developed [85 and 93]. For example, Ko and Pastore [62] established a fabric geometry model (FGM), which consists of four sets of idealized straight yarn segments with spatial orientations characterized by braiding angles. The elastic properties for each set of yarn segments can be locally calculated and then rotated to a 3-D braided composite frame. Eventually the overall effective elastic properties of the 3-D braided composite can be determined through summation of the stiffness of each yarn segment multiplied by its volume fraction.

The advantage of those 3-D models [85, 93, 94], including that of the Ko and Pastore model [62], is relatively simple and is easier to use in practice. However, they may not be able to provide satisfactory prediction in many cases. Particularly, in these models the geometry and architecture of fibers have to be greatly simplified and these simplifications may result in significant errors. To reduce some sources of these errors in an approximate manner, a modified homogenization scheme for evaluating the effective elastic properties of 3-D composites, in particular of 3-D braided composites can be used. The scheme is developed in such way that the requirement of continuity at interfaces is satisfied. Zuorong et al. call this as a perfect-interface-condition-based homogenization technique. With such a treatment more meso-structural characteristics of composite can be included [55].

2.4.1. Concept of fiber bundle

The computer-aided systems for testing the fibers and composites, as well as designing the geometry of different products made of fiber reinforced composite make it possible, moreover, require to study the relationships between the properties of the usually partially ordered fibrous structures and their macroscale strength in order to take them into consideration in planning structures built up of fibers or composites reinforced with fibers before manufacturing [7, 95 and 96].

The probabilistic theory of brittle materials has been founded by Weibull [97] essentially, the fundamental principle of which is the so called weakest link theory called often Weibull theory, too [98-102]. Another way of characterizing the strength of materials is fracture mechanics the method of which was reviewed by e.g. Cotterell [103].

Now it is clear that not only the single fibers but certain small assemblies of them formed by close fibers and so called fiber bundles can play an important role in the macroscale mechanical behavior of the fibrous structure in point.

An enormous number of studies have dealt with the problem of estimating or modeling and applying the statistical fiber bundle strength such as those of Hearle et al. [104-106], Zurek [107], Phoenix [108-111], Harlow and Phoenix [112 and 113] and recently Grishanov et al. [114]. Sutherland and Guedes Soares [102] gave a good review of this problem from the aspect of the strength of the composite materials. It has been shown that the damage accumulation, the failure of some adjacent fibers, initiates the failure of fiber reinforced composites [102, 112 and 113]. Wisnom [100] has discussed the size effect – among others – on the tensile and bending strength in detail. Some of the studies like those

of Phoenix et al. [108-111] and Vas et al. [115-118] have examined not only the probabilistic properties of the bundle strength but the damage process in time, too.

Vas et al. have worked out a modeling concept using a network of idealized fiber bundles cell (FBC) and applied to model the mechanical behavior of real fiber bundles like that for the flat bundle test of cotton fibers or twisted fiber bundles [116-118]. Vas et al. [95 and 96] have investigated this statistical modeling method, the special idealized fiber bundles to model the breakage and slippage of fibers during a mechanical test and the application of this method for modeling and analyzing the bending properties of unidirectional fiber reinforced composites.

2.4.2. Fiber bundle cells method for modeling fibrous structures

In general, the fibers as basic elements form amorphous and ordered, moreover super ordered parts in the fibrous structures. The fibers may be of different shapes and disposition in the space and their connection to the vicinity, consequently their mechanical behavior can differ, as well.

As it is well known, there is a close relationship between the course of the load-strain curve obtained for example in tensile tests and the structure in respect of the structural changes of fibrous products when elongating them gradually. In principle Figure 17 illustrates these changes [118].

The front part of the curve (O-A₂) is related to the elongating process with stretching the fibers – some of them are loose here – and elongating the best ordered fiber bundle.

With the first breakage or slippage at point A₂ the damaging process begins and through additional breakages and slippages it goes on until the bundle is completely broken (point F) [118].

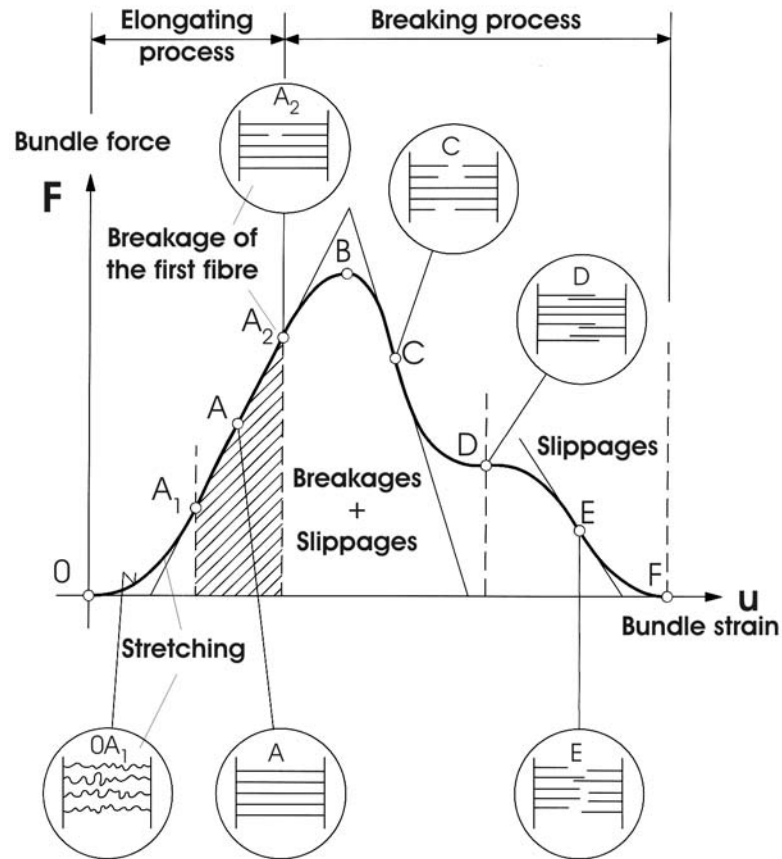


Figure 17 Characteristic parts of a load-strain curve obtained in a tensile test [114]

2.4.2.1. Statistical single fiber model

Making use of the known geometrical and mechanical properties of the given fibers, a statistical single fiber model, which is perfectly flexible and elastic but it breaks at a random value of load can be defined [115-118].

The tensile or shear test of the bundle induces the strain of the fibers. Assume that a tensile followed by a shear test are carried out on a fiber bundle, then the expression to calculate this strain ε of a fiber versus bundle strain u and bundle shear deformation w depends on the fiber position and is given by (see Figure 18):

$$\varepsilon = \frac{l}{l_0} - 1 = (1 + \varepsilon_0) \cdot \sqrt{\frac{(1+u)^2 + (T_0 + w)^2}{1 + T_0^2}} - 1. \quad (1)$$

In Eqn. (1) l_0 , ε_0 , e_0 , $L_0=x_0$, l , $L=x$ are the unloaded length, the initial strain before loading, and the initial excentricity or skewness of the fiber, of the initial and loaded lengths of the bundle, the loaded length of fiber after tensile and shear loads, respectively, as well as

$$u = \frac{\Delta L}{L_0} = \frac{L - L_0}{L_0}, \quad w = \frac{\Delta e}{L_0} = \frac{e - e_0}{L_0}, \quad (2, 3)$$

$$e_0^2 = y_0^2 + z_0^2, \quad e^2 = y^2 + z^2, \quad T_0 = \frac{e_0}{L_0}. \quad (4, 5, 6)$$

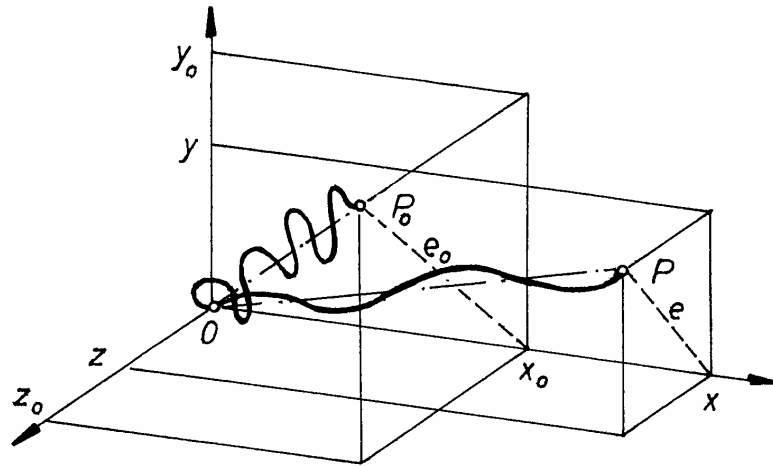


Figure 18 The arrangement of a single fiber in a flat fiber bundle before and after loading [95]

In case of a tensile test of an untwisted fiber bundle $w=0$ while at a shear test $u=0$ in Eqn. (1). If the fiber bundle is twisted then as an effect of the bundle strain caused by a tensile load the twist count of the bundle will change, consequently $w=w(u) \neq 0$. Later a tensile test is assumed to be carried out on the bundle in a point.

Eqn. (1) gives the basis of computing the tensile force in a single fiber using the real or an idealized relationship between strain and force, as well as the expected value of the bundle force utilizing the fact that all the parameters of the fiber and the bundle can be random variables with known probability distributions.

Since the fibers are considered perfectly flexible and the relationship between strain and force is assumed to be independent of the time, the force rising from stretching the fiber and transmitted by the fiber is zero if the fiber strain is less than zero:

$$F = K \cdot g(|\varepsilon|_+) = K \cdot g_+(\varepsilon) = \begin{cases} K \cdot g(\varepsilon), & \text{if } \varepsilon > 0 \\ 0, & \text{otherwise} \end{cases} \quad (7)$$

where $K > 0$ is the initial stiffness of the fibers, $|\varepsilon|_+$ is the positive part of ε , g_+ is defined by Eqn. (7) and mapping g ($g(0)=0$) can be given by an integral according to the Boltzmann-Persoz principle [16]:

$$g(\varepsilon) = \int_0^u \kappa(u-s, \varepsilon(s)) d\varepsilon(s), \quad (8)$$

where s is a running variable. If the fiber material is linear viscoelastic the core function (κ) in integral (8) is independent of ε , while it is non-linear elastic if $\kappa = \kappa(\varepsilon)$.

In the case of linear elastic behavior $g(u) \equiv u$ – that is $\kappa \equiv l$ – expression (8) takes a very simple form:

$$F(u(t)) = K|\varepsilon(u(t))|_+, \quad (9)$$

where t is the time. In the next examination the fibers will be considered linear elastic.

2.4.2.2. Idealized fiber bundle cells

The model of a flat bundle is built up of fibers independent of each other. In the real fiber bundles there can be well-ordered and amorphous parts. According to their arrangements within the bundle the fibers can be classified into subbundles which can be handled as bundle cells that are model elements in a modeling problem (Figure 19) [18, 20, 22, 24 and 37]:

- (1) **Well-ordered bundle cell** of normal fibers (E-bundle), in which the fibers have a linear (Hookean) strain-force relationship with random parameters like ultimate strain (ε_B) and ultimate tensile force (F_B), as well as they are gripped in parallel. These properties determine the **E-bundle** of ideal gripping. This bundle has been called classical fiber bundle in some studies [6].
- (2) **Preset bundle cell** (preloaded, pretensioned) (EH-bundle), in which the fibers can be randomly preloaded or precrimped. The **EH-bundle** is a preset E-bundle and its fibers have a random initial strain (ε_o). Preloading (prestretching) or precrimping means that $\varepsilon_o > 0$ or $\varepsilon_o < 0$. Because of the perfect flexibility, the fiber precrimped cannot transmit force until uncrimping. Supposing $\varepsilon_o > 0$ Phoenix [108] has defined an essentially similar one called generalized bundle.
- (3) **Slipping bundle cell** (ES-bundle), in which the fibers may randomly break or slip out the grips or each other. Fibers of the **ES-bundle** can be gripped at both ends or they are parts of a fiber-chain in the bundle. Their gripping is not ideal, that is why they can slip if the limit force of slippage (F_{SL}) is less than the ultimate tensile force (F_B). Both the limit force (F_{SL}) and the length of slippage (l_S) are random variables. The latter one is substituted with a relative displacement denoted by ε_S :

$$\varepsilon_S = \frac{l_S}{L_o}. \quad (10)$$

- (4) **Oblique bundle cell** (ET-bundle), in which the fibers are straight, however, neither they nor their chord are parallel to each other. Their initial relative declination ($T_o = e_o/L_o$), that is their obliquity (e_o) is a random variable. This obliquity of the **ET-bundle** means a kind of shearing of the fiber in question perpendicular to the

average direction of the bundle. According to that a bundle can be considered *sheared E-bundle* if its average orientation differs from the average direction.

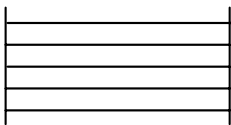
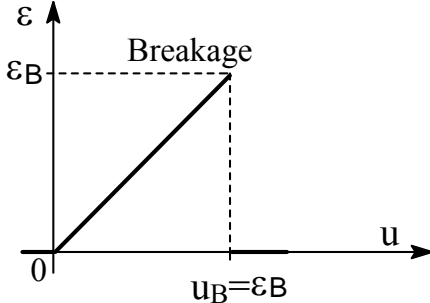
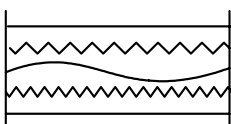
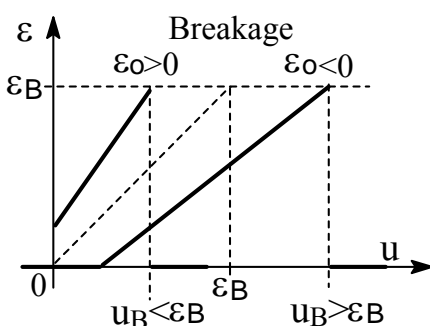
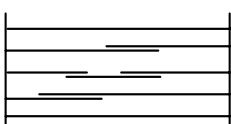
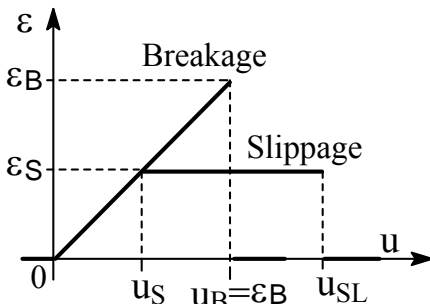
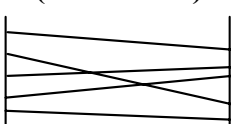
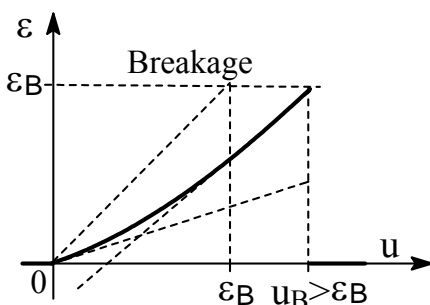
Idealized fiber bundle cells and their strain properties		
Line diagram	Relative strain of fibers	Random parameters
<p>Well-ordered bundle (E-bundle)</p> 		<ul style="list-style-type: none"> • Ultimate strain: $\epsilon_B > 0$
<p>Preset bundle (EH-bundle)</p> 		<ul style="list-style-type: none"> • Ultimate strain: $\epsilon_B > 0$ • Preloading: ϵ_0 • Prestretching: $\epsilon_0 > 0$ • Precrimping: $-1 < \epsilon_0 < 0$
<p>Slipping bundle (ES-bundle)</p> 		<ul style="list-style-type: none"> • Ultimate strain: $\epsilon_B > 0$ • Strain limit of slippage: $u_S = \epsilon_S > 0$ • Relative slippage length: $\epsilon_L > 0$ $u_{SL} = \epsilon_{SL} = \epsilon_S + \epsilon_L$
<p>Oblique bundle (ET-bundle)</p> 		<ul style="list-style-type: none"> • Ultimate strain: $\epsilon_B > 0$ • Initial relative declination: $T_0 = \epsilon_0 / L_0$

Figure 19 Properties of the idealized fiber bundle cells (FBCs) [95]

Taking into account the properties of the fiber bundle cells defined above the following general relationship between the fiber and bundle strain can be formulated:

$$\varepsilon(u, w) = \begin{cases} (1 + \varepsilon_o) \cdot \sqrt{\frac{(1+u)^2 + (T_o + w)^2}{1 + T_o^2}} - 1, & \text{if } 0 \leq u < \min(\varepsilon_B, \varepsilon_S) \\ \varepsilon_S, & \text{if } \varepsilon_S \leq u < \varepsilon_S + \varepsilon_{BL} \text{ and } \varepsilon_S < \varepsilon_B \\ 0, & \text{otherwise} \end{cases}. \quad (11)$$

To simplify the model, the probability distributions of all the random variables mentioned before are assumed to be normal. Thus, the expected value of the tensile force of the bundle cells ($E(F) = \bar{F}$) can be calculated. Dividing the expected value by the average ultimate tensile force of fibers, the so called normalized tensile force of bundle ($FH < 1$) can be computed as follows:

$$FH(z) = \frac{\bar{F}(z)}{n \cdot \bar{F}_B}, \quad (12)$$

where n and \bar{F}_B are the number and the average ultimate tensile force of fibers, respectively.

Variable z is the bundle strain normalized by the average ultimate strain of fibers:

$$z = \frac{u}{\bar{\varepsilon}_B}. \quad (13)$$

In general, the maximum value of the normalized force course is called the utilization factor of the fiber strength in the bundle and is denoted by $FH^* = FH(z^*)$ here.

Under the discussed conditions the normalized expected value process of a fiber bundle cell is given by the following expression ($\varepsilon = \varepsilon(z\bar{\varepsilon}_B)$):

$$\begin{aligned} FH(z) = & \frac{1}{\bar{F}_B} \cdot E[K \cdot g_+(\varepsilon(z\bar{\varepsilon}_B)) | -1 < \varepsilon < \min(\varepsilon_B, \varepsilon_S)] \cdot P(-1 < \varepsilon < \min(\varepsilon_B, \varepsilon_S)) + \\ & + \frac{1}{\bar{F}_B} \cdot E[K \cdot g(\varepsilon_S) | \varepsilon_S < \varepsilon_B, \varepsilon_S < \varepsilon < \varepsilon_{SL}] \cdot P(\varepsilon_S < \varepsilon_B, \varepsilon_S < \varepsilon < \varepsilon_{SL}) \end{aligned}. \quad (14)$$

Note that according to Eqn. (1) strain ε may be a random variable because of ε_o or T_o .

Table 2 contains the formulae determined on the basis of Eqn. (9) for calculating the expected value processes of the 4 fiber bundle cells discussed above [18, 20 and 37]. Here g_+ denotes the positive part of function g .

In Figure 20, Figure 21 and Figure 22 the normalized tensile force process calculated at different parameter values by using the formulae in Table 2 is plotted for the uniaxially oriented E-, EH- and ES-bundles.

In this kind of bundles the chords of fibers are parallel. The ultimate strain of fiber (ε_B) was assumed to be of normal distribution. Figure 20 illustrates the properties of these three types of idealized fiber bundle cells (FBCs).

The diagram in Figure 20 shows some normalized force-strain curves with value of the coefficient of variance of ultimate strain of fiber for the E-bundle ($VE=0, 0.05, 0.1, 0.2, 0.3, 0.4, 0.5$) [18, 20, 22 and 37]. The peak of these curves represents the best utilization of the fiber strength.

Type of fiber bundle cells	Normalized expected value of tensile force	
E-bundle	$FH(z) = z \cdot [1 - Q_{\varepsilon_B}(z\bar{\varepsilon}_B)]$	(15)
EH-bundle	$FH(z) = \int_{x=-1}^{\infty} h(z, x) _+ \cdot [1 - Q_{\varepsilon_B}(h(z, x)\bar{\varepsilon}_B)] dQ_{\varepsilon_o}(x\bar{\varepsilon}_B),$ where $h(z, x) = (1 + z\bar{\varepsilon}_B) \cdot (1 + x\bar{\varepsilon}_B) - 1$	(16) (17)
ES-bundle	$FH(z) = z \cdot [1 - Q_{\varepsilon_B}(z\bar{\varepsilon}_B)] \cdot [1 - Q_{\varepsilon_S}(z\bar{\varepsilon}_B)] + \int_{x=0}^z x \cdot [1 - Q_{\varepsilon_B}(x\bar{\varepsilon}_B)] \cdot [1 - Q_{\varepsilon_{SL}}((z-x)\bar{\varepsilon}_B)] dQ_{\varepsilon_S}(x\bar{\varepsilon}_B)$	(18)
ET-bundle	$FH(z) = \int_{x=-\infty}^{\infty} y(z, x) _+ \cdot [1 - Q_{\varepsilon_B}(y(z, x))] \cdot \frac{(1 + z\bar{\varepsilon}_B) dQ_{T_o}(x)}{\sqrt{(1 + z\bar{\varepsilon}_B)^2 + (x + w(z\bar{\varepsilon}_B))^2}},$ where $y(z, x) = \sqrt{\frac{(1 + z\bar{\varepsilon}_B)^2 + (x + w(z\bar{\varepsilon}_B))^2}{1 + x^2}} - 1$	(19) (20)

Table 2 Calculation formulae for the expected value processes of the fiber bundle cells ($z \geq 0$) [95]

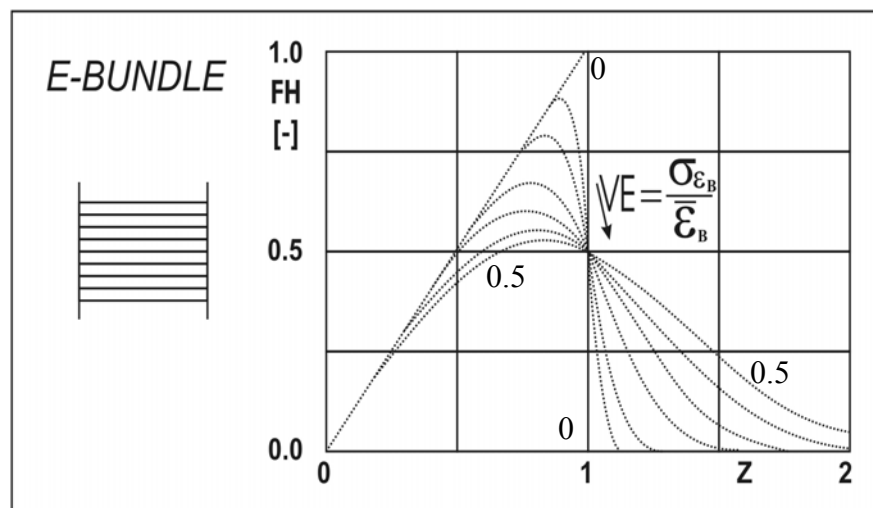


Figure 20 Normalized force-strain curves of the idealized E-bundle [95]

The diagram in Figure 21 shows the force-strain curves of EH-bundles calculated with the same average value of precrimping ($EH=0.5$) but with different variance of that ($VH=0, 0.05, 0.1, 0.2, 0.3, 0.5, 0.7$). Increasing this variance, the curve becomes flatter and at higher values the maximum slope will considerably decrease.

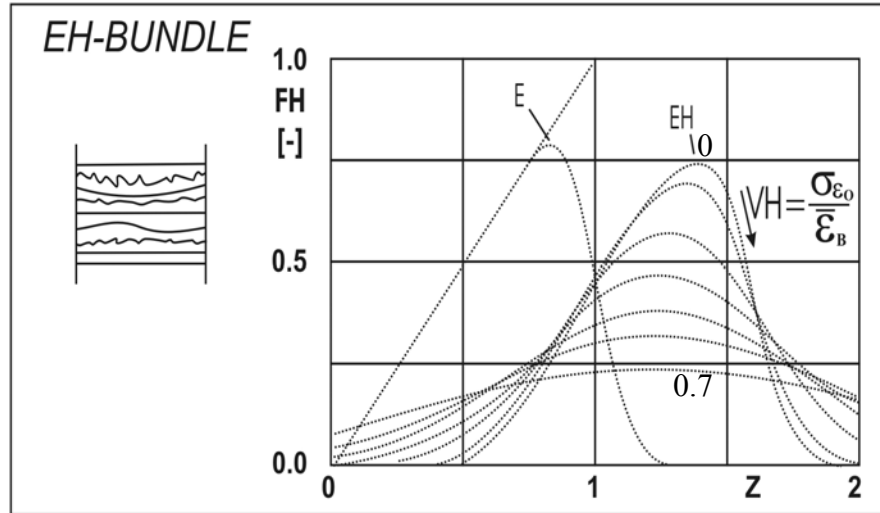


Figure 21 Normalized force-strain curves of the idealized EH-bundle [95]

Some typical force-strain curves of the ES-bundle are shown in Figure 22, where the average slippage strain (ES) and the average relative slippage length (EL) vary receiving the very same values ($ES=EL=0.1, 0.2, 0.5, 1.0, 1.5$). If they are small, most fibers will slip.

If the slippage strain is large, that is greater than the ultimate strain; fiber breakage dominates the process. If they are close to the ultimate strain value, then – as a result of slippages – a kind of plateau appears on the curve after the peak point.

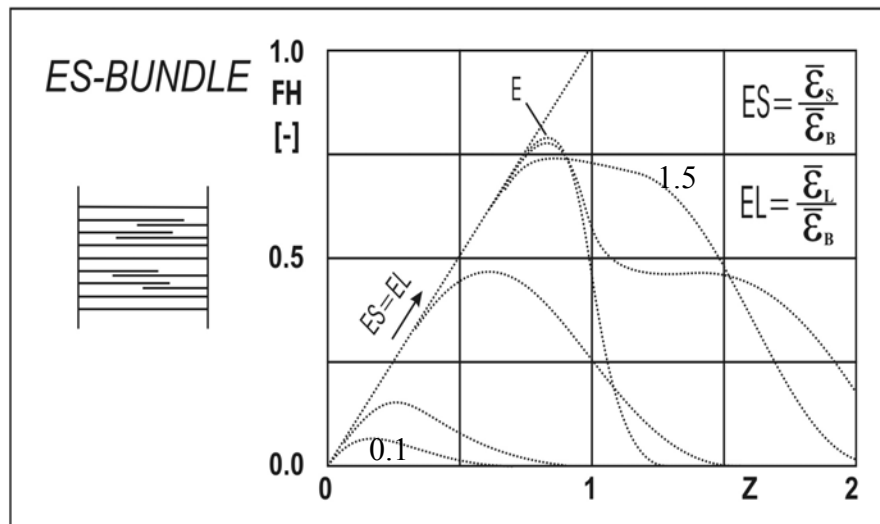


Figure 22 Normalized force-strain curves of the idealized ES-bundle [95]

It can be stated that the main types of changes in the structure of real uniaxially oriented fiber bundles and the course of their elongating and breaking process during the

tensile test can be described by using the idealized fiber bundle cells (FBCs) discussed above [18, 20, 22, 24 and 37].

The model of the *composite flat bundle* (see Figure 23) is constructed of these bundle cells connected parallel with chosen weight-ratios. The model structure of a three-dimensional fiber bundle is built up of composite flat bundles forming fiber layers.

The expected value process of a composite bundle built up of idealized parallel bundle cells connected parallel can be calculated as the weighted sum of the components (m is the number of components, w_i is the weight of the i -th component):

$$\bar{F} = \sum_{i=1}^m w_i \cdot \bar{F}_i \quad (21)$$

$$\sum_{i=1}^m w_i = 1 \quad (22)$$

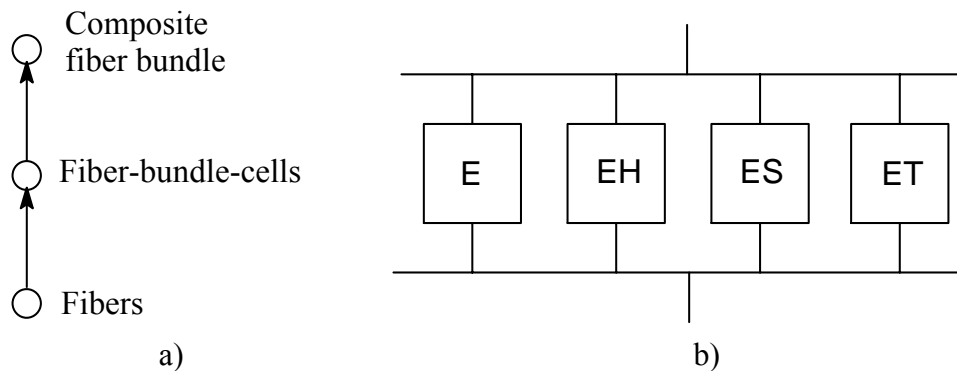


Figure 23 Structural levels (a) and the bundle cell structure (b) of a flat composite bundle [95]

2.4.2.3. Modeling the structure of unidirectional fiber reinforced composites

Figure 24 shows the structural levels of a fiber reinforced composite considered as built up of impregnated fiber layers in the approach of the statistical modeling method mentioned above.

The fibers are assumed to be parallel to the medium line of the specimen, which is, consequently, a unidirectional reinforced composite. The thin fiber layers of composite are essentially flat fiber bundles independent from each other. The independency means that there is no fiber migration between the layers and the random properties of the individual layers are statistically independent [95 and 96]. It can be noted that the principle of structural levels of composites (see Figure 24 a)) is able to be used in average cases as well as modeling the braided composites.

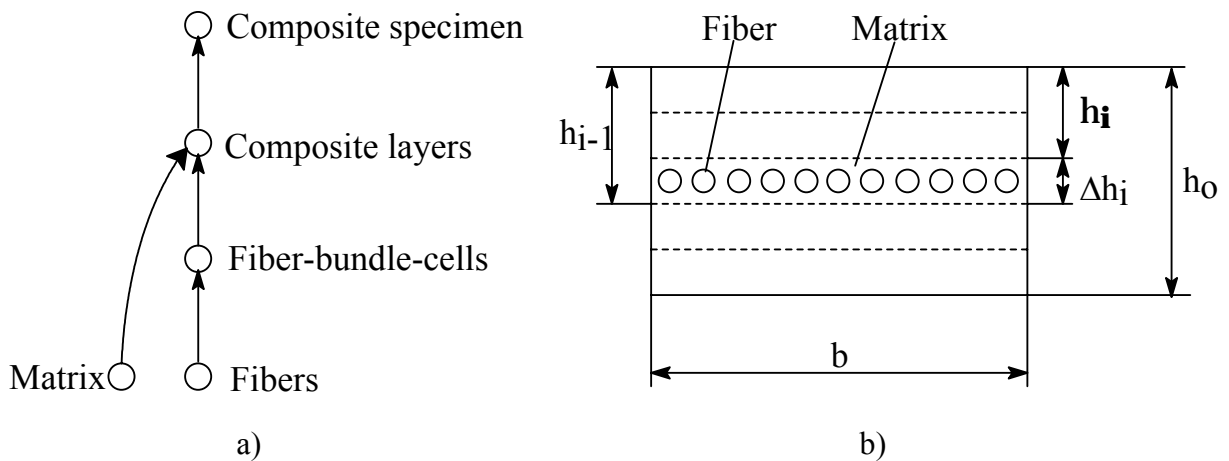


Figure 24 Structural levels (a) and cross section layer structure (b) of a composite specimen [95]

2.5. Targets of the dissertation

A thorough study of the literature available on the new type fiber reinforced composite structures revealed that braiding is still unexploited as a textile technology for producing composite profiles and tubes. These structural materials are advantageous in technical terms and provide attractive solutions for load-bearing beam and multiaxially loaded machine element production especially in case of structures subjected to tensile, bending, shearing or torsion.

The technology of electron treatment spread significantly among the polymer processing technologies for industrial curing. More than 1,500 industrial EB machines are working worldwide, mainly in crosslinking of heat resistant cables and shrinkable tubes for electronic isolation. In the last decade this technique also appeared in curing laminate and polymer composites. The main advantage of the technique is that the system, the fiber and the matrix resin, is handled together and the common beam treatment means a simultaneous excitation and this way gives a chance to a chemical connection on the fiber-matrix interface. Other advantages of the technology are that it produces cured structures a lot faster as compared to traditional curing methods and this structure involves a similar or even better interfacial adhesion.

The textile mechanical properties of braided structures are widely known but there is no simple and useable model developed for the tensile mechanical properties and failure of the composite itself when the braided element is the reinforcing structure. The fiber bundle cell model described in the literature seems to be able to model not only unidirectional but also variously oriented layers, hence it is able to predict the mechanical properties of braided composites. This procedure is not yet described.

The targets are summarized below:

1. Manufacturing of braided fiber reinforced composite profiles, tubes crosslinked by electron beam and analysis of their mechanical properties.
2. Modeling of braided composite tubes and analyzing their failure during tension.
3. Modeling of triaxially braided composite tubes during tension.
4. Investigation of the tensile force of braided composite tubes.
5. Examination of the applicability of the model based on measurements.

3. Experimental materials, machines and methods

In this Chapter the experimental materials, machines and methods will be summarized.

3.1. Experimental materials

3.1.1. Matrices and fibers

In our days epoxy resins and unsaturated polyesters are used as matrix in the production of carbon fiber reinforced (CFR) composites, because of their efficient interfacial connection and good mechanical properties. Epoxy resins have great adhesion properties, but in their traditional variants – connected by polyaddition – they are not crosslinkable by electron treatment. Epoxy-acrylate oligomers were used in our earlier experiments. Radiation crosslinking of free radical mechanism is well feasible here, initiated on the vinyl groups of epoxy-acrylates. EB crosslinking results in a composite material having good mechanical properties and extreme resistance to various chemicals [119-122].

Epoxy-acrylate

Epoxy-acrylate (vinylester) resins from DOW Chem. Co.: DERAKANE D 411 and D 470 have been used in our experiments (see Chapter 4).

Two main groups of crosslinking are distinguishable: chemically and physically initiated crosslinking (see Chapter 2.3):

Chemically initiated crosslinking

For comparison, conventional chemical crosslinking was also carried out by adding 2% Butanox M-50 (peroxy) catalyst, 2% dimethylaniline and 0.05% promoter leaving 36 hours at room temperature for crosslinking, according to the practice of our industrial partner.

Physically initiated crosslinking – EB curing

For the electron beam curing a LUE-8 type linear electron accelerator was chosen. The EB curing of the resins, composites occurred at room temperature, passing below the EB by a speed of about 2 m/min.

A thermal post-curing (80 °C, minimum 30 min) has been applied in all specimens with the aim of completing the curing and stress relieving. KDLC type air recirculation chamber were used made by HAGA Ltd, Hungary.

Fibers

The Hungarian carbon fiber roving contained 48,000 elementary fibers. It was produced from Panex[®]33 of Zoltek Rt. based on a polyacryl-nitril fiber precursor. The fibers were sized by ca. 2% epoxy resin, which has been washed out in our earlier experimental works by acetone (see Chapter 4).

The Tenax[®] STS 5631 carbon fiber rovings that contained 24,000 elementary fibers were used in our experimental work in which the amplified fiber bundle cell model output was compared with our experimental results (see Chapter 5.4). The STS type rovings were a special type suitable for modern industrial application as well as braiding. The fibers were sized by ca. 1% polyurethane. Table 3 shows the properties of applied carbon fibers.

Property	Panex [®] 33	Tenax [®] STS 5631
Tensile strength [MPa]	3,800	4,000
Tensile modulus [GPa]	228	240
Density [g/cm ³]	1.81	1.77
Fiber diameter [μm]	7.2	7
Number of elementary fibers	48,000	24,000

Table 3 Properties of Panex[®]33 and Tenax[®] STS 5631 rovings properties [123, 124]

It can be noted that Tenax roving was better than Zoltek roving for braiding: When Zoltek rovings were applied many fibers cracked near the spinning and braiding machine as well as the spinning ring, and unfortunately on the spinning bobbins, braiding carriers etc. these cracked fibers were raveled.

3.1.2. Production of specimens

EB-crosslinking of pure resins occurred in closed vials.

The impregnation of the braided reinforcing structure was carried out at room temperature. Afterwards vacuum foil technology was used to eliminate the oxygen bubbles and for perfect impregnation. Before radiation treatment the impregnated samples were rolled

in a release foil (PET). In both cases of pure resins as well as composite samples, a thermal after-treatment has been applied at 80 °C for 30 minutes.

3.2. *Experimental machines and methods*

3.2.1. *Braiding machines*

Figure 25 shows the Steeger vertical braiding machine made in Germany which were used in our earlier experiments (see Chapter 4) at Ribbon and String Factory Co. Ltd., Budapest, Hungary with 16 carriers, 8 laid-in and 4 stuffer roving inputs. The pulling speed can be modified.

Muratec J32 horizontal braiding machine made by Muratec Ltd., Kyoto, Japan which was set up in the Institute for Composite Materials at the University of Kaiserslautern, Germany was used to fabricate the circle profiles (see Chapter 5.4) as it can be seen in Figure 26. It had 32 carriers and 16 laid-in and arbitrary stuffer roving inputs. The bobbin and pulling speed can be modified.



Figure 25 The beginning of braiding on a Steeger type braider (16 carriers)



Figure 26 Muratec braider (32 carriers)

3.2.2. *Electron accelerator*

Many types of electron accelerators are used in radiation processing, although all types have some features in common. Electrons emitted by a cathode are accelerated in vacuum in an electromagnetic or electrostatic field passing through an exit window of metal foil into the air, where product irradiation takes place. The energy range of electron beams used in radiation processing varies from 0.15 to 10 MeV; lower-energy electrons are unsuitable because of

their low penetration, while higher-energy beams may induce radioactivity in some materials [125]. Beam powers (the product of electron energy and current) range from 5 to about 300 kW, although there are more powerful accelerators (500 kW and higher) as well [50].

For the high energy electron beam curing a LUE-8 type electron accelerator (see Figure 27 and Figure 28) was chosen, operating at 8 MeV and 650 μ A electron-current, at FE-MA Co. Budapest, Hungary.

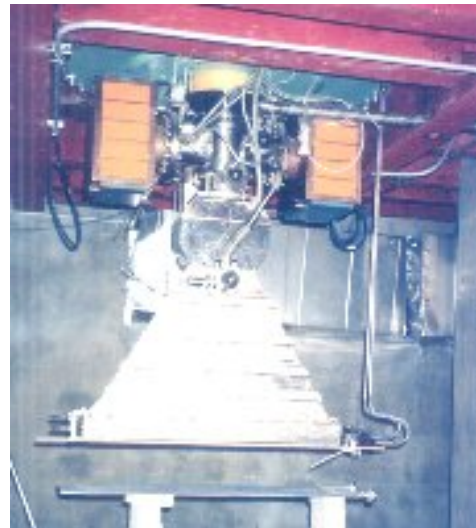
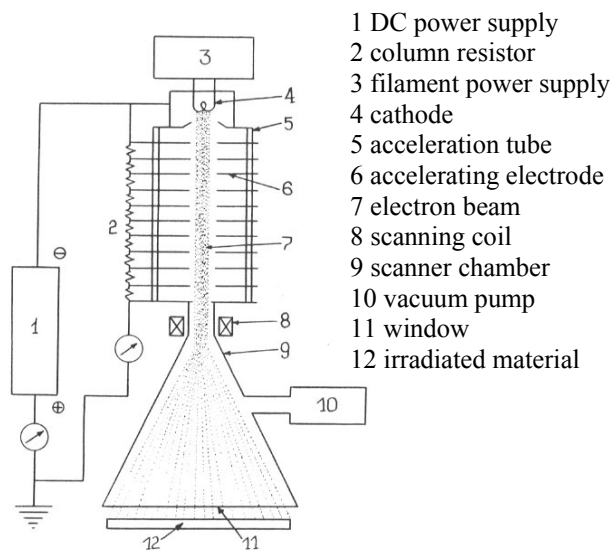


Figure 27 Linear electron-accelerator machine [50]

Figure 28 LUE-8 type electron accelerator [126]

3.2.3. Instrumental falling weight impact-tester

The composite profiles were tested at the Institute for Composite Materials of the University of Kaiserslautern, Germany (directed by K. Friedrich) which is equipped with a drop tower (see Figure 29) for research purposes. The falling weight system has a drop height of 15 m leading to a maximum impact velocity of 17.3 m/sec.

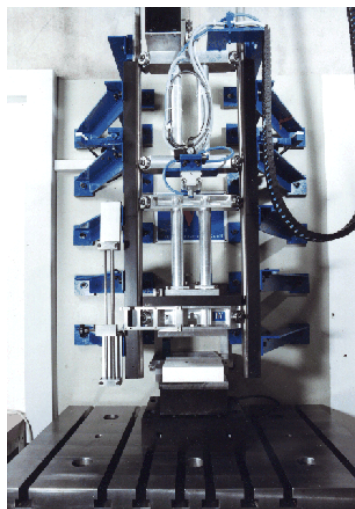


Figure 29 Drop tower in Kaiserslautern

The striker carriage with variable impact mass hits the specimen which is fixed on a piezoelectric load cell. Directly before the carriage impacts the specimen the initial impact velocity is measured by a light barrier. The impact force and the acceleration are measured by a piezoelectric load cell and an accelerometer. The displacement of the impacting carriage is measured by a laser system. For data acquisition a PC-based transient recorder is used with a maximum sampling rate of 300,000 samples/sec. In our experiments the falling mass was 40 kg and the impact velocity was about 4 m/s.

3.2.4. Tensile and bending tests

The mechanical testing of the crosslinked resin samples (for the bending modulus) as well as of the composite samples (for the tensile and bending properties) has been performed on a instrumented ZWICK Z020 (limit force 20 kN) and ZWICK Z050 (limit force 50 kN) electronic tensile tester. ZWICK Z005 (limit force 5 kN) was used to determine the tensile properties of elementary fibers. The offers of the following standards were considered: [127-133].

3.2.5. Determination of contraction parameter

The contraction parameter for applied fiber bundle cell model (see Chapter 5.1) was determined by Messphysik Videoextensometer ME-46 made by Messphysik Materials Testing GmbH, Austria on which simultaneous non-contacting measurement of both longitudinal and lateral strain can be performed.

3.2.6. Determination of fiber content

The fiber content of the composite materials was determined with burn out test. Before burning the geometry and the mass of composite specimens and afterwards the mass of elementary fibers were measured then density and mass as well as volume percent were calculated.

3.2.7. Image processing system

An image processing system was used to specify the diameter of the elementary fibers (ca. 100 elementary fibers were measured, see Appendix A) and braiding angle of the braided composites (ca. 12 angles/sample were determined, see Appendix D).

There are four steps to be completed in order to determine the diameter of the elementary fiber. The first step is sample preparation according to the standard instruction

[133]. Then the image is captured with the help of the CCD (charge coupled device) camera. And this microscopic image can be sent to the computer and transformed into a digital image stored in a file. Afterwards it is time for the stored image preprocessing which means that the object boundaries must be transformed into the coordinates of line segments. This procedure starts with segmentation, meaning the creation of a simplified image containing two kinds of pixel values: foreground and background. Noise may be removed by a filter that replaces each pixel value with a gray level value based on the average value of its immediate neighborhood. Contrast between the objects and the background may be enhanced by filtering techniques emphasizing sharp changes in gray level. The last step is image analysis, when the results are obtained and the actual examination is carried out [134].

The determination of the diameter of a fiber or a yarn with the help of a microscope is considered to be a conventional method. The disadvantages of it are the need for several measurements and the fact that the result depends on the person carrying out the investigation.

The image processing system working with a video camera gives a new way for determining the diameter of fibers and yarns [118]. Compared to the conventional method this method is very quick and the steps of the measurement can be programmed and so there is no possibility for carrying out the measurements in different ways and getting incorrect and unrepeatable results.

The measuring system, method (see Figure 30) and the frame software (with general image processing operations) were developed by KFKI Research Institute for Technical Physics and Materials Science, Budapest, Hungary and a special menu point was added to this in a research cooperation with our Department [135].

Some special measurements can be carried out with this device and its software named YARN besides the fiber or yarn diameter, for instance fiber orientation, surface twist angle (braiding angle) of yarns (and on the surface of a braided composite) and fiber assemblies are all possible to be investigated. The method to determine the fiber diameter is described in Figure 30 [135].

When fibers are inclined the contour-width measured is to be corrected using Y (see Figure 30) and taking into consideration the method of evaluation.

Measuring contour-width of single fibers

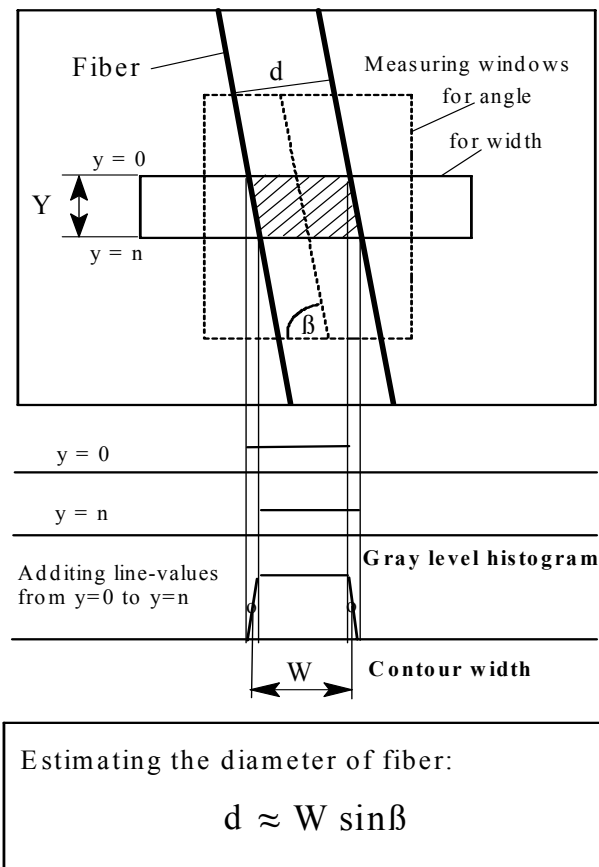


Figure 30 Measuring the contour-width of single fibers [134]

The above described system installed at the Department can be seen in Figure 31. There is a projection microscope type Projectina 4011-4016/MMA (1), the center of the measuring system. The CCD video camera (2) is fastened on the microscope instead of the eyepiece. Its task is to send the picture obtained with the help of a micro or macro objective (3) from the specimen (4) clipped on the stage to the computer (5). There are two monitors showing the picture taken of the specimen. One of them is a simple mono monitor for real-time displaying (6) and the other is an SVGA monitor (7). The two quartz-iodine lamps (8) provide light.

Braiding angles were measured on the surface of the braided composite and determined the following equation (use the marks of Figure 32):

$$\alpha_{0,i} = \begin{cases} 90^\circ - \beta_i, & \text{if } \beta_i \leq 90^\circ \\ \beta_i - 90^\circ, & \text{if } 90^\circ < \beta_i \leq 180^\circ \end{cases}, \quad (23)$$

where $\alpha_{0,i}$ is the i -th braiding, β_i is the i -th measured angle and i is the number of the measure.



Figure 31 The image processing system at our Department
 (1-Projectina 4011-4016/MMA, 2-CCD video camera, 3- objective, 4- specimen,
 5 Computer, 6- real-time monitor, 7- SVGA monitor, 8- quartz-iodine lamp)

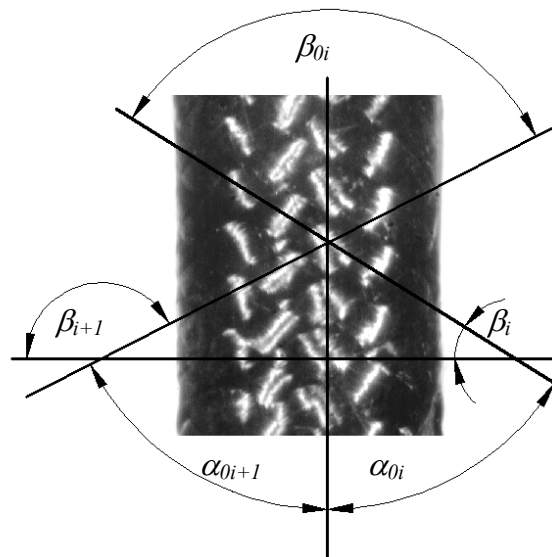


Figure 32 Surface of braided composite and the comparison of braiding and measured angle

4. Electron beam crosslinking of braided composite

In this Chapter the properties of resins, the rigidity of composites and the impact behavior of our new, braided carbon fiber reinforced composites, made by EB processing are compared. The results were published in [136-140].

4.1. EB crosslinking of epoxy-acrylates

The first question of our research was to decide which resin was more suitable to be used in our composite as matrix material. The most important features of the ideal composite matrix material – besides the perfect interfacial adhesion – are: adequate modulus and toughness. We have to note that the high modulus of elasticity – which is reflected in high inflexibility in bending – and the high impact resistance on the other hand are in most cases opposite requirements; it is difficult to fulfill them simultaneously. For the analysis of these features of the resins, the bending test seemed to be the most effective.

3-point bending test was made on EB cured resins. Because of the shape and the L/D proportion of the specimens these tests provided only comparative results, but for the purpose to decide which type of resin we should use for the composite, we found it adequate.

The specimens cured by EB were subject to subsequent heat treatment for different time periods (0-60 min) at the temperature of 80 °C with the aim of completing the curing and stress relieving. Figure 33 shows the mechanical properties of the resins that obtained different curing doses as a function of the time of the heat treatment. It can be seen clearly that the 30-minute-long heat treatment has already a satisfactory stabilizing effect on the mechanical properties.

Concluded from these experiences during the following tests of our composites, after electron treatment as well as after chemical crosslinking, every sample was submitted to a 30-minute-long 80 °C post-treatment.

Figure 34 reveals the difference between the mechanical behavior of the two resins. The force-deflection figure shows that the resin type D470 is more rigid, and seems unfavorable from the point of view of possible catastrophic failure. The D411 possesses a significant “reserve” load-bearing capacity after reaching the maximum value of force, while D470 is brittle. The same is reflected in the area below the curves, which is proportional to the measure of toughness. I considered the toughness as the major aspect, so I chose the D411 resin for the manufacturing of braided composites.

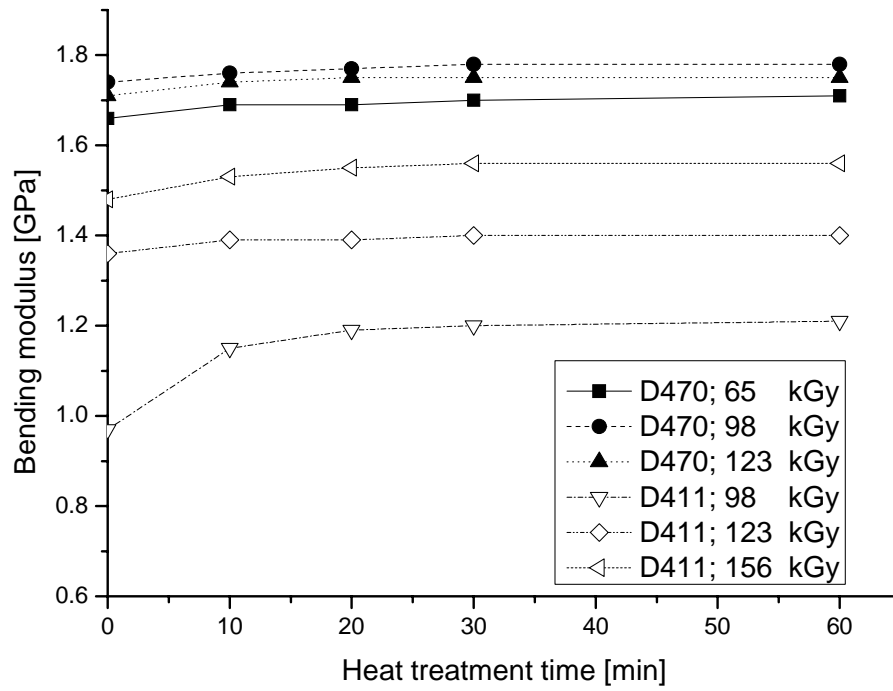


Figure 33 The change of the bending modulus as a result of thermal post-treatment at 80 °C (cp. Appendix B, Table T1 and Table T2)

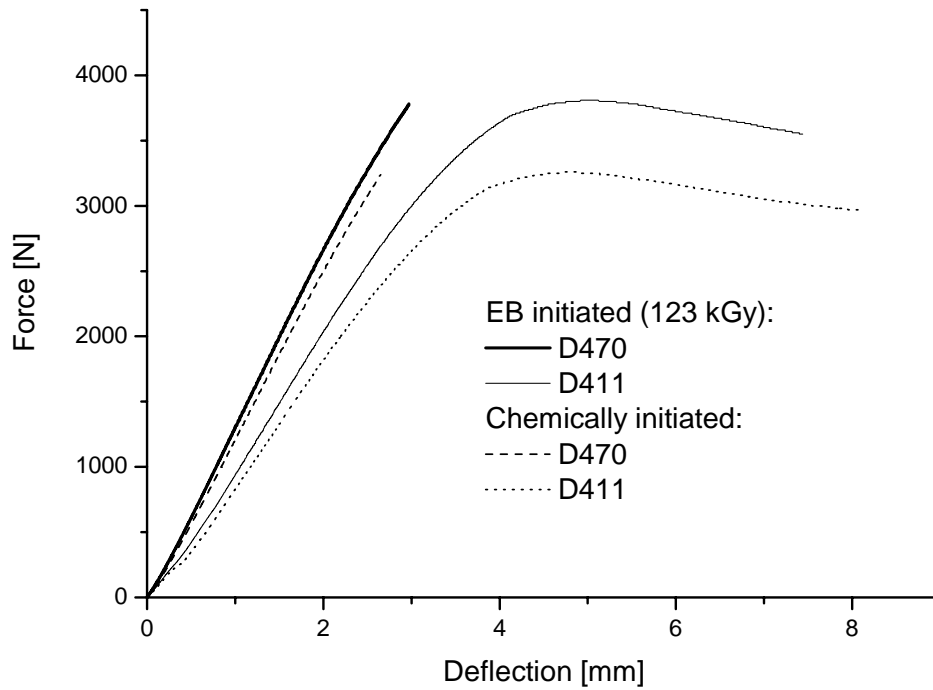


Figure 34 Bending behavior of D411 and D470 type resins (cp. Appendix B, Table T1 and Table T2)

4.2. Carbon fiber reinforced epoxy-acrylate composites

First the asymmetric (non-circular) carbon fiber reinforced (CFR) braided composite profiles (Figure 35 illustrates the cross section of its) were tested for 3-point bending (support distance: 250 mm). From the initial bending stiffness (up to 2 mm deformation) a bending modulus was calculated. The fiber content of the composites was typically 25 v%. The results are seen as a function of the dose in Figure 36.

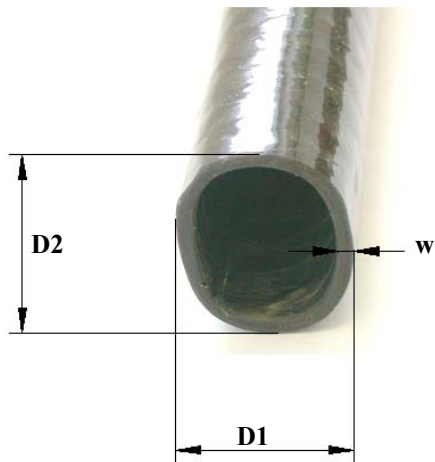


Figure 35 Cross-section of the composite profiles

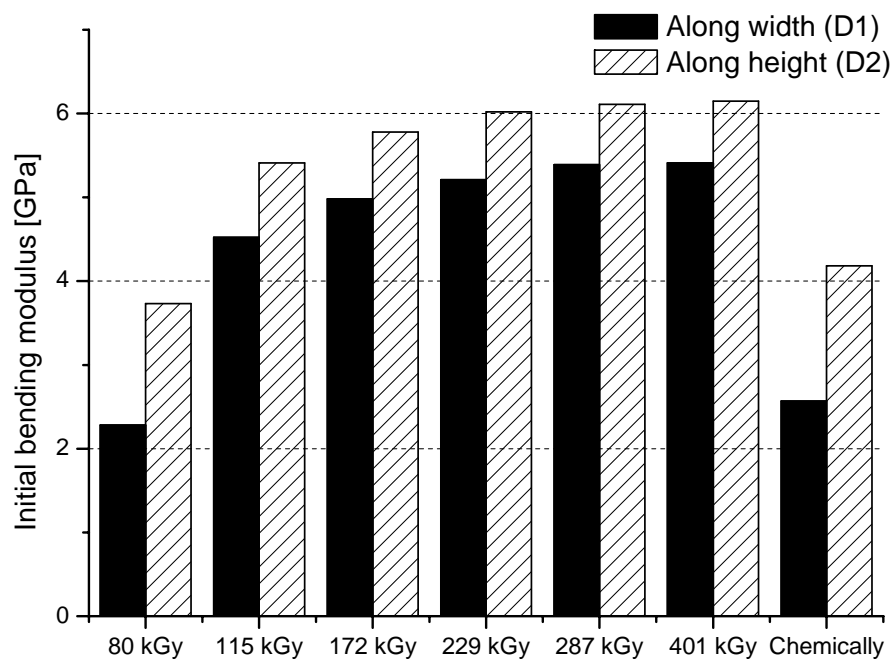


Figure 36 Initial bending modulus of the asymmetric composite profiles (cp. Appendix C, Table T4)

As it can be seen in Figure 36, about 120 kGy is enough to reach a significant bending stiffness level of the EB treated braided CFR epoxy profiles. The initial bending modulus of

this EB treated composite is at least 30% higher than the corresponding, conventionally (chemically) treated composite.

In the followings wall samples taken from the composite profile have been tested for interlaminar shear strength (3-point bending test with 10 mm support distance: short-beam test). As it is seen in Figure 37 no dose higher than 175 kGy was applied and the results were compared again with that of conventional chemical curing. EB curing is about 30-50% more efficient than chemical crosslinking in all these aspects (cp. Appendix C, Table T5).

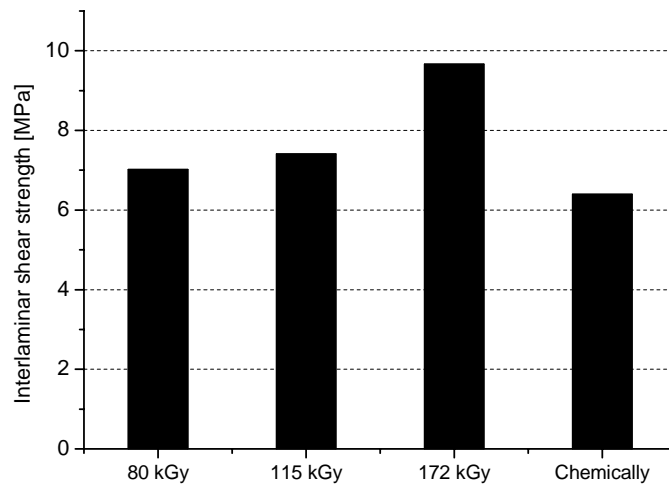


Figure 37 Interlaminar strength measured in the composite wall

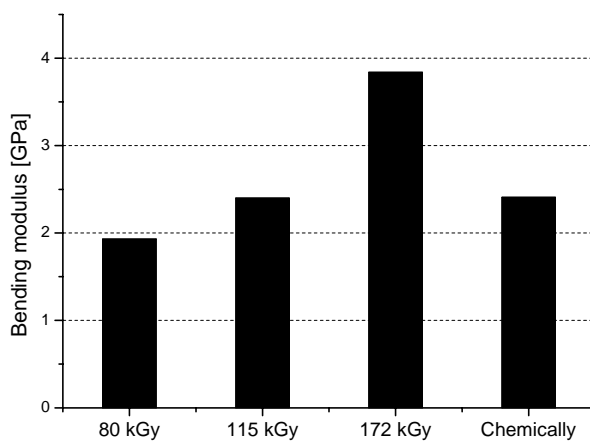


Figure 38 Bending modulus of the composite wall

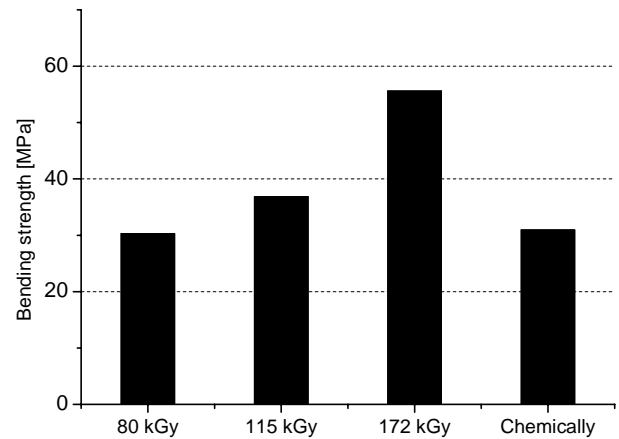


Figure 39 Bending strength of the composite wall

Similar benefit of EB is shown in Figure 38 and Figure 39, where bending modulus and strength were calculated.

4.3. Crash test of EB treated braided CFR composites

The composite profiles (D1xD2x100 mm) were tested at the Institute for Composite Materials of the University of Kaiserslautern, Germany, equipped with a “drop tower” for research purposes.

Figure 40 shows the results and trends of the crash tests on the EB treated, braided CFR epoxy composites. Curves b) show a typical behavior of the profile: high impact resistance along the whole displacement area. Practically 9 samples out of 10 behave similarly. Curve a) shows an unfavorable behavior: buckling. This behavior was exceptional (less than 10% of all tests). These results were comparable with Chapter 2.2.2 and Figure 13.

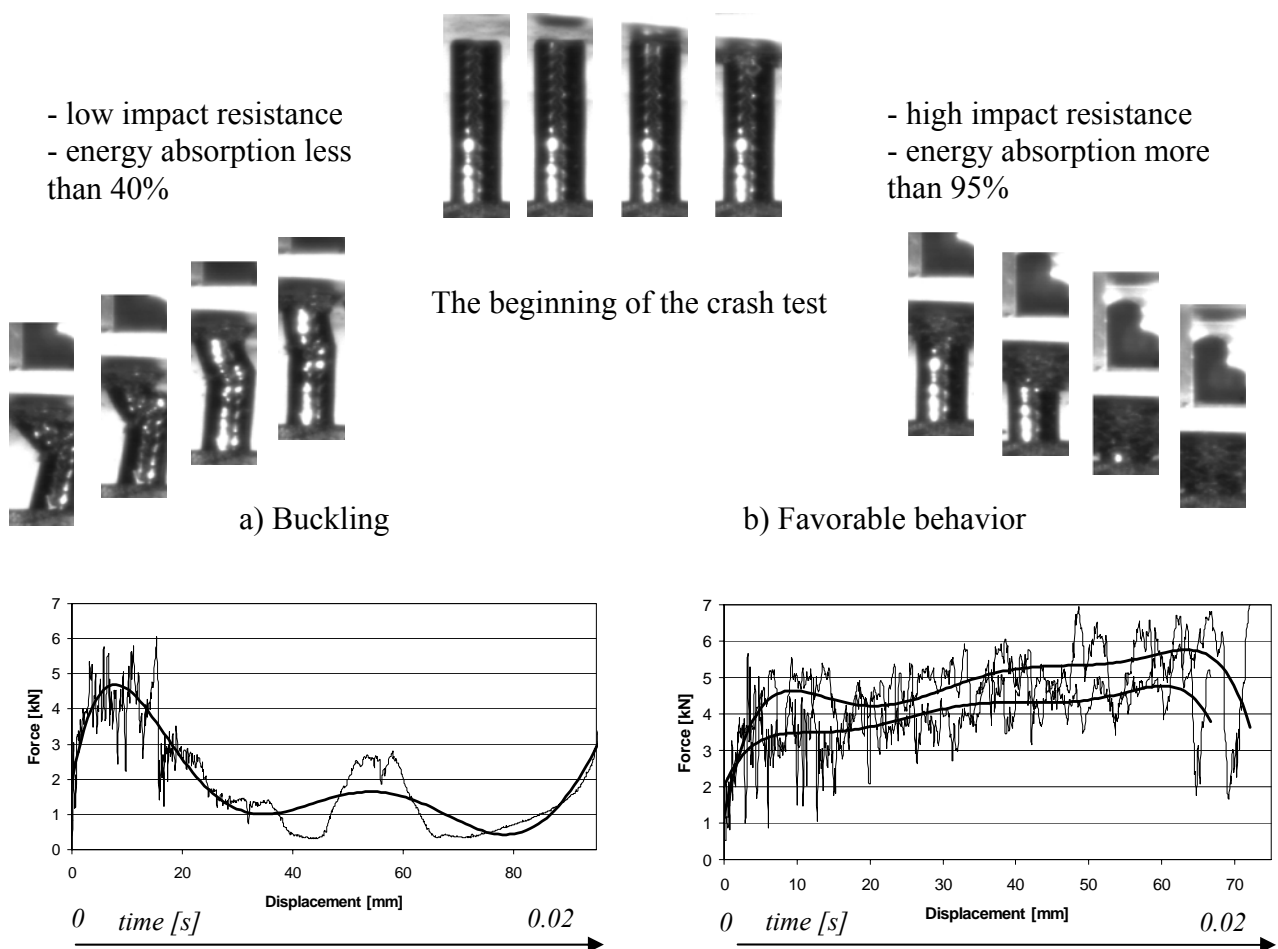


Figure 40 Crash experiments; comparing a) buckling and b) favorable behavior

5. Modeling of the tensile process of braided composite tubes

In this Chapter the whole tensile process of circular cross-sectional braided composite tubes subjected to tensile loading is modeled with a fiber bundle cell model and modeling method (see Chapter 2.4). As the first step the tensile state of fibers is examined. The obtained results are applied to tensile loading of circular cross-sectional braided composite tubes from the simplest to the more complicated cases, which contain a lot of random parameters, then arbitrary braided structures are also able to be modeled.

5.1. Examination of the tensile state of fibers in braided composite tubes

Suppose that the fibers are on the middle surface of the composite tube. There is tensile stress in the fibers of the loaded composite if the elongation is positive, i.e. the loaded length (l) is higher than unloaded one (l_0) (see the notations of Figure 41: $l \geq l_0$):

$$\sqrt{4R_k^2 \cdot \pi^2 + L^2} = l \geq l_0 = \sqrt{4R_{k0}^2 \cdot \pi^2 + L_0^2} . \quad (24)$$

where L_0 , R_{k0} and L , R_k are the unloaded and loaded length and middle radius of the composite, respectively. Let $L = L_0 \cdot (1 + u)$, where $u = \frac{\Delta L}{L_0}$ is the strain of the composite.

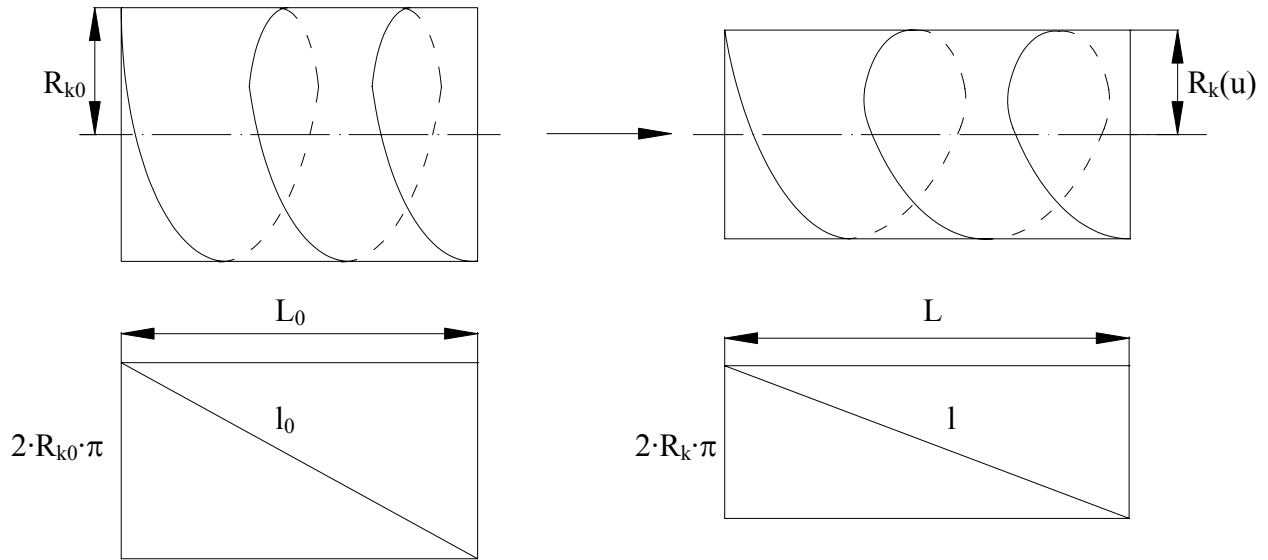


Figure 41 Deformation of a tow in the middle surface of the braided composite

The following quantities are introduced

$$k_0 = \frac{R_{k0}}{L_0}; \quad \rho_k(u) = \frac{R_k(u)}{R_{k0}}; \quad k(u) = \frac{R_k(u)}{L_0} = \frac{R_{k0}}{L_0} \cdot \frac{R_k(u)}{R_{k0}} = k_0 \cdot \rho_k(u). \quad (25, 26, 27)$$

Eqns (25, 26, 27) are substituted into Eqn. (1) and then it is squared and sorted:

$$\rho_k^2(u) \geq 1 - \frac{(1+u)^2 - 1}{4\pi^2 \cdot k_0^2}. \quad (28)$$

The condition of elongation above should be completed with the fact that the loaded middle radius ($R_k(u)$) is less than the original (R_{k0}):

$$1 \geq \rho_k(u) \geq \sqrt{1 - \frac{(1+u)^2 - 1}{4\pi^2 \cdot k_0^2}} = \rho_{kA}(u), \quad (29)$$

where $\rho_{kA}(u)$ is the low boundary function.

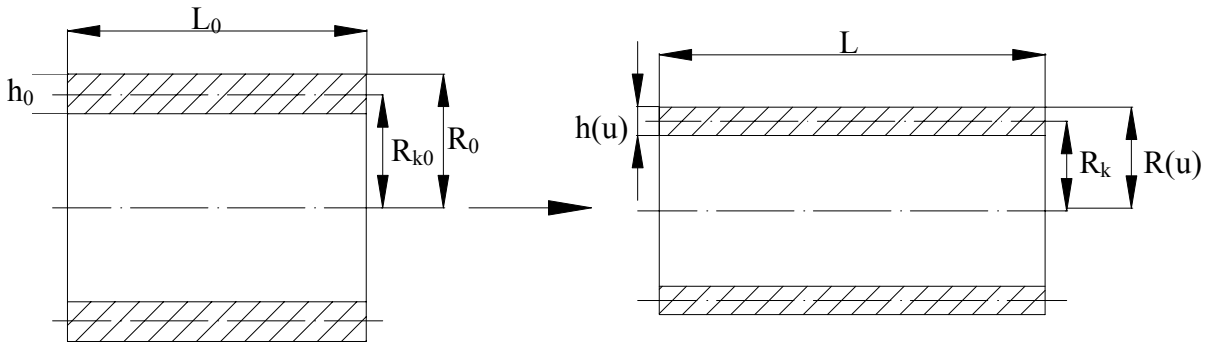


Figure 42 Changing volume of a braided composite tube

External radii ($R_0, R(u)$) and thickness ($h_0, h(u)$) are used to determine the radius ratio (Figure 42):

$$\rho_k(u) = \frac{R(u) - \frac{h(u)}{2}}{R_0 - \frac{h_0}{2}}, \text{ introducing: } \Phi_0 = \frac{h_0}{R_0}, \text{ hence} \quad (30, 31)$$

$$\rho_k(u) = \frac{\frac{R(u)}{R_0} - \frac{\Phi_0}{2} \cdot \frac{h(u)}{h_0}}{1 - \frac{\Phi_0}{2}}, \text{ using additionally: } \delta(u) = \frac{h(u)}{h_0}, \quad (32, 33)$$

on the other hand the external radii is described with Eqn. (29)

$$\rho(u) = \frac{R(u)}{R_0} \geq \left(1 - \frac{\Phi_0}{2}\right) \cdot \rho_{kA}(u) + \frac{\Phi_0}{2} \cdot \delta(u). \quad (34)$$

It is to be noted that the right side of Eqn. (34) is the convex linear combination of $\rho_{kA}(u)$ and $\delta(u)$ functions

If the volume change is considered

In the case of the pure tensile loading of the continuum, the volume cannot decrease (using the notations of Figure 42).

$$V \geq V_0 \quad (35)$$

$$\left(R^2(u) - (R(u) - h(u))^2\right) \cdot \pi \cdot L_0 \cdot (1 + u) \geq \left(R_0^2 - (R_0 - h_0)^2\right) \cdot \pi \cdot L_0 \quad (36)$$

$$\left(2R(u) \cdot h(u) - h^2(u)\right) \cdot (1 + u) \geq (2R_0 - h_0) \cdot h_0 \quad (37)$$

transformed and divided with R_0^2 :

$$\left(2 \frac{R(u)}{R_0} - \frac{h(u)}{R_0}\right) \cdot \frac{h(u)}{R_0} \geq \frac{\left(2 - \frac{h_0}{R_0}\right) \cdot \frac{h_0}{R_0}}{1 + u} \quad (38)$$

$$\left(\rho(u) - \frac{\Phi_0}{2} \cdot \delta(u)\right) \cdot \Phi_0 \cdot \delta(u) \geq \frac{2 - \Phi_0}{1 + u} \cdot \Phi_0 \quad (39)$$

$$\left(\rho(u) - \frac{\Phi_0}{2} \cdot \delta(u)\right) \cdot \delta(u) \geq \frac{1}{2} \cdot \frac{2 - \Phi_0}{1 + u} \quad (40)$$

Obviously

$$0 < \Phi_0 \leq 1; 0 < \rho(u) \leq 1; 0 < \delta(u) \leq 1. \quad (41, 42, 43)$$

In Eqn. (40) the equality means constant volume. $\rho(u)$ and $\delta(u)$ are monotonously decreasing functions ($0 \leq u < \infty$).

When solid rod is stretched $h_0=R_0$, $\Phi_0=1$, $\rho(u)=\delta(u)$, hence (40) takes the following form:

$$\left(\rho(u) - \frac{1}{2} \cdot \rho(u)\right) \cdot \rho(u) \geq \frac{1}{2} \cdot \frac{1}{1 + u} \quad (44)$$

$$\delta(u) = \rho(u) \geq \frac{1}{\sqrt{1 + u}} \quad (45)$$

Eqn. (45), the right side limit function is generalized e.g. with choice:

$$\delta(u) = \rho(u) \geq \frac{1}{(1 + u)^a} \geq \frac{1}{\sqrt{1 + u}}; 0 < a \leq \frac{1}{2}. \quad (46)$$

Similar process can be carried out for hollow rods (tubes) as well. Although $\delta(u) \neq \rho(u)$ in that case, hence only one of them can be chosen in the way described above. In case of the other quantity, conditions (34) and (40) should also be considered.

Let accordingly (for the simpler conditions)

$$\delta(u) = \frac{1}{(1 + u)^a}, \quad (47)$$

where $a > 0$.

If Eqn. (47) is substituted into Eqns (34) and (40), the following results is obtained

$$1 \geq \rho(u) \geq \frac{\Phi_0}{2} \cdot \frac{1}{(1+u)^a} + \left(1 - \frac{\Phi_0}{2}\right) \cdot \sqrt{1 - \frac{(1+u)^2 - 1}{4\pi^2 \cdot k_0^2}}, \quad (48)$$

and

$$1 \geq \rho(u) \geq \frac{\Phi_0}{2} \cdot \frac{1}{(1+u)^a} + \frac{2 - \Phi_0}{2} \cdot \frac{1}{(1+u)^{1-a}}. \quad (49)$$

If $a > 1$, the second block of Eqn. (49) tends to infinity if $u \rightarrow \infty$ which contradicts the $\rho(u) \leq 1$ condition, hence condition $0 < a \leq 1$ must be fulfilled.

The right part of Eqn. (49) can give an upper boundary function of the same form as (47) which is made stricter but also more simplified than Eqn. (49):

$$\rho(u) \geq \rho_2(u) = \frac{1}{(1+u)^{b_2}}, \quad b_2 = \min(a, 1-a), \quad (50)$$

since e.g. if $a < 1-a$

$$\frac{\Phi_0}{2} \cdot \frac{1}{(1+u)^a} + \frac{2 - \Phi_0}{2} \cdot \frac{1}{(1+u)^{1-a}} \leq \left(\frac{\Phi_0}{2} + \frac{2 - \Phi_0}{2}\right) \cdot \frac{1}{(1+u)^a} = \frac{1}{(1+u)^a}. \quad (51)$$

Figure 43 illustrates the expressions above. It is to be noted that Eqn. (51) can be constricted further, obviously.

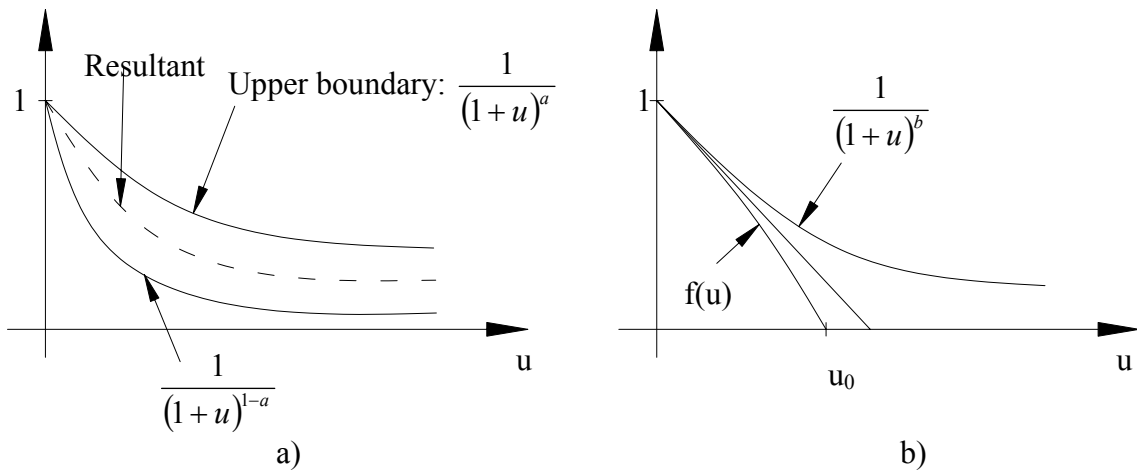


Figure 43 Explanation of the boundary functions

Similarly to (51), a boundary function or a simpler condition that can be used more easily is looked for. For this purpose, the second term in Eqn. (48) is examined.

If function (52) and its derivative (53) are studied

$$f(u) = \sqrt{1 - \frac{(1+u)^2 - 1}{4\pi^2 \cdot k_0^2}}; \quad f(0) = 1, \quad (52)$$

$$\frac{d}{du} f(u) = \frac{1}{2 \cdot \sqrt{1 - \frac{(1+u)^2 - 1}{4\pi^2 \cdot k_0^2}}} \cdot \left(-\frac{2 \cdot (1+u)}{4\pi^2 \cdot k_0^2} \right) < 0. \quad (53)$$

It can be seen from Eqn. (53) that function $f(u)$ is monotonously decreasing (Figure 43), moreover the derivative is concave downward. Let $f(u)=0$, i.e.

$$u_0 : 1 = \frac{(1+u_0)^2 - 1}{4\pi^2 \cdot k_0^2} \Rightarrow u_0 = \sqrt{1 + T_0^2} - 1, \text{ where } T_0^2 = 4\pi^2 \cdot k_0^2. \quad (54, 55)$$

Accordingly

$$f(u) \leq \frac{1}{(1+u)^b} = g(u), \text{ if} \quad (56)$$

$$\left. \frac{d}{du} f(u) \right|_{u=0} \leq \left. \frac{d}{du} g(u) \right|_{u=0}, \quad (57)$$

where

$$\frac{d}{du} g(u) = -\frac{b}{(1+u)^{1+b}}. \quad (58)$$

$$\left. \frac{d}{du} f(u) \right|_{u=0} = -\frac{1}{2} \cdot \frac{2}{4\pi^2 \cdot k_0^2} = -\frac{1}{T_0^2} \leq -b = \left. \frac{d}{du} g(u) \right|_{u=0}, \text{ i.e.} \quad (59)$$

$$\frac{1}{T_0^2} \geq b \Leftrightarrow \left. \frac{d}{du} f(u) \right|_{u=0} \leq \left. \frac{d}{du} g(u) \right|_{u=0}. \quad (60)$$

Consequently

$$\begin{aligned} & \frac{\Phi_0}{2} \cdot \frac{1}{(1+u)^a} + \left(1 - \frac{\Phi_0}{2}\right) \cdot \sqrt{1 - \frac{(1+u)^2 - 1}{4\pi^2 \cdot k_0^2}} \leq \frac{\Phi_0}{2} \cdot \frac{1}{(1+u)^a} + \frac{1 - \frac{\Phi_0}{2}}{(1+u)^{\frac{1}{T_0^2}}} \leq \\ & \leq \frac{\Phi_0}{2} \cdot \frac{1}{(1+u)^a} + \frac{1 - \frac{\Phi_0}{2}}{(1+u)^{b_1}} = \frac{1}{(1+u)^{b_1}}, \end{aligned} \quad (61)$$

where $b_1 = \min\left(a, \frac{1}{T_0^2}\right)$.

Thus

$$1 \geq \rho(u) \geq \rho_1(u) = \frac{1}{(1+u)^{b_1}}. \quad (63)$$

Finally a simple, applicable (while constrictable) condition is obtained for $\rho(u)$ as Eqns (50) and (63) are connected:

$$1 \geq \rho(u) \geq \max(\rho_1(u), \rho_2(u)) = \max\left(\frac{1}{(1+u)^{b_1}}, \frac{1}{(1+u)^{b_2}}\right) = \frac{1}{(1+u)^b}, \quad (64)$$

i.e.

$$1 \geq \rho(u) \geq \frac{1}{(1+u)^b}, \text{ where } b = \min\left(a, 1-a, \frac{1}{T_0^2}\right). \quad (65)$$

If $\rho(u) \geq \frac{1}{(1+u)^b}$, conditions (34) and (40) are fulfilled and that is equivalent to

$$\rho(u) = \frac{1}{(1+u)^c} \geq \frac{1}{(1+u)^b}, \quad (66)$$

$$\text{where } 0 < c \leq b = \min\left(a, 1-a, \frac{1}{T_0^2}\right). \quad (67)$$

The results above are being published in [143].

5.2. Modeling the tensile loading of braided circular cross-sectional composites

First of all, the neglections, assumptions and the parameters that influence the failure of the tensioned braided composite are reviewed. Then the constants and random parameters with the help of which modeling are carried out in the sub-chapters.

The followings neglections were applied during modeling:

- a) matrix loading
 - shearing (axial and in bias direction),
 - compression (on the cylindrical surface in axial and bias direction),
 - radial forces (taken into consideration implicitly with contraction);
- b) reinforcing fibrous structure loading
 - radial compression forces (taken into consideration implicitly with contraction),
 - changed tensile loading of axial braids in case of contraction,
 - in case of contraction, normal braids loosen (taken into consideration implicit with contraction),
 - sliding of fibrous structures,
 - loosening of fibrous structures (except for axial fiber introductions, see Chapter 5.4),

- fibers are perfectly flexible, hence do not transmit compression;
- c) composite structure
 - sliding when clamped,
 - deforming when clamped,
 - neck-forming (it can be taken into consideration implicitly with contraction),
 - fiber/matrix connection failure.

The following assumptions were applied during modeling:

- a) for the matrix:
 - linear elastic (Hookean),
 - the fracture is of brittle type, i.e. after reaching the ultimate strain of the matrix the transmitted force is zero;
- b) for the fibers (ET-bundle):
 - linear (Hookean) strain-force relationship (which is independent of the time) with random parameters like ultimate strain (ε_s) and ultimate tensile force (F_s), as well as they are gripped in parallel,
 - perfectly flexible, i.e. do not transmit compression,
 - fracture of an elementary fiber is of brittle type,
 - the ultimate strain is random variable with Q_{ε_s} normal distribution function, $\overline{\varepsilon_s}$ limited average ultimate strain and σ_{ε_s} standard deviation,
 - the elementary fibers are unidirectional in the rovings;
- b) for the composite:
 - it does not slid when clamped,
 - it does not deform when clamped into the grip,
 - neck does not form,
 - the adhesion between the fiber and the matrix is ideal, i.e. the deformations of the components are identical.

In case of braiding the following parameters are considered as independent, random variables of finite expected value and standard deviation: ultimate tensile force (F_s) -, tensile stiffness (K) -, ultimate tensile strength (σ_s) -, ultimate strain (ε_s) - and its standard deviation (σ_{ε_s}) of elementary fibers; angle of braiding cone (β_0), braiding angle (α_0). Additionally, the carriers of the braider in one direction ($n_j=n$), the number of elementary fibers in a defined

roving ($N_i=N$), the fiber volume content (φ) and the tensile modulus of the matrix (E_M) are considered to be constant.

The ET fiber bundle cell (oblique cell) defined in the fiber bundle cell method is used (see Chapter 2.4) following the structural levels of Figure 24 a) from Chapter 2.4.2.3. The applied unit cell is shown in Figure 44: the braided structure is laid out first then a repetitive unit (unit cell) is chosen to be used in the calculations. The advantage of modeling is that the equations are developed at micro level (level of elementary fibers) and they are extended to macro level, to bundles and finally to the braided structure and composite.

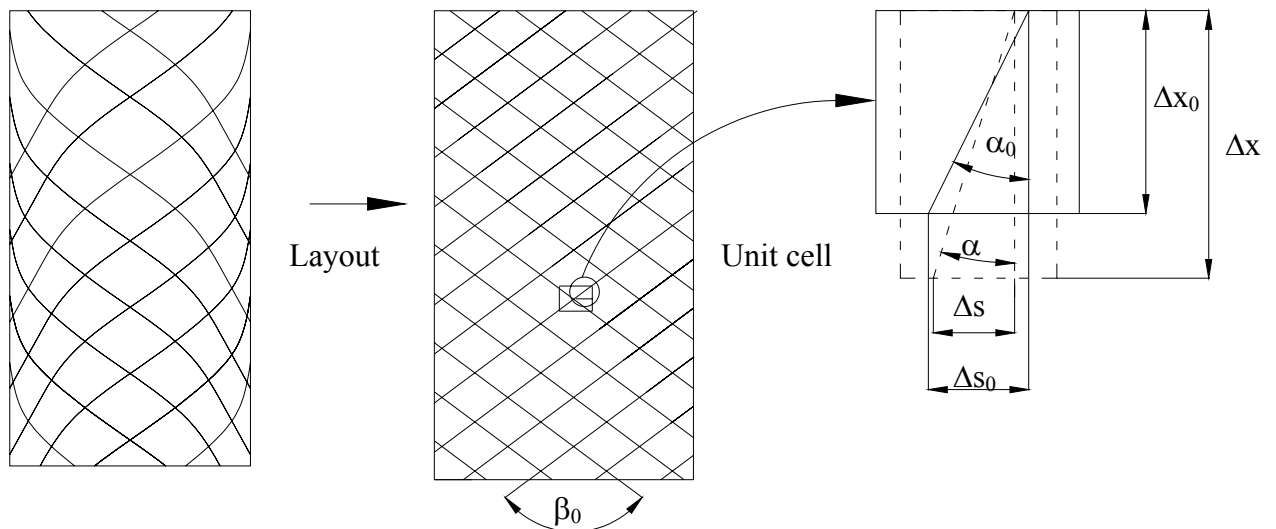


Figure 44 The unit cell of a braid

The cases to be processed are summarized in Table 4 where ϵ_0 is the initial strain of fiber.

No.	ϵ_0	α_{0i}	
Chapter 5.2.1 /a	0	$\alpha_{01}=\alpha_{02}=\alpha_0$	
Chapter 5.2.1 /b	0	$\alpha_{01}=\alpha_{02}=N(\overline{\alpha_0}, \sigma_{\alpha_0})$	
Chapter 5.2.2 /a	$\neq 0$ const.	$\alpha_{01}=\alpha_{02}=\alpha_0$	
Chapter 5.2.2 /b	$\neq 0$ const.	$\alpha_{01}=\alpha_{02}=N(\overline{\alpha_0}, \sigma_{\alpha_0})$	
Chapter 5.3 /a	0	$\alpha_{01}=\alpha_{02}=\alpha_0$	Axial fiber introduction
Chapter 5.3 /b	$\neq 0$ const.	$\alpha_{01}=\alpha_{02}=\alpha_0$	Axial fiber introduction
Chapter 5.4 ET&EH-bundle	$\neq 0$ prob. var.	$\alpha_{01}=\alpha_{02}=\alpha_0$	Axial fiber introduction

Table 4 Problems to be solved

5.2.1. Application of non-pretensioned fiber bundles

In this model the pretensioning ($\varepsilon_0=0$) of the fibers is not considered, i.e. the fibers are not pretensioned.

a) Constant braiding angle

In this case the initial braiding angle is constant ($\alpha_0=\text{const.}$).

The strain in the ET-bundle (see Chapter 2.5) is the following if Eqn.(1) is simplified

$$\varepsilon = (1 + \varepsilon_0) \cdot \sqrt{\frac{(1+u)^2 + e^2}{1+e_0^2}} - 1 = \sqrt{\frac{(1+u)^2 + e^2}{1+e_0^2}} - 1, \quad (68)$$

where (Figure 44) $e_0 = \frac{\Delta s_0}{\Delta x_0} = \tan(\alpha_0)$ – initial obliquity. (69)

Based on Chapter 5.1 suppose that

$$e = e_0 \cdot \frac{1}{(1+u)^b}, \quad (70)$$

where b is the contraction parameter.

The resultant force in the fiber bundle is

$$F_B = \sum_{j=1}^n (F_{ET1,j} + F_{ET2,j}), \quad (71)$$

where n is the number of fiber bundles in direction 1 and 2, F_{ET1} , F_{ET2} the forces in arising the direction of loading and are calculated (without indices) this way [7, 95]:

$$F_{ET} = \sum_{i=1}^N K_i \cdot \varepsilon_i \cdot \cos(\alpha_0) \cdot \chi(\varepsilon_i, \varepsilon_{S,i}), \quad (72)$$

where N is the number of elementary fibers in the given roving, K_i is the tensile stiffness of the i -th elementary fiber, $\varepsilon_{S,i}$ is the strain at the maximal force and $\chi(\varepsilon_i, \varepsilon_{S,i})$ is the window function:

$$\chi(\varepsilon_i, \varepsilon_{S,i}) = \begin{cases} 1, & \text{if } 0 \leq \varepsilon_i < \varepsilon_{S,i} \\ 0, & \text{otherwise} \end{cases} \quad (73)$$

$$0 \leq \varepsilon_i < \infty, \quad (74)$$

the expected value of which is [7]:

$$E[\chi(\varepsilon_i, \varepsilon_{S,i})] = P(\varepsilon_i \leq \varepsilon_{S,i}) = 1 - P(\varepsilon_{S,i} < \varepsilon_i) = 1 - Q_{\varepsilon_{S,i}}(\varepsilon_i), \quad (75)$$

where $Q_{\varepsilon_{S,i}}(\varepsilon_i)$ is the normal distribution function of the ε_i function and $\varepsilon_{S,i}$ is its expected value. α_0 , $\varepsilon_{S,i}$ and ε_i parameters are independent.

The expected value of F_B (71) is:

$$E[F_B] = n \cdot (E[F_{ET1}] + E[F_{ET2}]). \quad (76)$$

The expected value of F_{ET} (72) (without indices) is:

$$\begin{aligned} E[F_{ET}] &= \overline{F_{ET}} = N \cdot E[K \cdot \varepsilon \cdot \cos(\alpha_0) \cdot \chi(\varepsilon, \varepsilon_S)] = \\ &= N \cdot \overline{K} \cdot E[\varepsilon] \cdot E[\cos(\alpha_0)] \cdot E[\chi(\varepsilon, \varepsilon_S)] = \\ &= N \cdot \overline{K} \cdot \varepsilon \cdot E[\cos(\alpha_0)] \cdot (1 - Q_{\varepsilon_S}(\varepsilon)), \end{aligned} \quad (77)$$

where $1 - Q_{\varepsilon_S}(\varepsilon)$ is the expected value of $\chi(\varepsilon, \varepsilon_S)$ window function based on (75). In this case since $\alpha_0 = \text{const.}$, hence $E[\cos(\alpha_0)] = \cos(\alpha_0)$.

If $\alpha_{01} = \alpha_{02}$ symmetry exists (and in case of braiding is realized), then $\cos(\alpha_{01}) = \cos(\alpha_{02})$ hence instead of Eqn. (76) the following formula can be used:

$$E[F_B] = \overline{F_B} = 2n \cdot E[F_{ET}]. \quad (78)$$

The tensile force of the composite is

$$F_C = \overline{F_B} + F_M, \quad (79)$$

where F_M is the tensile force of the matrix.

The simplified rule of mixture was applied to determine the tensile stress of the composite [141]:

$$\sigma_C = \varphi \cdot \sigma_B + (1 - \varphi) \cdot \sigma_M. \quad (80)$$

Eqn. (80) was normalized with σ_S , which is the average tensile strength of elementary fibers:

$$\frac{\sigma_C}{\sigma_S} = \varphi \cdot \frac{\overline{F_B}}{2n \cdot N \cdot \overline{F_S}} + (1 - \varphi) \cdot \frac{\sigma_M}{\sigma_S}, \quad (81)$$

where $\overline{F_S}$ is the average ultimate tensile force of elementary fibers. Eqn. (81) practically combines the normalized force and stress, since in case of fibers the tensile force of one elementary fiber and in case of the matrix the stress is more advantageous to apply, furthermore this form is better than Eqn. (79) to investigate the effects of parameters.

z is introduced instead of u in order to be able to simpler and more compact representation z defined as shown below (as in Eqn. (13))

$$z = \frac{u}{\varepsilon_S} \Rightarrow u = z \cdot \overline{\varepsilon_S}, \quad (82, 83)$$

where $\overline{\varepsilon_S}$ is the average ultimate strain of elementary fibers. The maximum value of z is obviously

$$z_{\max} = \frac{\max(\varepsilon_{S_{\max}}, \varepsilon_{M_{\max}})}{\varepsilon_S}, \quad (84)$$

where $\varepsilon_{S_{\max}}$ and $\varepsilon_{M_{\max}}$ are the maximal ultimate strain of elementary fibers and matrix, respectively, therefore the curves are graphed until the z_{\max} of the composite.

It is to be noted that z values can be increased, of course, but the curve segment above this value has no physical meaning (since there is no composite the ultimate strain of which is more than $\max(\varepsilon_{S_{\max}}, \varepsilon_{M_{\max}})$), furthermore z_{\max} only depends on the basic data.

The expected tensile strength is calculated as the local maximum of Eqn. (81) if the $[0, z_{\max}]$ closed interval is multiplied with σ_S .

In Table 5 the applied parameters are summarized based on Chapter 3 (standard deviations are only listed where they were applied in the model). In order to be able to trace the consequence of the change of a variable and its impact on the normalized tensile stress of the composite, only one parameter is modified at a time, all the others are substituted with values shown in Table 5.

α_0	σ_{α_0}	$\overline{\varepsilon_S}$	σ_{ε_S}	$\overline{\sigma_S}$	n	N	$\overline{F_S}$	\overline{K}	$\overline{E_M}$	$\overline{\varepsilon_M}$	b	φ
[°]	[°]	[%]	[%]	[MPa]	[piece]	[piece]	[N]	[N]	[GPa]	[%]	[-]	[v%]
30	5	1.44	0.35	2857.6	16	24,000	0.128	8.66	3.2	4.5	0.32	30

Table 5 Values of the parameters applied in the model

15, 30 and 45° cases are indicated (where it is possible) in the figures since the easiest modifiable machine parameter is the braiding angle and the common effect given with the parameter on the tensile strength is also analyzed. Hereafter it is supposed for the numerical analyses that the ultimate strain ε_S is of $N(\overline{\varepsilon_S}, \sigma_{\varepsilon_S}^2)$ normal distribution where $\sigma_{\varepsilon_S} < \frac{\overline{\varepsilon_S}}{3}$.

Figure 45 shows the effect of fiber content on the normalized tensile stress. $\varphi=0$ v% and $\varphi=100$ v% describes the tensile stress of the matrix and the fiber bundle (theoretically, since it is not easy to make a composite without matrix which has 30° braiding angle), respectively.

It is obvious that the change in fiber content has a significant impact on the normalized tensile stress and initial tensile stiffness of the composite (e.g. [142]). It can be seen as well that the simultaneous changing of the braiding angle and the fiber content results in a large deviation in the tensile strength (Figure 46).

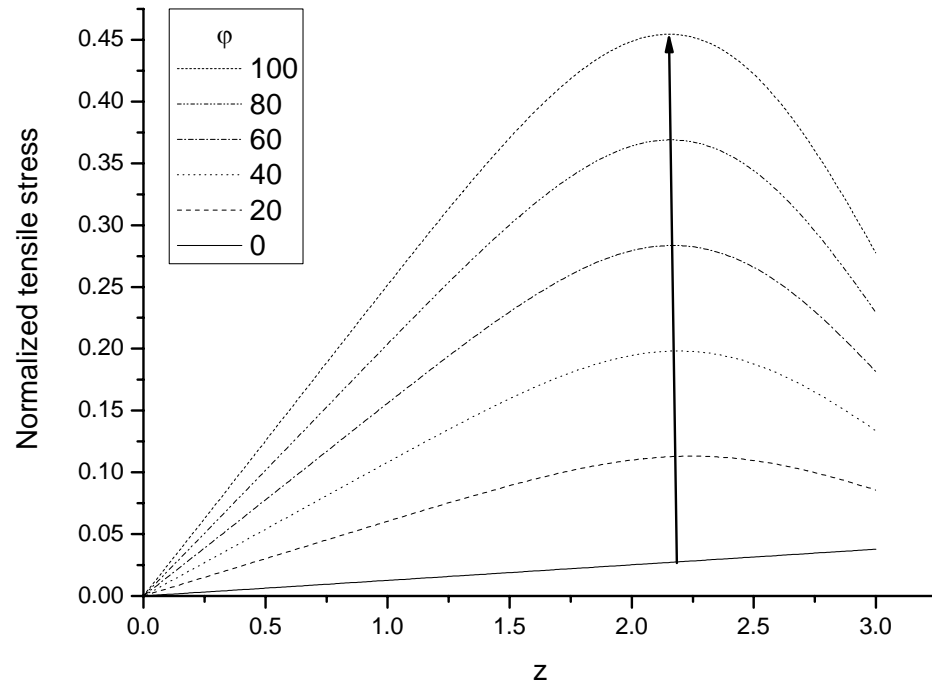


Figure 45 Effect of fiber content (φ) on the normalized tensile stress

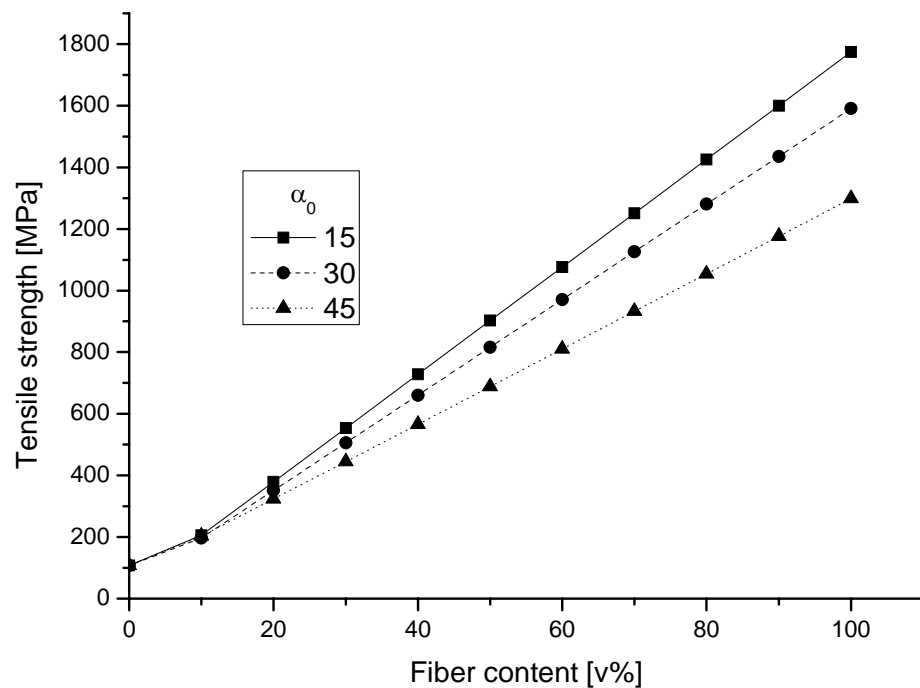


Figure 46 Effect of fiber content (φ) on tensile strength (at $\alpha_0=15^\circ, 30^\circ, 45^\circ$)

The effect of braiding angle on the normalized tensile stress can be seen in Figure 47. If the braiding angle, $\alpha_0=0^\circ$ tensioned parallel to the direction of fibers takes place that corresponds to the tensile force of a unidirectional composite with $\varphi=30$ v% fiber content. It can be seen that the braiding angle has a significant impact on the normalized tensile stress

and initial tensile stiffness (Figure 47). Figure 48 reveals that even a small extent change in the braiding angle influences tensile strength remarkably.

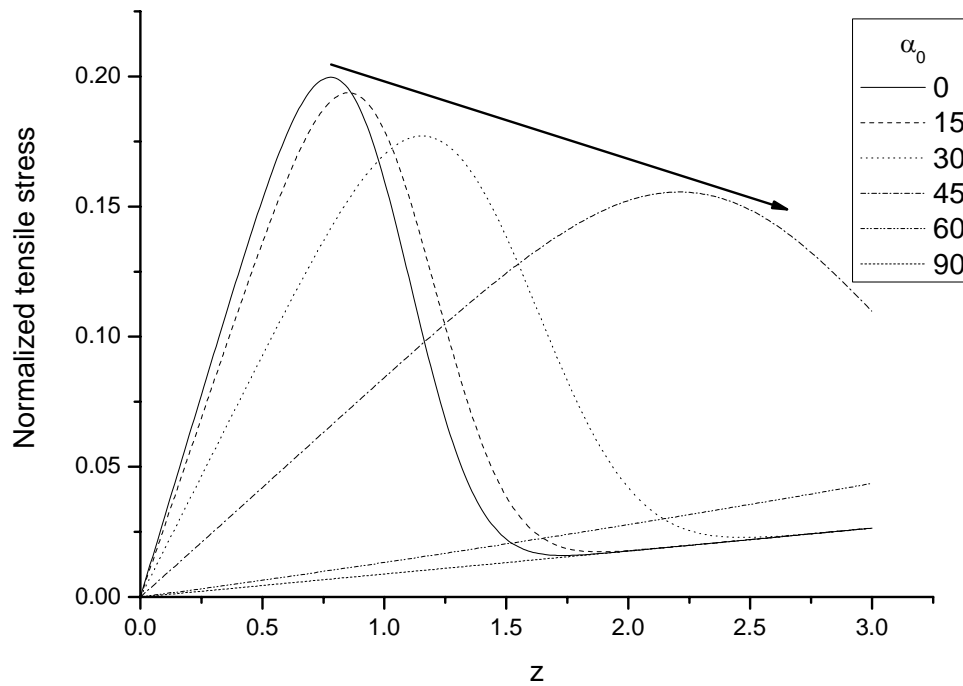


Figure 47 The effect of braiding angle (α_0) on the normalized tensile stress

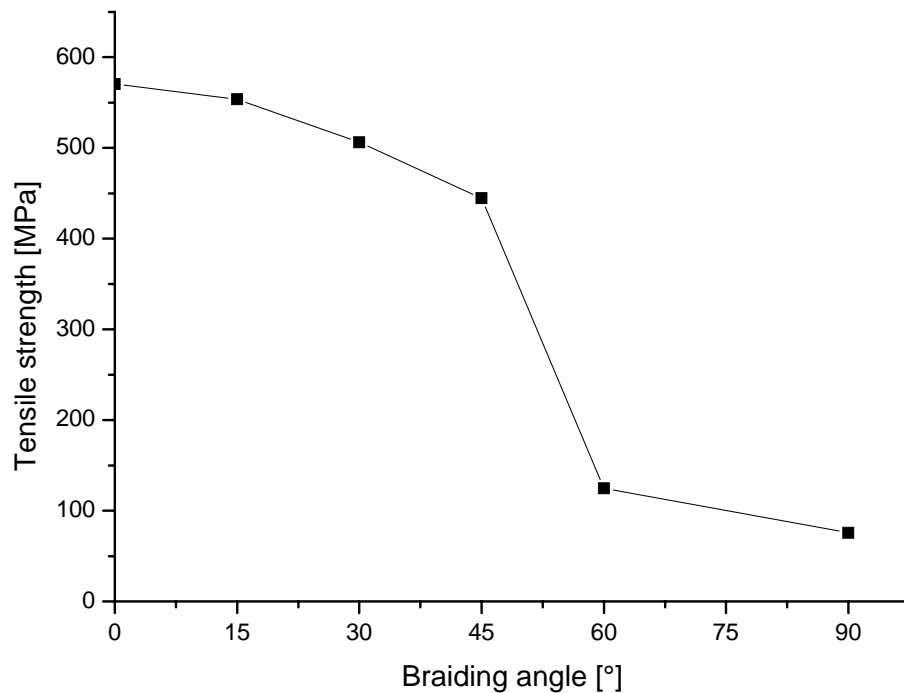


Figure 48 The effect of braiding angle (α_0) on tensile strength

It can also be observed that the braiding angle in case of tensile loading is not advisable to set higher than 45° (without axial fiber introduction, see Chapter 5.2.3), because the tensile strength decreases rapidly then.

The contraction parameter influences the normalized tensile stress, the location of maximums (cp. (68)-(70)) and hence the initial tensile stiffness as well as revealed in Figure 49.

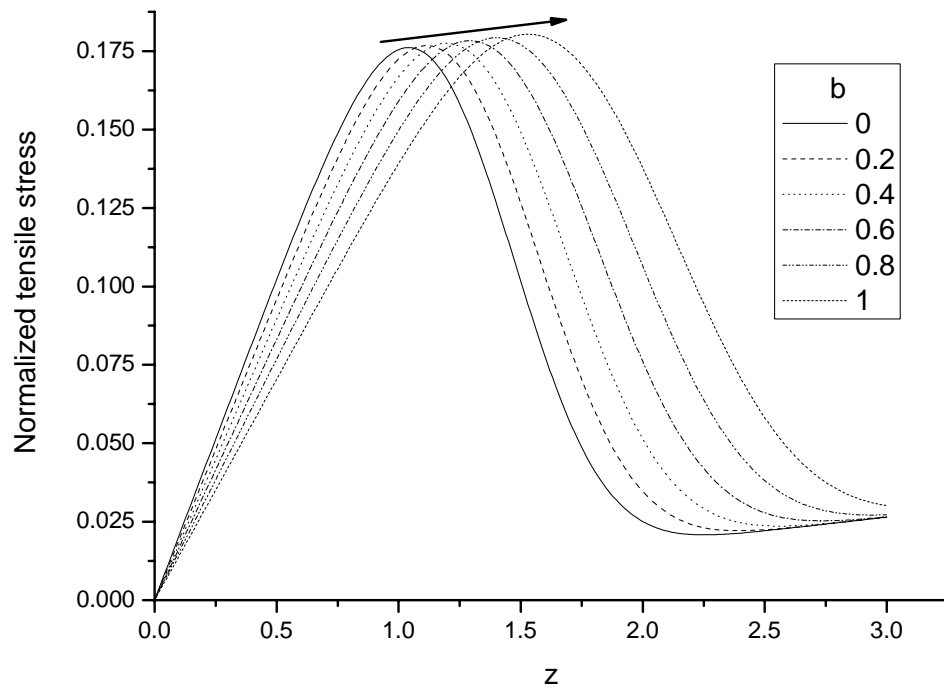


Figure 49 The effect of contraction parameter (b) on the normalized tensile stress ($\alpha_0=30^\circ$)

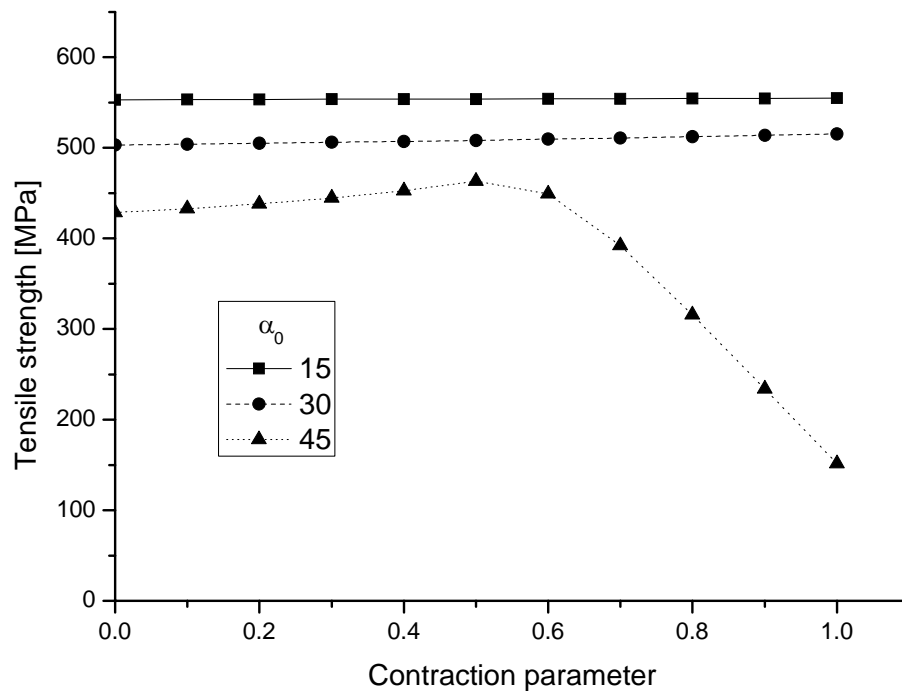


Figure 50 The effect of contraction parameter (b) on tensile strength (at $\alpha_0=15^\circ, 30^\circ, 45^\circ$)

The value of 0.5 corresponds to the contraction factor of ideal rubber in case of small deformations. Here a smaller value should be used. Value 0.32 is chosen on the basis of my measurements.

Figure 50 reveals a small extent change in tensile strength as a function of the contraction parameter for different braiding angles.

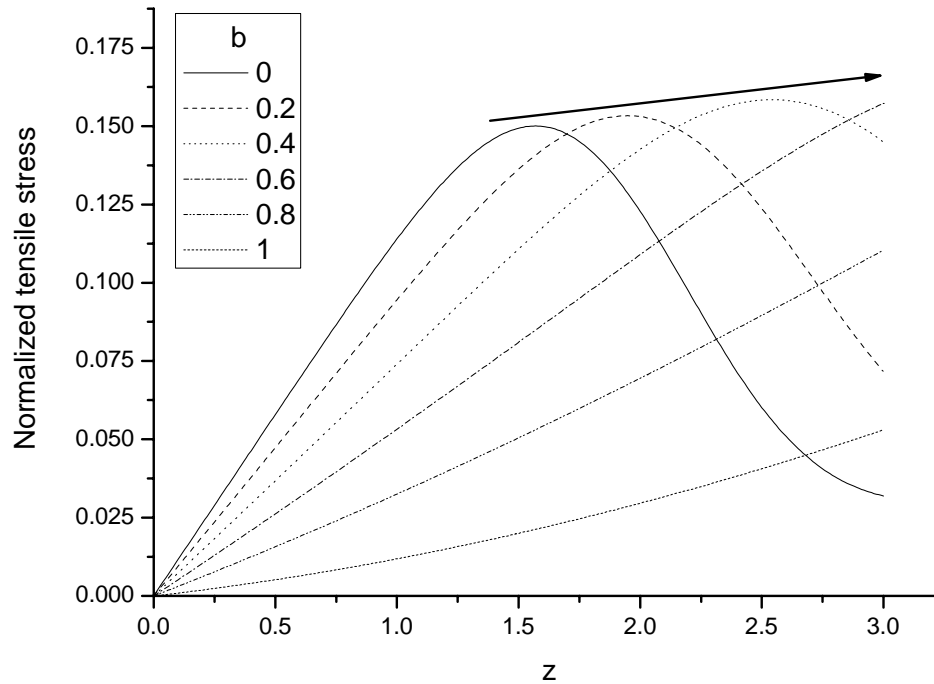


Figure 51 The effect of contraction parameter (b) on the normalized tensile stress ($\alpha_0=45^\circ$)

It is to be noted that when braiding angle $\alpha_0=45^\circ$ and contraction parameter $b>0.5$ the value of the function at z_{max} , a local maximum (the reason for the decrease) is visible (Figure 50). This is illustrated in Figure 51. It can be observed that the simultaneous change of the two parameters here causes a significant deviation in the initial tensile stiffness.

b) Braiding angle with standard deviation

In this case the initial braiding angle is handled as an average value but with a small (max. 5°) standard deviation.

If α_0 is supposed to be of $N(\bar{\alpha}_0, \sigma_{\alpha_0}^2)$ normal distribution then $(\alpha_0 - \bar{\alpha}_0)$ is of $N(0, \sigma_{\alpha_0}^2)$ distribution, hence its density function is the following:

$$f_{\alpha_0 - \bar{\alpha}_0}(x) = \frac{1}{\sqrt{2\pi} \cdot \sigma_{\alpha_0}} \cdot e^{-\frac{x^2}{2 \cdot \sigma_{\alpha_0}^2}} \quad (85)$$

The following simplification is carried out:

$$\begin{aligned} \cos(\alpha_0) &= \cos(\overline{\alpha_0} + \alpha_0 - \overline{\alpha_0}) = \cos(\overline{\alpha_0}) \cdot \cos(\alpha_0 - \overline{\alpha_0}) - \sin(\overline{\alpha_0}) \cdot \sin(\alpha_0 - \overline{\alpha_0}) \approx \\ &\approx \cos(\overline{\alpha_0}) \cdot \cos(\alpha_0 - \overline{\alpha_0}), \end{aligned} \quad (86)$$

using that the standard deviation (σ_{α_0}) of α_0 is small

$$|\alpha_0 - \overline{\alpha_0}| \text{ small} \Rightarrow \sin(\alpha_0 - \overline{\alpha_0}) \approx \alpha_0 - \overline{\alpha_0} \Rightarrow E[\alpha_0 - \overline{\alpha_0}] = 0, \quad (87)$$

hence

$$E[\cos(\alpha_0)] \approx \cos(\overline{\alpha_0}) \cdot E[\cos(\alpha_0 - \overline{\alpha_0})]. \quad (88)$$

The second term is extracted:

$$E[\cos(\alpha_0 - \overline{\alpha_0})] = \int_{-\frac{\pi}{2}}^{\frac{\pi}{2}} \cos(x) \cdot \frac{1}{\sqrt{2\pi} \cdot \sigma_{\alpha_0}} \cdot e^{-\frac{x^2}{2\sigma_{\alpha_0}^2}} dx \approx \int_{-\infty}^{\infty} \cos(x) \cdot \frac{1}{\sqrt{2\pi} \cdot \sigma_{\alpha_0}} \cdot e^{-\frac{x^2}{2\sigma_{\alpha_0}^2}} dx = e^{-\frac{\sigma_{\alpha_0}^2}{2}}, \quad (89)$$

using [98] and accordingly

$$\int_0^{\infty} \cos(x) \cdot \frac{1}{\sqrt{2\pi} \cdot \sigma_{\alpha_0}} \cdot e^{-\frac{x^2}{2\sigma_{\alpha_0}^2}} dx = \frac{\sqrt{\pi}}{2 \cdot \frac{1}{\sqrt{2} \cdot \sigma_{\alpha_0}}} \cdot e^{-\frac{1}{4 \cdot \frac{1}{2\sigma_{\alpha_0}^2}}} = \frac{\sqrt{\pi} \cdot \sigma_{\alpha_0}}{\sqrt{2}} \cdot e^{-\frac{\sigma_{\alpha_0}^2}{2}}, \quad (90)$$

thus

$$E[\cos(\alpha_0)] \approx \cos(\overline{\alpha_0}) \cdot e^{-\frac{\sigma_{\alpha_0}^2}{2}}. \quad (91)$$

If this result (91) is substituted in Eqn. (77), the following equation is obtained:

$$\begin{aligned} E[F_{ET}] &= \overline{F_{ET}} = N \cdot \overline{K} \cdot \varepsilon \cdot E[\cos(\alpha_0)] \cdot (1 - Q_{\varepsilon_S}(\varepsilon)) = \\ &= N \cdot \overline{K} \cdot \varepsilon \cdot \cos(\overline{\alpha_0}) \cdot e^{-\frac{\sigma_{\alpha_0}^2}{2}} \cdot (1 - Q_{\varepsilon_S}(\varepsilon)). \end{aligned} \quad (92)$$

The impact of the standard deviation of each parameter on the normalized tensile stress is studied.

The effect of the standard deviation of the ultimate strain of fibers (σ_{ε_S}) is revealed in Figure 52. The significant role of even fiber quality is well visible. On the basis of Figure 53 it can be stated that the simultaneous change of σ_{ε_S} and the braiding angle results in a cumulated impact since a remarkable decrease occurs in strength.

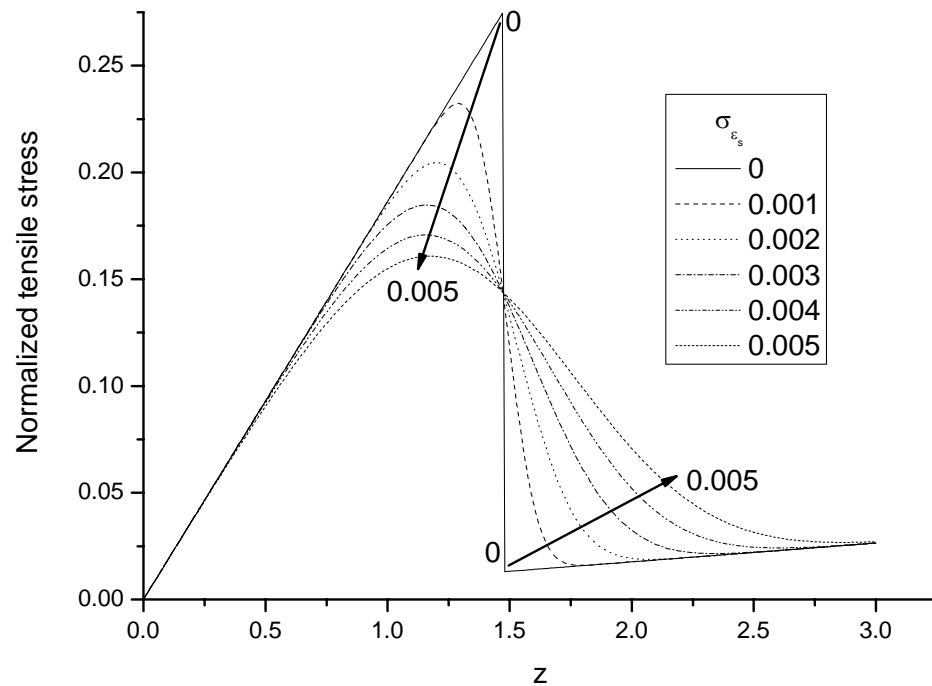


Figure 52 The effect of the standard deviation of the ultimate strain of fibers (σ_{ε_s}) on the normalized tensile stress

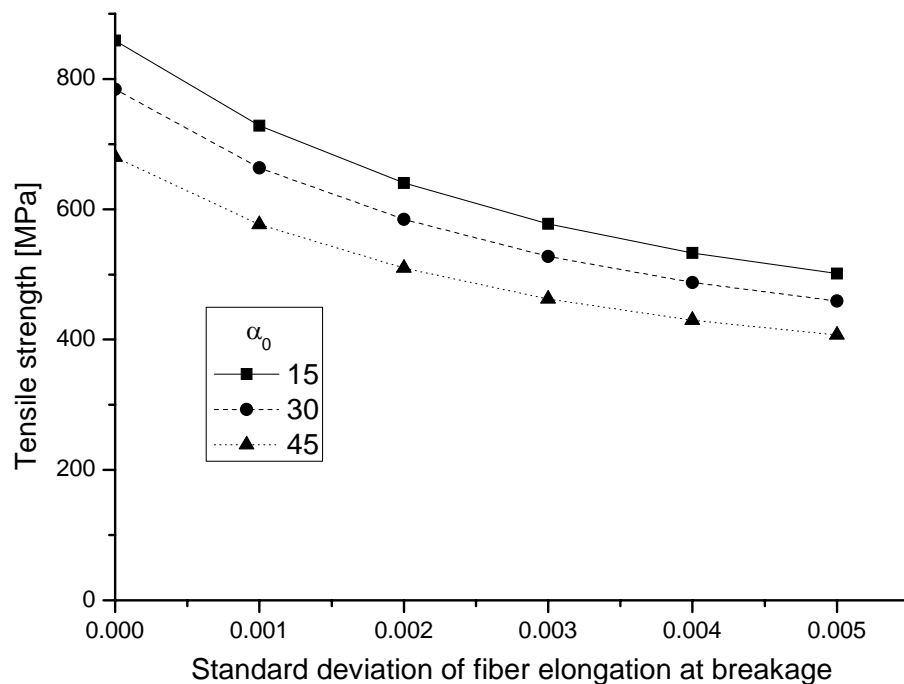


Figure 53 The effect of the standard deviation of the ultimate strain of fibers (σ_{ε_s}) on the tensile strength (at $\alpha_0=15^\circ, 30^\circ, 45^\circ$)

The impact of the standard deviation of the braiding angle on the normalized tensile stress – based on (91) – is shown in Figure 54. It is also of industrial importance that the small extent deviation around the average value of the braiding angle does not influence the

normalized tensile stress significantly (it can also be seen from Eqns. (90)-(91)) and this is also illustrated in Figure 55.

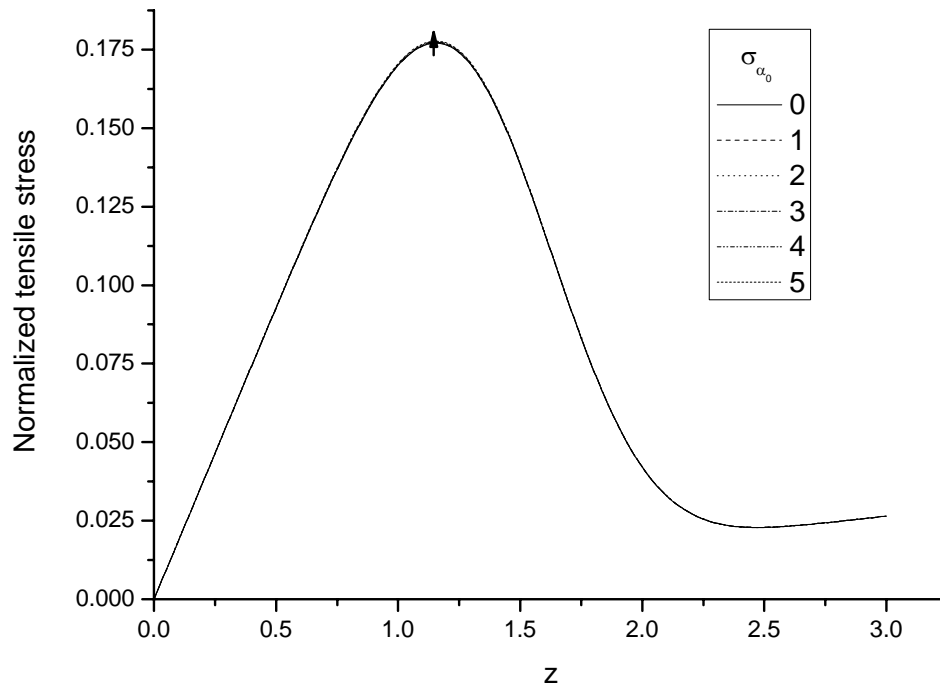


Figure 54 The effect of the standard deviation of braiding angle (σ_{α_0}) on the normalized tensile stress standard deviation is shown in degrees

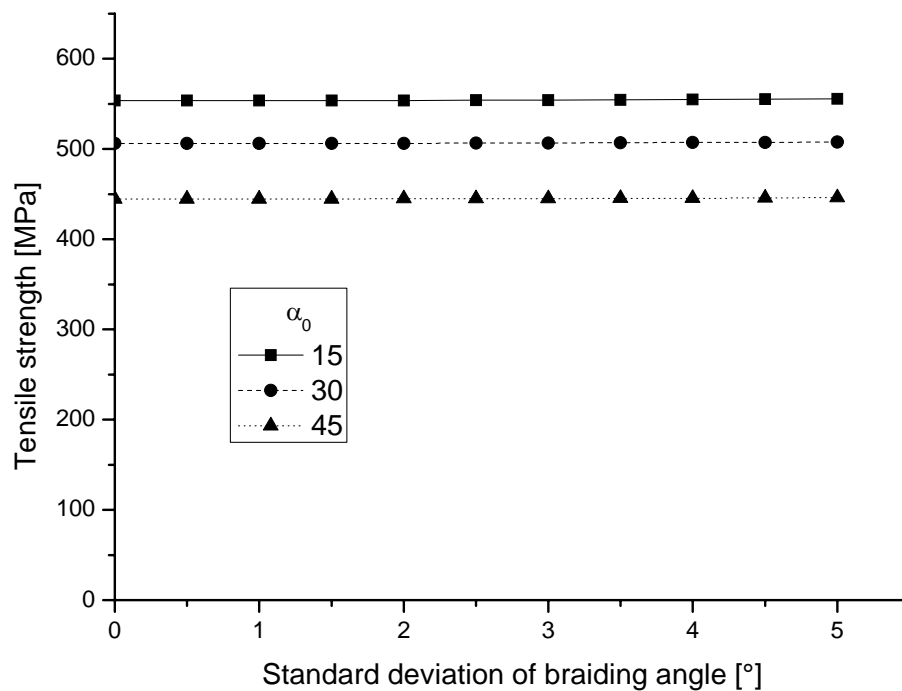


Figure 55 The effect of the standard deviation of braiding angle (σ_{α_0}) on the tensile strength (at $\alpha_0=15^\circ, 30^\circ, 45^\circ$)

5.2.2. Application of pretensioned fiber bundles

In this model, the fibers have initial strain ($\varepsilon_0 > 0$). The previous Chapter showed that the standard deviation of the braiding angle has no significant impact on the normalized tensile stress of the braided composite, hence the a) and b) cases of Table 4 are handled together in this Chapter supposing that the braiding angle is constant ($\alpha_0 = \text{const.}$).

a-b) Constant pretensioned

It is supposed that the fibers have constant initial length and that the braiding angle is constant. Then Eqn. (68) can be written in the following form:

$$\varepsilon = (1 + \varepsilon_0) \cdot \sqrt{\frac{(1+u)^2 + e^2}{1+e_0^2}} - 1. \quad (93)$$

The a) model in Chapter 5.2.1 can be used in the calculations and Eqn. (68) instead of Eqn. (93) is applied.

It was expected and is proven by Figure 56 and Figure 57 that pretension does not have a significant impact on the normalized tensile stress of the composite although it influences the location of the maximum, since pretension moves the curve into the negative direction and can reach the maximal value before and it can be concluded that this occurs at smaller strains.

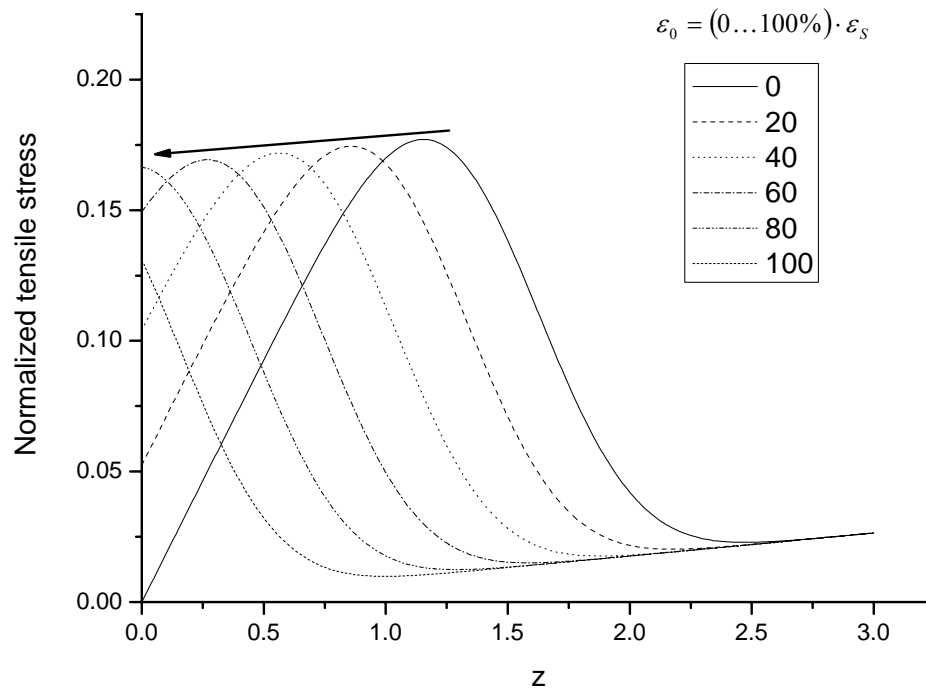


Figure 56 The effect of pretension (ε_0) on the normalized tensile stress in the percentage of ultimate strain of fibers

It is to be noted that the initial dropping end of the curves show the value of the function at 0. Obviously, this value decreases due to large pretension. It can also be concluded that pretension higher than 80% of ε_s results in a decrease in strength (a significant force is necessary already 10-30% pretensions and this is difficult to achieve without the cracking of the elementary fibers in the rovings).

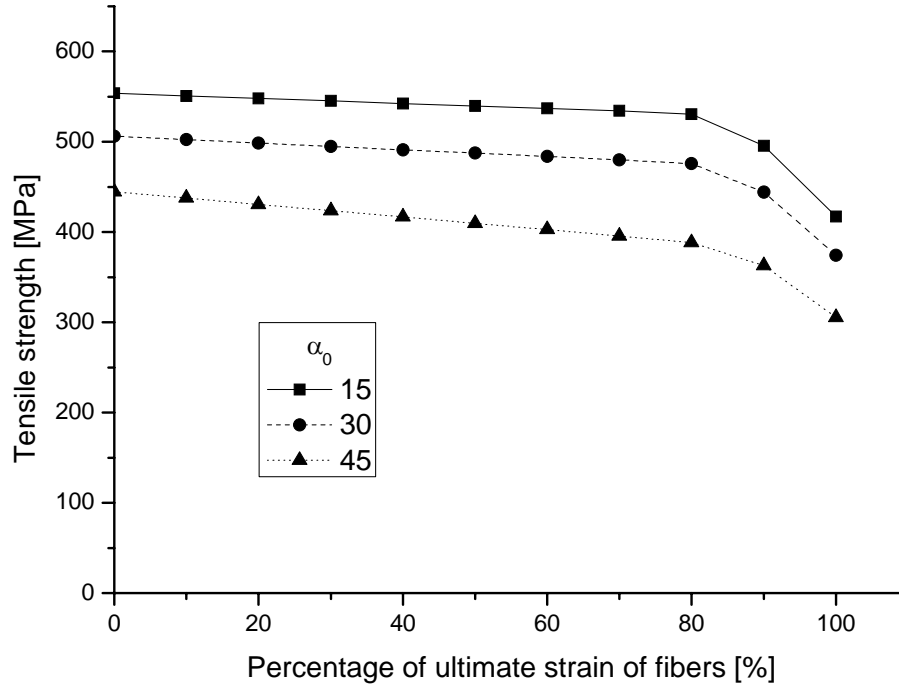


Figure 57 The effect of pretension (ε_0) on the tensile strength in the percentage of ultimate strain of fibers (at $\alpha_0=15^\circ, 30^\circ, 45^\circ$)

5.2.3. The effect of axial fiber introduction

Braided composites are usually produced in triaxially braiding in practice (see Figure 9) in order to reach a sufficient tensile (and bending) strength and stiffness, hence one of my aims is to model this kind of composites. If the model mentioned already are expanded and supposing that the axial fibers are not pretensioned ($\varepsilon_{0,a}=0$), and Eqns (76) and (78) are used:

$$E[F_B] = \overline{F_B} = 2n \cdot E[F_{ET}] + n_a \cdot E[F_{ET,a}], \quad (94)$$

where index a refers to axial fiber introduction. If Eqn. (49) is used:

$$E[F_{ET,a}] = \overline{F_{ET,a}} = N \cdot \overline{K} \cdot \varepsilon_a \cdot (1 - Q_{\varepsilon_s}(\varepsilon_a)), \quad (95)$$

which is the expected value of the 0° ET-bundle tensile force provided that the same roving is used for axial fiber introductions for braiding. Thus (81) is modified accordingly:

$$\frac{\sigma_C}{\sigma_S} = \varphi \cdot \frac{\overline{F_B}}{(2n + n_a) \cdot N \cdot \overline{F_S}} + (1 - \varphi) \cdot \frac{\sigma_M}{\sigma_S}, \quad (96)$$

$$\frac{\sigma_C}{\sigma_S} = \varphi \cdot \frac{\{2n \cdot \cos(\alpha_0) \cdot \varepsilon \cdot [1 - Q_{\varepsilon_S}(\varepsilon)] + n_a \cdot \varepsilon_a \cdot [1 - Q_{\varepsilon_S}(\varepsilon_a)]\} \cdot N \cdot \bar{K}}{(2n + n_a) \cdot N \cdot \bar{F}_S} + (1 - \varphi) \cdot \frac{\sigma_M}{\sigma_S}, \quad (97)$$

where

$$\varepsilon_a = u, \quad (98)$$

since $e_{0,a}=0$ and $\varepsilon_{0,a}=0$.

Figure 58 shows the impact of axial fiber introduction on the normalized tensile stress in case of different braiding angles (30 and 45°). It can be stated in general that axial fiber introductions increased the value of the initial tensile stiffness in each cases.

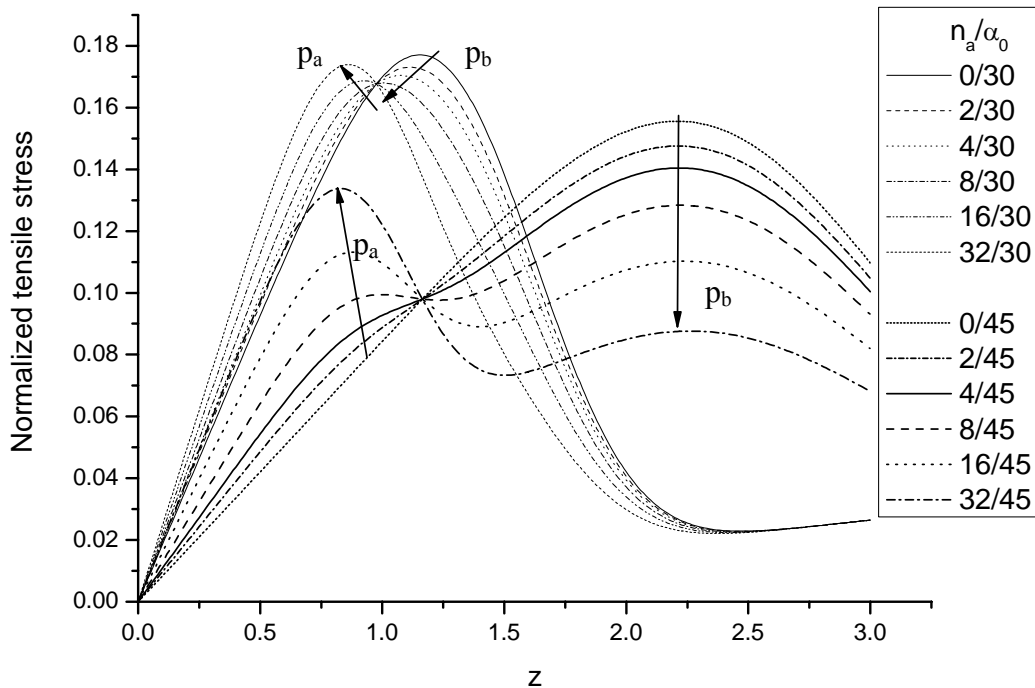


Figure 58 The effect of axial fiber introduction on the normalized tensile stress for different braiding angles (axial fiber introduction/braiding angle)

Eqn. (97) clearly reveals that the synergic effect of the two distribution functions is present and the terms (braided tows and axial fiber introductions) are considered with different weights. As a consequence, the resultant normalized tensile stress is obtained from the superposition of the two distribution functions. Two peaks can be defined: p_a for axial fiber introductions and p_b caused by the braided tows. These peaks can be observed well in the 45° case: if the number of axial fiber introductions increases p_a grows, while if peak p_b decreases since the weight of axial fiber introductions increases. In case of 16 and 32 axial fiber introductions it can be observed that these materials have a significant strength reserve since after the first peak the environment of the second peak can also bear significant loading, hence a tough materials is obtained. A direct reference for the existence and movement of the

two peaks can be seen in the 30° case but since the weight of tows (2x16 tows) is still comparable with that of the axial fiber introduction, these peaks do not appear as sharply as in the 45° case.

Since the number of axial fiber introductions in a given braiding machine is limited, it is advisable to use thicker or more tows held together if the aim is to increase the tensile (bending) modulus or strength.

If the axial fibers are evenly pretensioned (which is easy to set on most braiding machines, i.e. $\varepsilon_{0,a} \neq 0$), Eqn. (99) is obtained provided that only the axial fibers are pretensioned and if Eqn. (93) is applied in Eqns (94)-(97):

$$\frac{\sigma_C}{\sigma_S} = \varphi \cdot \frac{\{2n \cdot \cos(\alpha_0) \cdot \varepsilon \cdot [1 - Q_{\varepsilon_S}(\varepsilon)] + n_a \cdot \varepsilon_a^* \cdot [1 - Q_{\varepsilon_S}(\varepsilon_a^*)]\} \cdot N \cdot \bar{K}}{(2n + n_a) \cdot N \cdot \bar{F}_S} + (1 - \varphi) \cdot \frac{\sigma_M}{\sigma_S}, \quad (99)$$

where

$$\varepsilon_a^* = (1 + \varepsilon_{0,a}) \cdot (1 + u) - 1, \quad (100)$$

since $\varepsilon_{0,a} = 0$ és $\varepsilon_{0,a} \neq 0$.

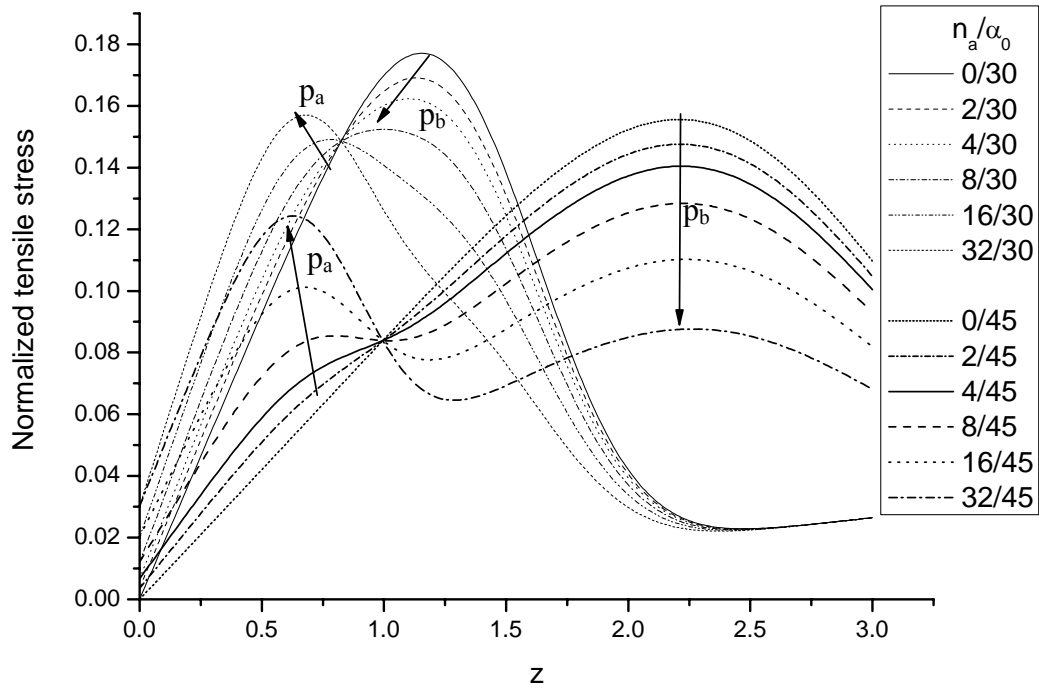


Figure 59 The effect of pretensioned ($\varepsilon_0 = 0.2 \cdot \bar{\varepsilon}_S$) axial fiber introduction on the normalized tensile stress for different braiding angles (axial fiber introduction/braiding angle)

The impact of pretensioned axial fiber introduction on the normalized tensile stress for different braiding angles can be studied well in Figure 59 if compared with Figure 58. It can

be seen that already $\varepsilon_0 = 0.2 \cdot \overline{\varepsilon_s}$ pretension has a favorable impact and peak p_a and p_b separates more as well.

5.3. Fiber bundle cell model of arbitrary braided structures

So far several parameters have been considered constant (e.g. same material, same direction of tows). This Chapter deals with the fiber bundle cell model of arbitrary braided structures (considering ET-bundles).

Composites are usually claimed to be parallel combination of the fiber (bundle) and the matrix and the matrix material parts – up to separation or breakage –, hence the tensile force that acts on the composite is the sum of the forces arising the parts and obviously fiber and matrix cross-sections can be added within a given cross-section (Figure 60).

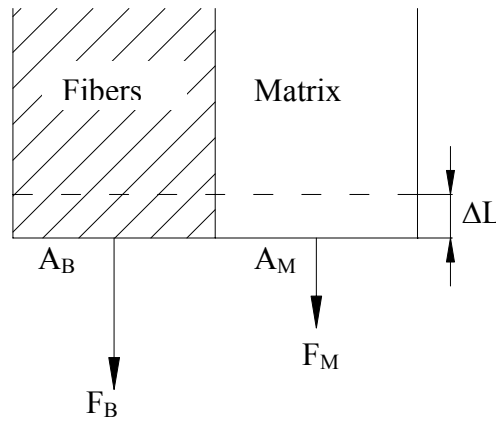


Figure 60 Cross-sections of the fibers and the matrix and the explanation of the arising axial forces

On the basis of the considerations above and using the notations of Figure 60:

$$F_C = F_B + F_M \quad (101)$$

$$A_C = A_B + A_M, \quad (102)$$

where F_C is the force that acts on the composite, while F_B on the fibers (bundles), F_M is the axial tensile force which the matrix is subjected, A_C is the cross-section area of composite element, A_B is that of the fibers (bundles) and A_M is that of the matrix.

The fibers in the considered composite intersect all cross-sections in the same proportion, hence the volume fraction of fibers/matrix is also constant along the length of the composite (the oblique angle of the bias fibers is constant along their length).

Hence for instance

$$\frac{A_B}{A_C} = \frac{A_B \cdot \Delta L}{A_C \cdot \Delta L} = \frac{V_B}{V_C} = \varphi_B =: \varphi ; \quad \frac{V_M}{V_C} = \varphi_M = 1 - \varphi , \quad (103, 104)$$

where φ_B is the volume fraction of the fiber, while φ_M is that of the matrix.

It is more reasonable to use the stresses instead of the forces:

$$\frac{F_C}{A_C} = \frac{F_B}{A_B} \cdot \frac{A_B}{A_C} + \frac{F_M}{A_M} \cdot \frac{A_M}{A_C} \quad (105)$$

$$\sigma_C = \frac{F_C}{A_C} = \frac{F_B}{A_B} \cdot \varphi + \frac{F_M}{A_M} \cdot (1 - \varphi). \quad (106)$$

If the matrix is considered to be homogenous, hence it is true that:

$$\sigma_M = \frac{F_M}{A_M}, \quad (107)$$

then (108) can be used instead of (106):

$$\sigma_C = \frac{F_B}{A_B} \cdot \varphi + \sigma_M \cdot (1 - \varphi). \quad (108)$$

The resultant bundle force:

$$F_B = \sum_{j=1}^o \sum_{i=1}^{N_j} F_{ij}, \quad (109)$$

where N_j is the number of elementary fibers in the j -th bundle, o is the number of bundles in the braided structure, F_{ij} is the axial force in the i -th fiber in the j -th direction, which – using the notations of Figure 61 – can be calculated according to (110):

$$F_{ij} = F_{f,ij} \cdot \cos(\alpha_{ij}), \text{ additionally} \quad (110)$$

$$A_{f,ij} = \frac{d_{ij}^2 \cdot \pi}{4} \quad (111)$$

$$A_{ij} = \frac{A_{f,ij}}{\cos(\alpha_{ij})}, \quad (112)$$

where $F_{f,ij}$ is the i -th force arising in the j -th bundle, α_{ij} is the angle between the fiber and the direction of loading (braiding angle), $A_{f,ij}$ is the cross-section area of the i -th fiber in the j -th bundle, d_{ij} is the fiber diameter, A_{ij} is its cross-section area perpendicular to the direction of loading. Obviously

$$\alpha_{ij} = \begin{cases} \neq 0, & \text{for oblique fibers} \\ = 0, & \text{for axial fiber introductions} \end{cases} \quad (113)$$

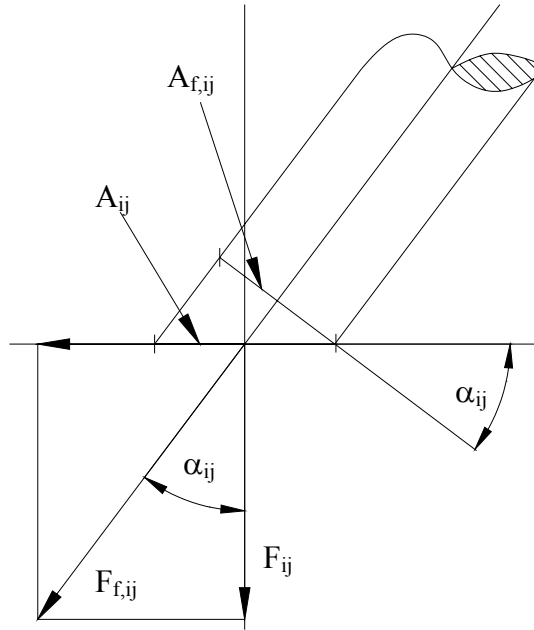


Figure 61 Oblique fibers

The tensile force of the bundle, where u is the strain of the composite can take the following form if Eqns (109) and (110) are used:

$$F_B = \sum_{j=1}^o \sum_{i=1}^{N_j} F_{ij} = \sum_{j=1}^o \sum_{i=1}^{N_j} F_{f,ij} \cdot \cos(\alpha_{ij}), \quad (114)$$

and using additionally Eqn. (112):

$$A_B = \sum_{j=1}^o \sum_{i=1}^{N_j} A_{ij} = \sum_{j=1}^o \sum_{i=1}^{N_j} \frac{A_{f,ij}}{\cos(\alpha_{ij})}. \quad (115)$$

The expected value of bundle forces (114):

$$E[F_B] = \overline{F_B} = \sum_{j=1}^o N_j \cdot \overline{F_{ij}} = \sum_{j=1}^o N_j \cdot E[F_{f,ij} \cdot \cos(\alpha_{ij})]. \quad (116)$$

The average tensile stress correspondent to the expected value of bundle forces:

$$\overline{\sigma_B} = \frac{\overline{F_B}}{A_B}. \quad (117)$$

Suppose that instead the bundle ($j=1, \dots, o$) the average cross-section areas of the fibers are:

$$A_{f,j} \approx A_{f,ij}, \quad \forall i, \quad (118)$$

and the braiding angles are:

$$\alpha_j \approx \alpha_{ij}, \quad \forall i, \quad (119)$$

hence it is supposed that the fibers within one given fiber bundle are of the same diameter and direction. Using Eqns (115) and (118):

$$A_B = \sum_{j=1}^o \sum_{i=1}^{N_j} \frac{A_{f,ij}}{\cos(\alpha_{ij})} = \sum_{j=1}^o N_j \cdot \frac{A_{f,j}}{\cos(\alpha_j)}, \quad (120)$$

and Eqns (116) and (119).

$$\overline{F}_B = \sum_{j=1}^o N_j \cdot \overline{F}_{f,j} \cdot \cos(\alpha_j). \quad (121)$$

It is to be noted that then α_j is not a random parameter, obviously.

The average ultimate force of fibers in the j -th bundle: $\overline{F}_{S,j}$ and its tensile strength:

$$\overline{\sigma}_{S,j} = \frac{\overline{F}_{S,j}}{A_{f,j}}, \quad (122)$$

and their maximum of these:

$$\sigma_S = \max_j(\overline{\sigma}_{S,j}), \quad (123)$$

or

$$\sigma_S = \frac{\max_j(\overline{F}_{S,j})}{A_{f,k}}, \text{ where} \quad (124)$$

$$k : \max_j(\overline{F}_{S,j}) = \overline{F}_{S,k}, \quad (125)$$

or average A_f can be used instead of $A_{f,k}$

$$\sigma_S = \frac{\max_j(\overline{F}_{S,j})}{A_f} = \frac{\overline{F}_S}{A_f}, \text{ where} \quad (126)$$

$$\overline{F}_S = \max_j(\overline{F}_{S,j}) \quad (127)$$

$$A_f = \frac{1}{N \cdot o} \cdot \sum_{j=1}^o A_{f,j} \cdot N_j \quad (128)$$

$$N = \sum_{j=1}^o N_j, \quad (129)$$

where A_f is an average cross-section area of all the fibers (perpendicular).

If (108) is used together with Eqns (117) and (120):

$$\frac{\sigma_C}{\sigma_S} = \varphi \cdot \frac{\overline{F}_B}{\sigma_S \cdot A_B} + (1 - \varphi) \cdot \frac{\sigma_M}{\sigma_S}. \quad (130)$$

Concluding from Eqn. (121) e.g. with Eqn. (123) (using Eqns (120) and (122)):

$$\frac{\overline{F}_B}{\sigma_S \cdot A_B} = \frac{\sum_{j=1}^o N_j \cdot \overline{F}_{f,j} \cdot \cos(\alpha_j)}{\max_j \left(\frac{\overline{F}_{S,j}}{A_{f,j}} \right) \cdot \sum_{j=1}^o N_j \cdot \frac{A_{f,j}}{\cos(\alpha_j)}}, \quad (131)$$

or with Eqn. (126) because not the stress but rather the extreme value is to be normalized to 1:

$$\frac{\overline{F}_B}{\sigma_S \cdot A_B} = \frac{\sum_{j=1}^o N_j \cdot \overline{F}_{f,j} \cdot \cos(\alpha_j)}{\frac{\overline{F}_S}{A_f} \cdot \sum_{j=1}^o N_j \cdot \frac{A_{f,j}}{\cos(\alpha_j)}} = \frac{\overline{F}_B}{\overline{F}_S \cdot \frac{A_B}{A_f}} = \frac{\overline{F}_B}{N_B \cdot \overline{F}_S} = \frac{\overline{F}_B}{\overline{F}_S} = \frac{\overline{F1}}{\overline{F1}}, \quad (132)$$

where N_B is a kind of weighted cardinality, i.e.

$$N_B = \frac{A_B}{A_f}, \quad (133)$$

additionally, the whole fiber system is a tensile force related to 1 fiber:

$$\overline{F1} = \frac{\overline{F}_B(u)}{N_B} = \overline{F}_B \cdot \frac{A_f}{A_B} = \frac{\overline{F}_B}{N \cdot o \cdot \psi}, \quad (134)$$

where using Eqns (128) and (129):

$$N_B = \frac{A_B}{A_f} = \frac{\sum_{j=1}^o N_j \cdot \frac{A_{f,j}}{\cos(\alpha_j)}}{\frac{1}{N \cdot o} \cdot \sum_{j=1}^o N_j \cdot A_{f,j}} = N \cdot o \cdot \psi, \quad (135)$$

furthermore

$$\psi = \sum_{j=1}^o \frac{1}{\cos(\alpha_j)} \cdot \frac{N_j \cdot A_{f,j}}{\sum_{j=1}^o N_j \cdot A_{f,j}}, \quad (136)$$

which is the average of $\frac{1}{\cos(\alpha_j)}$ -s weighted with the fiber type total cross-section areas.

Finally, the normalized tensile stress of the arbitrary braided composite is obtained with the help of Eqns (130) and (132):

$$\frac{\sigma_C}{\sigma_S} = \varphi \cdot \frac{\overline{F1}}{\overline{F1}} + (1 - \varphi) \cdot \frac{\sigma_M}{\sigma_S}. \quad (137)$$

5.4. Evaluation of the model as compared to measured values

The further developed fiber bundle cell model and the impact of the parameters of the model on the normalized tensile stress have been detailed in Chapters 5.1-5.3. In this Chapter the measured tensile force and stiffness of different braided composites are compared with the result of the model (the initial parameters of the studied composites are taken into consideration, of course).

5.4.1. Braided composite tubes without axial fiber introduction

The applied materials, technologies, manufacturing technique of the specimens and the conditions of the measurements were summarized in Chapter 3. It is to be noted that before the tensile test the braiding angle and the geometry (external, internal diameters, wall thickness, clamping distance) were measured on each specimen, while fiber content was determined after the measurement. The longitudinal and bias strains were tracked with a videoextensometer due to neck-forming appeared and then the contraction parameter was determined. In all cases the notations below the figures show which parameters were used. The experimental results are summarized in Appendix D.

The tensile force of the composite, obtained from Eqn. (81) in the way shown below, is graphed in the comparative figures:

$$F_C = \varphi \cdot \frac{\overline{F_B}}{2n \cdot N \cdot \overline{F_S}} \cdot \sigma_S \cdot \overline{A_C} + (1 - \varphi) \cdot \sigma_M \cdot \overline{A_C}, \quad (138)$$

which is simplified, using Eqns (76)-(78):

$$F_C = \varphi \cdot \overline{K} \cdot \varepsilon \cdot \cos(\overline{\alpha_0}) \cdot (1 - Q_{\varepsilon_S}(\varepsilon)) \cdot \frac{\overline{A_C}}{A_S} + (1 - \varphi) \cdot \overline{E_M} \cdot u \cdot \overline{A_C}. \quad (139)$$

It is worth observing that Eqn. (139) does not depend directly either on the number of elementary fibers in the rovings or on the number of carriers in the braiding machine. The question whether the size of the braiding machine (the number of carriers) and the number of rovings do not influence the tensile mechanical properties of the composite may arise. The answer is – of course – that they do influence it: these factors appear e.g. in the volume fraction indirectly. If a roving that contains relatively few elementary fibers (24k) is used in a braiding machine having a low number (16) of carriers, only a very high braiding angle can be achieved in order to be able to provide a complete covering. In case smaller braiding angles are to be reached on the same machine under the same circumstances, gaps may form among the rovings and these voids will be filled with the matrix, hence fiber content would decrease.

Thus, in practice high number of carriers (64-144) and thin (4-6k) rovings are applied so that the usual range of braiding angles (10-80°) can be obtained and a sufficient coverage is provided and as a result fiber content becomes as high as possible.

First the effect of the braiding angle is studied. As it could be seen in Figure 47 and Figure 48 even a little change in the braiding angle has a significant impact on the tensile strength. This fact is verified in the measurements, as well (Figure 62). Figure 62 shows the typical tensile force of braided composites (not to the whole failure, see that later): after one maximum is reached where the matrix cracks, neck-forming starts (Figure 63), tensile force drops, continuous neck-forming sets in to which ca. half the maximal force is necessary. Since the braiding angles are relatively large, the impact of fiber bundles on failure is negligible, while the matrix becomes the dominant load-bearing element. It can be observed that the model describes the initial tensile stiffness well in both cases, even in case of such huge braiding angles.

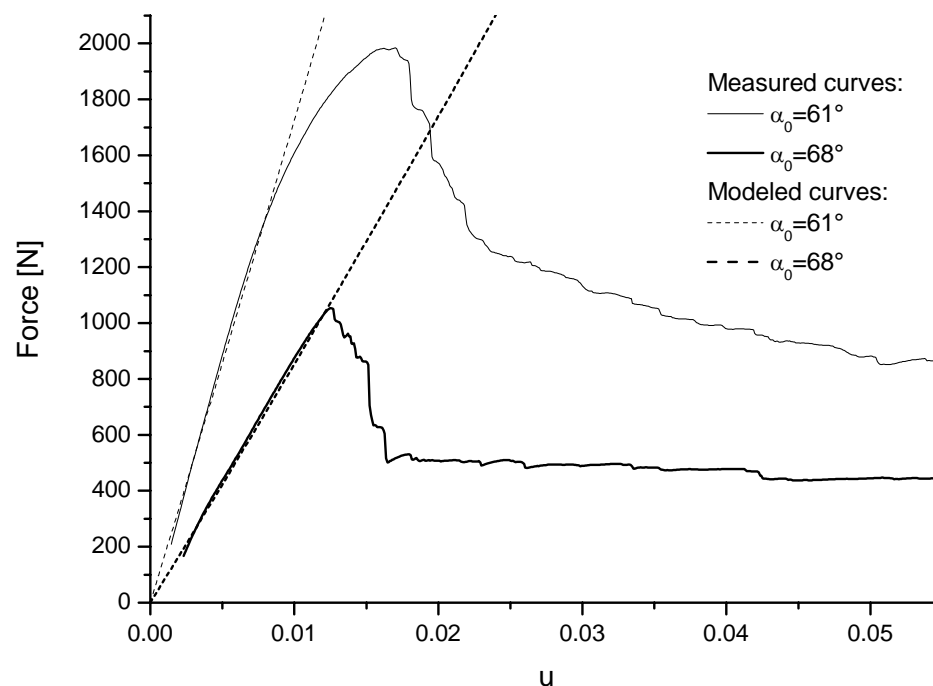


Figure 62 The effect of the change of the braiding angle on the tensile force of composites ($n=8$, $\varphi=0.23$; $\alpha_0=61^\circ$ and $\alpha_0=68^\circ$)

Figure 64 shows the ratio of external radii as a function of the longitudinal strain. It can be seen clearly that the modeled contraction function (using Eqn. (64)) estimates the real ratio of external radii up to neck-forming (cp. Figure 62) well.



Figure 63 Neck-forming of tensile-loaded marked braided composite

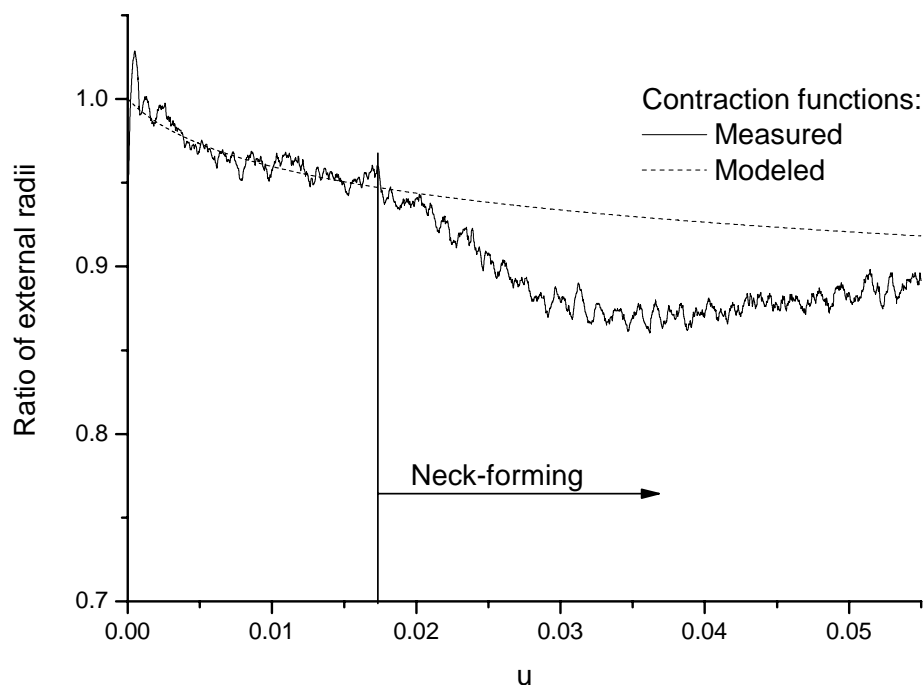


Figure 64 The measured and the modeled contraction functions
($n=8$, $\varphi=0.23$; $\alpha_0=61^\circ$)

Figure 65 shows the measured and the modeled maximal forces (up to neck-forming) (for explanation see Eqn. (140)). It can be seen clearly, in comparison with Figure 48, that the measurements show similar tendencies to the modeled values, i.e. the maximal force and obviously the stress as well decrease significantly above 45° .

$$F_{C,Max} = \max\left(F_C(\varepsilon_M), \max_{u < \varepsilon_M}(F_C(u))\right). \quad (140)$$

The figure also reveals that almost the half of the estimated values could be reached. For a more accurate evaluation the relative average square of errors is to be calculated

between the estimated and the measured values. As the first step, the square of errors is calculated:

$$\overline{H_*^2} = \sum_{i=1}^t (y_i - \xi \cdot Y_i)^2, \tag{141}$$

where t is the number of the measurements, y_i is the measured, Y_i is the modeled value and ξ is the average proportionality factor ($0 < \xi < 1$). This way the average square of errors can be computed as follows:

$$h_* = \sqrt{\frac{1}{n} \cdot \overline{H_*^2}}, \tag{142}$$

with the help of which the relative average square of errors:

$$\mu = \frac{h_*}{\max(y_i, \xi \cdot Y_i)}. \tag{143}$$

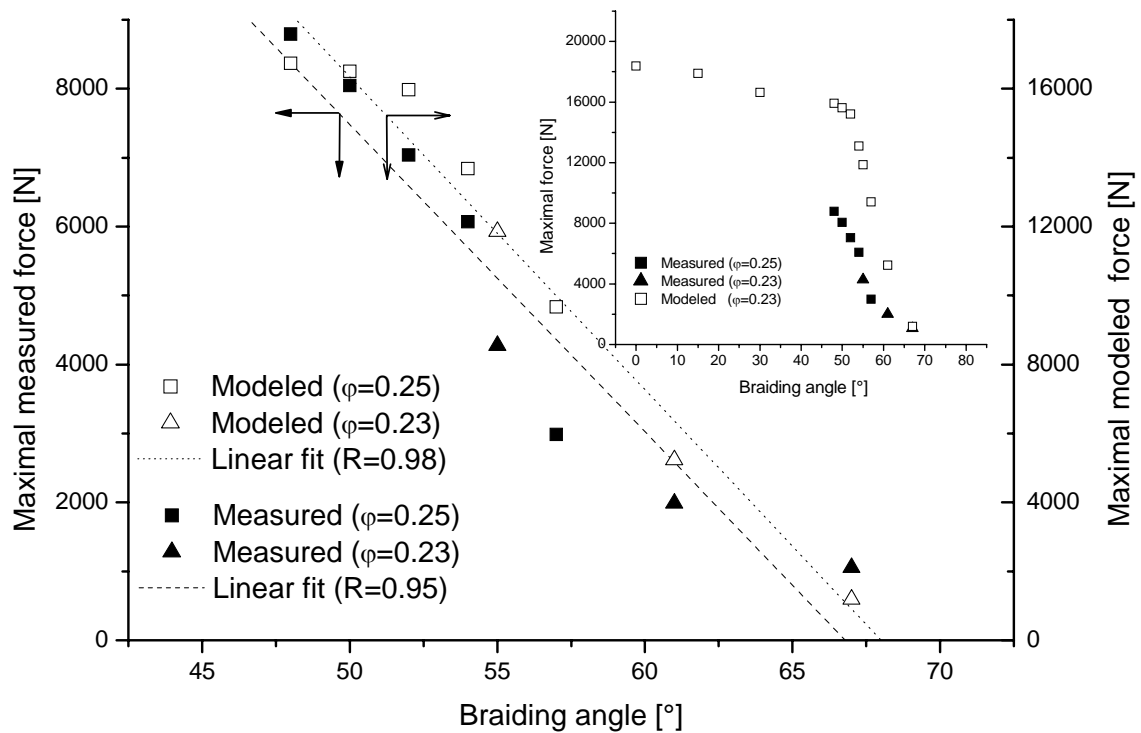


Figure 65 The maximal measured (up to neck-forming) and the modeled forces

If (143) is minimized, it turns out that 44% of the maximal value was reached in average concerning the first breakage peak (up to neck-forming) (the value of the relative average square of error was 11.9%). If the 44% of the modeled values are graphed as a function of the measured values, Figure 66 is obtained, which reveals that the correlation coefficient of the fitted linear curve is $R=0.95$ that reveals a strong correlation.

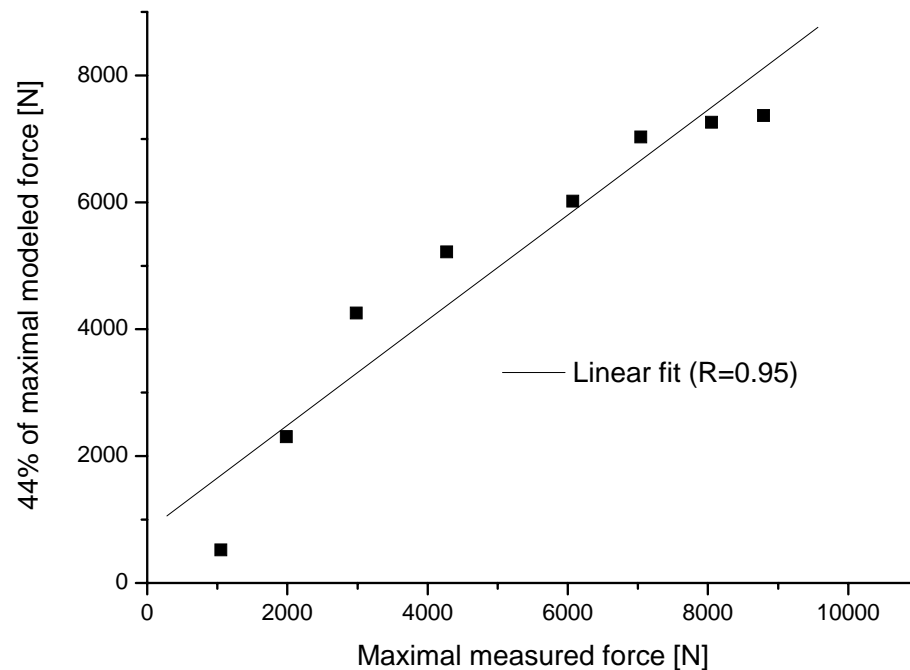


Figure 66 44% of the maximal force as a function of the measured forces

It can be stated that the average gradient of the decrease in the measured values is approximately the same as the one estimated with the theory (the ratio of the measured and the converted estimated values is 0.98), furthermore a relatively small extent change in the fiber content (2%) did not cause a significant value offset in the measured and the estimated data.

The whole tensile failure process is shown in Figure 67. The whole tensile failure process of the studied braided composite tubes can be divided into four, well-separable parts of deformation: *I. Range of engineering applications*, where the load-uptake is quasi-linear (it is to be noted that this is the range that can be modeled so far). It is visible that after neck-forming takes place along the whole clamping distance (*II. Range of continuous neck-forming*) a significant tensile force reserve evolves since the initial diameter has already dropped and the wall thickness increased (the cross-section area remained quasi constant), additionally the fiber bundles are oriented in the direction of loading (slipping on one another) this way the process ended in impregnated bundle tension (*III. Range of the impregnated bundle tension*). This resulted in a three times higher tensile force compared to the initial, local maximum. It can be mentioned that the fiber content changed only to a small extent (<0.5%) meanwhile. Finally, the rovings started to break continuously after the maximum and the final failure took place (*IV. Range of final failure*). The model estimates the initial tensile stiffness well, even in this case.

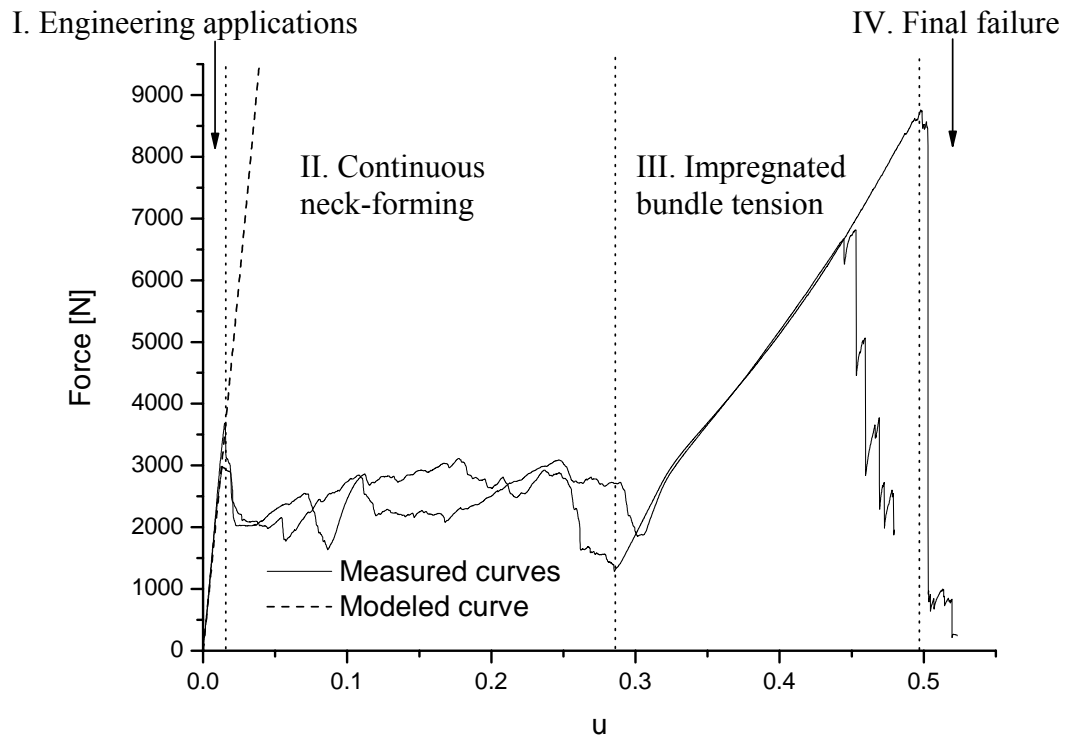


Figure 67 The whole tensile process of braided composites
($n=16$; $\alpha_0=55^\circ$, $\varphi=0.25$)

In Figure 68 a composite with a smaller braiding angle than the foregoing one can be seen. The model estimates the initial tensile stiffness well in this case, too.

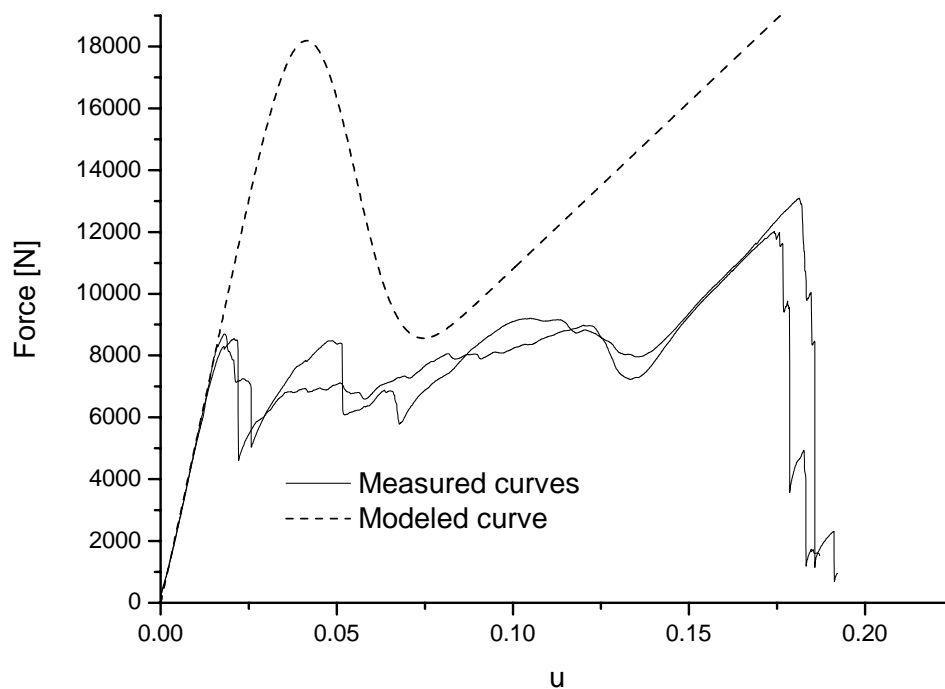


Figure 68 The whole tensile process of braided composites
($n=16$; $\alpha_0=48^\circ$, $\varphi=0.25$)

It can be noticed that the initial neck-forming maximum exceeds the similar values of composites that have larger braiding angle significantly (with 2-3,000 N) compared to Figure 67, additionally the same can be stated about the global maximum arising from the bundle tension. The peak experienced during the parameter variation can be seen in the appropriate scale. This peak describes the tensile force of the ideal composite produced from bundles of given braiding angle.

The above detailed results are being published in [144].

As it was revealed in part b) of Chapter 5.2.1, the small standard deviation of the braiding angle does not have a significant impact on the strength, hence on the maximal tensile force. In Figure 70 a few elements of a specially prepared series of tensile forces are shown. These measurements were carried out on samples that scatter around one braiding angle. In order to claim even statistically that the braiding angle was of normal distribution, more angles (52 pieces) than usual were measured on the surface of the specimens. Figure 69 as well as the chi-squared test carried out at 95% level verifies the statement that specimens with normal distribution of braiding angle were successfully produced, and the average value of the distribution was 57.09° , while the standard deviation turned out to be 3.52° . It can be concluded that the standard deviation of the braiding angle can be considered as small ($<5^\circ$), not significant in this aspect.

It can also be stated that the small extent standard deviation of the braiding angle does not influence the tensile force, hence tensile strength of the braided composite significantly. This means the following:

- a) the small extent standard deviation (max. 5°) of the even braiding angle is not a significant parameter provided that it is managed to be kept around a certain average value in the technology;
- b) the composite manufacturers, who use braided tapes or belts as the pre-product, and produce circular cross-sectional braided composites, and have an error in the production due to technological deficiency (i.e. the angle cannot be kept at a constant value because it scatters around a given average value) are not affected by a significant decrease in the strength values.

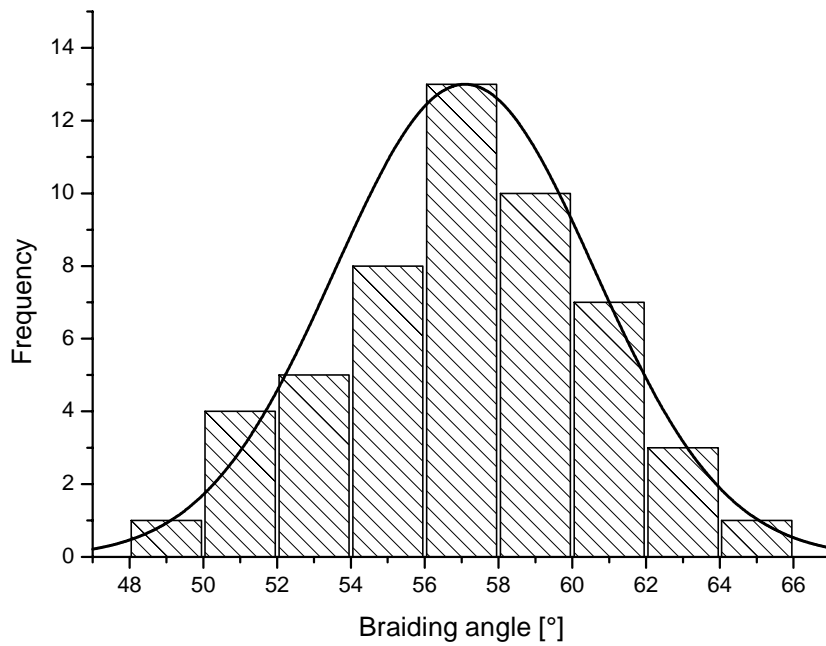


Figure 69 Histogram and density function of braiding angle ($\bar{\alpha}_0 = 57.09^\circ$, $\sigma_{\alpha_0} = 3.52^\circ$)

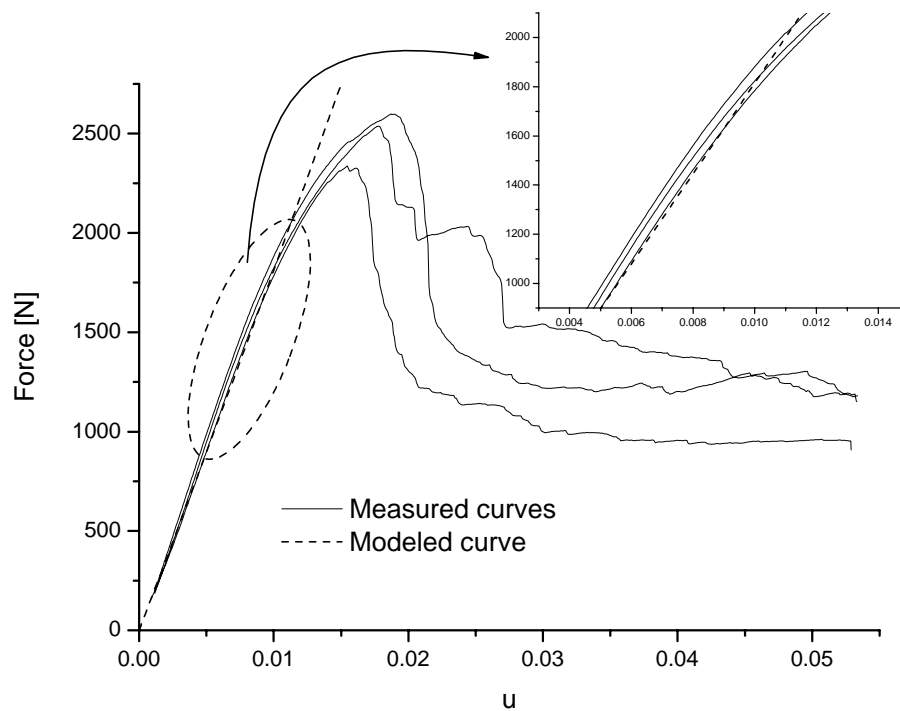


Figure 70 Tensile forces of braided composites with a braiding angle of normal distribution ($n=16$, $\varphi=0.25$, $\bar{\alpha}_0 = 57.09^\circ$, $\sigma_{\alpha_0} = 3.52^\circ$)

5.4.2. Braided composite tubes with axial fiber introduction

The impact of axial fiber introduction was studied using Eqn. (97)-t (since is considered to be $\varepsilon_{0,a} \approx 0$) and the principle revealed in (138). On the basis of Figure 71 it can be claimed that this form of the model cannot be applied for the description of the properties of composites with axial fiber introduction, hence the model is to be developed further. The comparison with Figure 67 shows that the axial fiber introduction has a significant impact, as it had been expected.

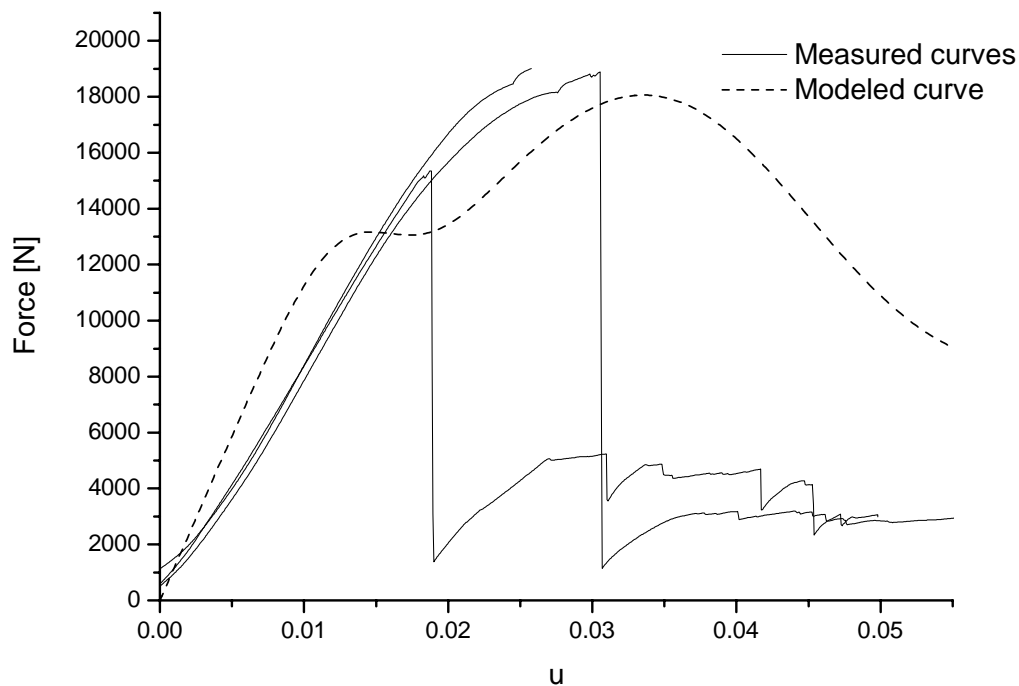


Figure 71 Measured and modeled curves of axial fiber introduction composites
($n=8, n_a=8, \alpha_\theta=55^\circ, \varphi=0.25$)

Supposedly, the assumption is wrong, i.e. the pretension of axial rovings is not zero ($\varepsilon_{0,a} \neq 0$). Nevertheless, this is not pretension but loosening that can be described with the EH-bundle (see Chapter 2.5). This statement can be explained since in practice, during composite manufacturing, the pretension of axial rovings could not be provided continuously at least to a minimal extent, and as a consequence some fibers were always loose, hence the axially introduced tows are considered to be describable with EH-bundles (this is only valid for the axial tows, the initial tensile stiffness of braided tows in this angular range is characterized with the ET-bundle, as it was derived before).

5.4.3. The improvement of the axial fiber introduction model of braided composite tubes – modeling with ETH-bundle

In case of the crimped or preloaded flexible tensile fiber bundle, i.e. the EH-bundle (Figure 72) the u relative strain related to the L_0 free clamping distance of the bundle is usually not the same as the ε relative strain related to the unloaded length of single fibers owing to the preload $\varepsilon_{0,a} \neq 0$ (the meaning of which is crimping if $\varepsilon_{0,a} < 0$ denoted by ε_0 hereinafter for the sake of simplicity). If the L_0 clamping length of the bundle is reduced, the value of ε_0 may even reach -1 (if $L_0=0$), namely the two ends of a fiber of finite length join ($u > 0$):

$$-1 < \varepsilon_0 < \varepsilon(u, \varepsilon_0) = \varepsilon_0 + (1 + \varepsilon_0) \cdot u < \varepsilon_s, \tag{144}$$

using (1), i.e.

$$\varepsilon(u, \varepsilon_0) = (1 + \varepsilon_0) \cdot (1 + u) - 1 \tag{145}$$

$$\varepsilon(u, \varepsilon_0) = \varepsilon_0 + (1 + \varepsilon_0) \cdot u \tag{146}$$

Note that ε_0 is a random parameter in this case.

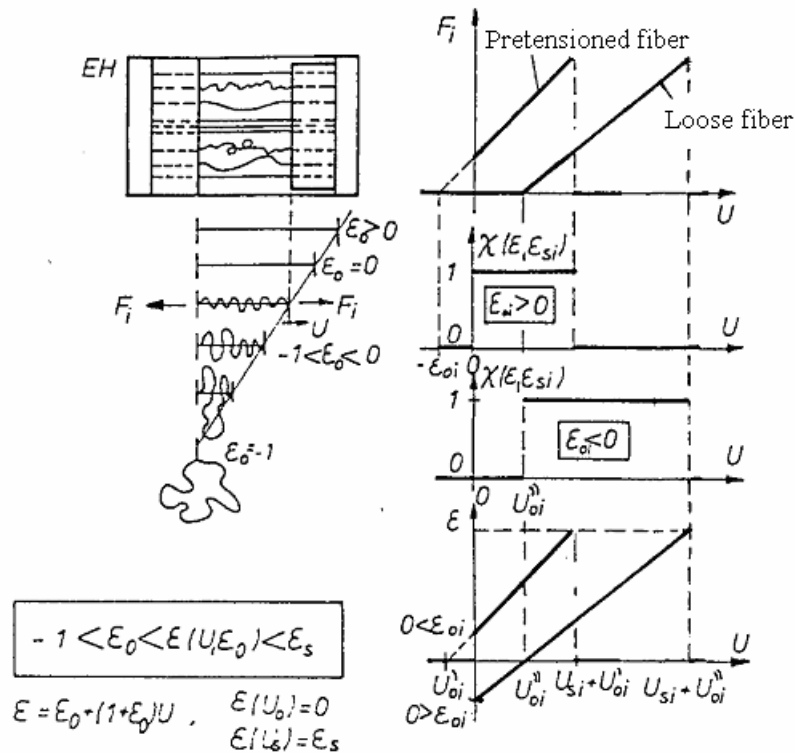


Figure 72 Structural draft of the EH- bundle and the strain of one of its fibers as well as the evolving tensile force as a function of bundle strain [7]

Consider an EH-bundle tensile force, which involves N fibers:

$$F_{EH} = \sum_{j=1}^N K_j \cdot \varepsilon_j(u, \varepsilon_0) \cdot \chi(\varepsilon_j(u, \varepsilon_0), \varepsilon_{S,j}), \quad (147)$$

the expected value of which (without indices) is

$$E[F_{EH}] = \overline{F_{EH}} = N \cdot \overline{K} \cdot E[\varepsilon(u, \varepsilon_0) \cdot \chi(\varepsilon(u, \varepsilon_0), \varepsilon_S)]. \quad (148)$$

The simplifications used in the calculation of the expected value of the ET-bundle (77) cannot be applied here, hence

$$\overline{F_{EH}} = N \cdot \overline{K} \cdot \int_{x=-1}^{\infty} |(1+x) \cdot (1+u) - 1|_+ \cdot [1 - Q_{\varepsilon_S}((1+x) \cdot (1+u) - 1)] \cdot dQ_{\varepsilon_0}(x), \quad (149)$$

where $|\cdot|_+$ denotes the positive part of the function, since according to the supposed fiber properties (perfectly flexible fibers) the transmitted force is zero if $\varepsilon < 0$ force zero.

In case the axial bundles are considered to be characterized with EH-bundles and the braided ones with ET-bundles, Eqn. (94) can be modified in the following way:

$$E[F_B^{ETH}] = \overline{F_B^{ETH}} = 2n \cdot E[F_{ET}] + n_a \cdot E[F_{EH}], \quad (150)$$

where $\overline{F_B^{ETH}}$ is the average tensile force of ET and EH compound bundle, n_a is the number of axial introductions, and there are N fibers in all the bundles (96):

$$\frac{\sigma_C}{\sigma_S} = \varphi \cdot \frac{\overline{F_B^{ETH}}}{(2n + n_a) \cdot N \cdot \overline{F_S}} + (1 - \varphi) \cdot \frac{\sigma_M}{\sigma_S}. \quad (151)$$

The form of (138) is advantageous when it is graphed. This form is obtained from the multiplication of the normalized tensile stress and the A_C cross-section area of the composite:

$$F_C = \varphi \cdot \frac{\overline{F_B^{ETH}}}{(2n + n_a) \cdot N} \cdot \frac{A_C}{A_S} + (1 - \varphi) \cdot E_M \cdot u \cdot A_C. \quad (152)$$

The loosening is supposed to be of normal distribution, i.e. $N(\overline{\varepsilon_0}, \sigma_{\varepsilon_0}^2)$. Hence (149) can be modified in the following way:

$$\overline{F_{EH}} = N \cdot \overline{K} \cdot \int_{x=\frac{u}{1+u}}^{\infty} |(1+x) \cdot (1+u) - 1|_+ \cdot [1 - Q_{\varepsilon_S}((1+x) \cdot (1+u) - 1)] \cdot q_{\varepsilon_0}(x) \cdot dx, \quad (153)$$

where $q_{\varepsilon_0}(x)$ is the density function of ε_0 , and the fact that owing to the $|\cdot|_+$ positive part, if is $\varepsilon < 0$, the integral is zero, too is considered, hence it is enough to complete the integration on the $\varepsilon_0 = x$ values from which $\varepsilon \geq 0$, namely

$$\varepsilon(u, \varepsilon_0) = (1+x) \cdot (1+u) - 1 \geq 0, \quad (154)$$

$$x \geq -\frac{u}{1+u}. \quad (155)$$

This extended model is studied using Eqns (152) and (153) and compared to the results of the previous model that contained only ET-bundle. In Figure 73 it can be seen that the modified model gives a good estimation for the initial tensile stiffness of a braided composite with 8 axial fiber introductions – as opposed to the simpler model.

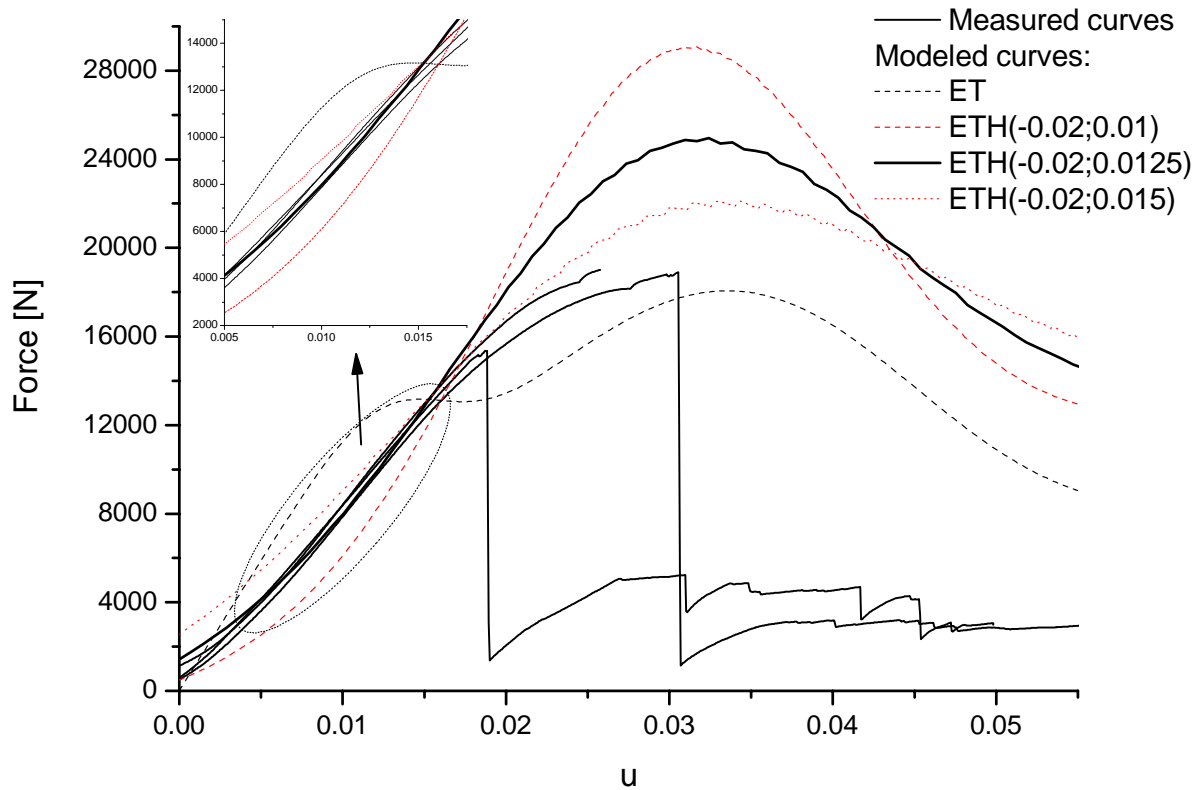


Figure 73 The measured and modeled curves of axial fiber introductions (ET-, ETH-bundles) ($n=8, n_a=8, \alpha_0=55^\circ, \varphi=0.25$)

The average value and standard deviation of loosening cannot be measured directly hence, they had to be estimated on the basis of the fitted model and the following values were obtained: $\overline{\varepsilon_0} = -0.02$, $\sigma_{\varepsilon_0} = 0.0125$. This means 4 mm loosening in case of a 200-mm-long composite tube, and this value can be accepted as real considering the technology. The significant effect of the standard deviation of preload, precrimp can be observed, and the lack of peaks p_a and p_b in case of the ETH-bundle can be observed although the parameters are similar. The explanation is that these peaks disappear and fit into the initial, increasing part of the curve.

Figure 74 shows the tensile force of a braided composite manufactured with 4 axial fiber introductions. It can be observed that the ETH model provided a better result for the initial tensile stiffness in this case, too.

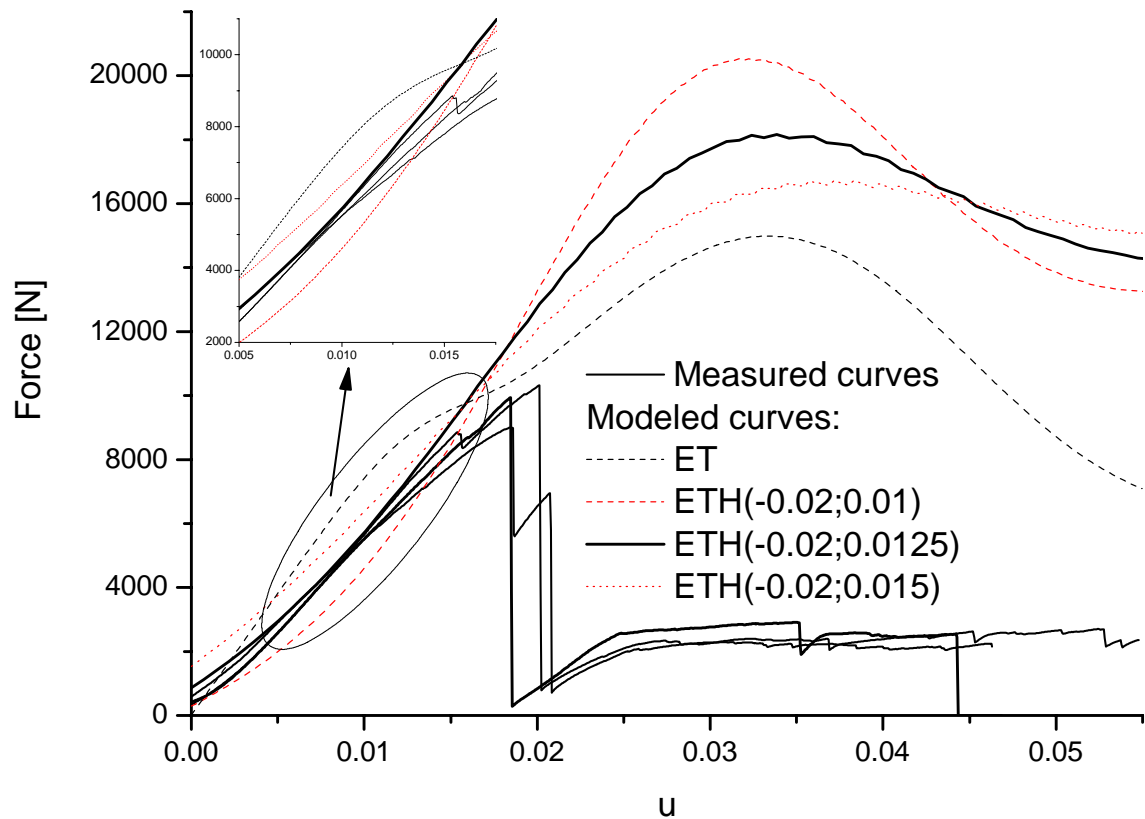


Figure 74 The measured and modeled curves of axial fiber introductions (ET- and ETH-bundles) ($n=8$, $n_a=4$, $\alpha_f=55^\circ$, $\varphi=0.25$)

A further interesting result is that the selection of the same parameters provided the ability to estimate the initial tensile stiffness of braided composites with 4 and 8 axial fiber introductions. The statements above reveal that loosening and its standard deviation primarily depends only on the technology, since braided composites with 4 and 8 axial fiber introductions could be modeled using the same parameters. Thus, it can be claimed that the application of the modified model, the EH-bundle, in case of axial fiber introduction.

6. Discussion

6.1. Evaluation of mechanical behavior of braided profiles

The aim of my dissertation was to develop a high strength composite profile of closed cross-section for the transportation-, automotive-, or machine-building industry. In such elements the basic requirements are the high load-bearing capacity, high stiffness and harmonized impact resistance. On the other hand, good productivity in the manufacturing technology is also important. The technical parameters of such a composite product should be comparable or higher than those of the closed steel profiles now available on the market. First the materials, then the technologies had to be selected. Carbon fiber was chosen as reinforcing material because of its advantageous mechanical properties, proven in several application fields such as the aircraft industry. Braiding was chosen as profile-building technique, since it is a well known, productive textile technology, creating a weave-like, self-reinforced structure. In fact, the braiding is still not widely spread in composite technology. The reason may be the conservatism of some important industries in the potential market. Moreover the braiding machine developers do not have experience with high performance carbon fibers, which have considerably different properties as compared to the typical braiding fibers, such as polyesters, polyamides etc.

The conventional, chemically initiated crosslinking of the advanced composite matrices, such as unsaturated polyesters or epoxies is relatively slow (from 6-8 hours to several days). There are only few exceptions such as the hot pressing of the sheet molding compounds. A faster crosslinking technology had to be found to make whole composite profiles, possibly in continuous mode of operation. An advanced technology used in the crosslinking of polyethylene and shrinkable tubes, which has been a well known and applied technology for more than 30 years was chosen, that is the crosslinking initiated by accelerated electrons. Nowadays more than 1,500 industrial electron accelerators are serving the plastics processing industry worldwide in this function. The EB crosslinking is not only a “cool”, energy-conserving, fast technology but also generates better mechanical properties in the crosslinked polymer products. In my case the electron beam has a possibility to activate not only the cross-linkable matrix but also the surface of the fibers, therefore it can result in a better cooperation between the main components of the composite. This is essential for the repeated, dynamical load-bearing capacity of the composite.

In the first part of my dissertation I had to prove the electron beam crosslinkability of the vinylester type (epoxy-acrylate) resin itself. The electron beam curing of the resin resulted in better mechanical properties (ca. 15% better) than that of the conventional, chemically initiated method, but even more significant differences were revealed in the mechanical properties of composites (30-50% better). As the static mechanical tests showed, the EB processing of braided CFR epoxy composite profiles demonstrated better cooperation between fiber and matrix, as related to the conventional chemical crosslinking. This is visible specifically in the better values of the interlaminar shear strength, but also in the better bending strength and modulus measured on the wall of the composite product. It has been shown that not only the high bending modulus characterized the new braided carbon fiber reinforced composite, but also an advantageous (“accordion-like”) impact (crash) behavior. The majority of my braided EB treated composite profiles showed high energy absorbing capacity all along the displacement, which is of great benefit in applications such as an automobile drive shaft or steering column. Due to these advantageous properties composite profiles were manufactured by electron beam in the rest of my dissertation.

Basic engineering constants, e.g. modulus and strength have to be predictable on the mechanics of main components of the braided composites to be used in structural applications. Several models are available to describe these properties. The fiber bundle cell modeling method was applied, because of the evident analogies between the braided structure and the multifilament yarns and tows. The braided structure itself consists of rovings, bundles and these bundles consist of several thousands of elementary fibers. The simplest geometry (circular tube) and load (tensile) were used to determine the properties above.

First the contraction of the braided composite tube was modeled during tensile loading and it was summarized in a contraction function then the tensile force of the composite was described with the fiber bundle cell model. The effect of the parameters of tensile force, their standard deviations, common impact and finally the role of axial fiber introduction on the normalized tensile stress was examined. All parameters influenced the normalized tensile stress, but – in my opinion – the most important parameter is the braiding angle, as this parameter can be modified in the easiest way on the braiding machine (with the speed of pulling or carriers) hence mean in the technology as well. Theoretically the small value of the standard deviation around the average value of the braiding angle has practically no effect on the normalized tensile stress and this fact is supported by measurements. This is an important result for the industry, too, that the small extent standard deviation (max. 5°) of the even braiding angle is not a significant parameter provided that it is managed to be kept around a

certain average value in the technology; the composite manufacturers, who use braided tapes or belts as the pre-product, and produce circular cross-sectional braided composites, and have an error in the production due to technological deficiency (i.e. the angle cannot be kept at a constant value because it scatters around a given average value) are not affected by a significant decrease in the strength values.

Before hand the failure of the circular cross-sectional braided composite tube was revealed. I have pointed out that the tensile process can be divided into four, well separable parts of deformation: *I. Range of engineering applications*, where the load-uptake is quasi-linear (it is to be noted that this is the range that can be modeled so far). It is visible that after neck-forming takes place along the whole clamping distance (*II. Range of continuous neck-forming*) a significant tensile force reserve evolves since the initial diameter has already dropped and the wall thickness increased (the cross-section area remained quasi constant), additionally the fiber bundles are oriented in the direction of load (slipping on one another), and this way the process ended in impregnated bundle tension (*III. Range of the impregnated bundle tension*). This resulted in a three times higher tensile force compared to the initial, local maximum. It can be mentioned that the fiber content changed only to a small extent (<0.5%) meanwhile. Finally, the rovings started to break continuously after the maximal load and the final failure took place (*IV. Range of final failure*).

In Range I the simplest model (only oblique bundle) describes the tensile force, therefore the initial tensile stiffness well, but this model does not estimate the properties of the composites with axial fiber introduction well. This statement can be explained since in practice, during composite manufacturing, the pretension of axial rovings could not be provided continuously at least to a minimal extent, and as a consequence some fibers were always loose, hence the axially introduced tows are considered to be describable with EH-bundles (this is only valid for the axial tows, the initial tensile stiffness of braided tows in this angular range is characterized with the ET-bundle, as it was derived before). The modified model estimates the tensile force well. The significant effect of the standard deviation of preload, precrimp can be observed. A further noticeable result is that the selection of the same parameters provided the ability to estimate the initial tensile stiffness of braided composites with 4 and the 8 axial fiber introductions. The statements above reveal that loosening and its standard deviation primarily depends only on the technology, since braided composites with 4 and 8 axial fiber introductions could be modeled using the same parameters. Supposedly the above mentioned modification does not have to be made in case of continuous operation, thus precrimping avoidable then.

A successful attempt was made to create the fiber bundle cell model of an arbitrary braided structure that can be applied to estimate the tensile force of the hybrid composite. It reveals that the fiber bundle cell model is most suitable, therefore my further aim of research is to describe the properties of the braided composite to another loads (e.g. torsion, bending and impact resistance).

6.2. Possibility of the continuous operation

One target of the dissertation is to consider the alternatives of the continuous manufacturing process of composites, namely the “serial connection” of braiding, impregnation, shaping and crosslinking. The synchronized steps of production provide the greatest advantage compared to the discontinuous processes.

Braiding is possible in the wet as well as the dry state. The roving may be impregnated first and braided afterwards. The advantage of this method is that the roving is thoroughly wetted ensuring the basic criterion of a good fiber-matrix connection. After braiding the excess resin can be pressed out and evenly distributed on the surface with the help of caliper rings.

There are different ways of **profile shaping**.

- a) Shaping with a temporary core that must be removed at the end of the process. This process is uneconomical but can be applied in the development stages.
- b) In the fully developed continuous process it would be favorable to replace the removable core by forming a pin in the tool.
- c) The most promising method considering both the composite properties and the profile stability seems to be applying a permanent insert (core), and as a result a sandwich structure composite beam with a well defined shape is formed. This permanent core could be made of hard polyurethane (PUR), or other polymer foam, used for example in helicopter rotor blades.

Crosslinking can be completed in two ways.

- A) The resin is crosslinked in a conventional thermochemical way. In this case several technological problems arise. Adding the catalyst to the resin creates an initiated system having a limited pot-life.
- B) The treatment with high energy electrons brings significant technological benefits. Using EB, the crosslinking density can be regulated well. A thermo-tunnel is only necessary for the thermal post curing and it has to be of small size, since the final

product will be available in the form of beams (bars) of limited (several meter) length.

A significant problem of the EB crosslinking of polyester type resins is the inhibiting effect of oxygen on the surface. The possible solutions are the following:

- A release foil may be applied before the electron treatment and this way the even wall thickness and surface quality are assured. This solution can be used for products of any shape (even for square profiles). For this purpose a suitable winding machine is necessary where the workpiece is stationary but the winding head rotates.
- The treatment can also be carried out in an inert atmosphere. Other inertisation methods can be applied to eliminate the unfavorable effect of atmospheric oxygen.

Figure 75 shows in schematic form a possible arrangement for continuous products.

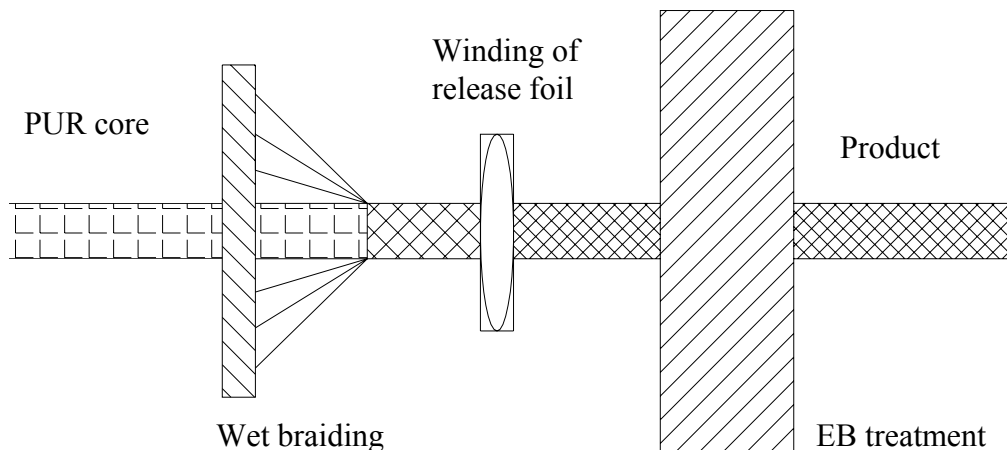


Figure 75 A possibility of continuous production

6.3. Applicability of the braided composites

Nowadays research has been carried out in Hungary (at our Department of Polymer Engineering) to develop a state-of-the-art technology to manufacture braided (Ribbon and String Factory Ltd. Co.) composite profiles (both circular and rectangular cross-sections) crosslinked by electron beam (FE-MA Ltd.). These high strength and lower weight profiles have good chance to substitute sheet metal profiles, e.g. in the transport applications, since loss in weight and hereby energy saving can be achieved this way, too. This dissertation provided a good basis further development work. The fiber bundle cell modeling method makes it possible to design the mechanical properties of the composites to be produced and

even the steps of the technology can be planned taking into consideration the desired mechanical properties of the composites.

6.4. Tasks to be solved

After summarizing and evaluating the results the following questions have arisen:

The impact of interfacial adhesion and the possibilities to increase it have not been examined directly in this work. It would be worth investigating the formation process and properties of this interaction (possibly a primary bond) since electron treatment affects the fiber as well not only the matrix. The application of new type, modified cationic epoxy resins is also promising [36].

Since the applicability of the fiber bundle model has only been studied in a small range of angles (48-67°), it would be important to check whether this model can characterize the initial tensile stiffness adequately in a wider range of angles (~10-80°), too. If further bundle types were introduced, obviously a more exact estimation would be obtained for not only the modulus but also for the strength. A further task is to describe the other sections of the whole failure process, as well. The modification of the contraction function is supposedly sufficient to be able to describe failure Range II.

Since the composite has only been tensile tested, the model would be worth interpreting to bending and even to torsion, since the benefits of the braided structure are likely to appear better there. A tube of circular cross-section has been examined in this work (this is the most favorable case considering analytical modeling) but modeling different (rectangular) profiles should also be dealt with in further investigations, although this requires a more complex finite element model. The range of the initial neglects should also be narrowed and this way the real failure process can be approached.

The literature review has also referred to the increasing role of braided hybrid (containing e.g. both carbon and aramid fibers) composites. It would be recommended to examine the applicability of the generalized model for these types of composites as well. The impact resistance properties and a detailed description of braided structures also require further explanation and investigation.

However, the most important mission is to develop composite profiles such as steel closed profiles (e.g. box section) which provide a good chance to be used in e.g. transportation, automotive and building industry.

Theses

The results are summarized in the theses below:

1. I have demonstrated that the electron beam (EB) initiated crosslinking of carbon fiber reinforced braided epoxy-acrylate matrix composite systems improves the mechanical properties as related to the conventional, chemical crosslinking. Relevant mechanical properties such as bending modulus and interlaminar shear strength of the EB treated (172 kGy) composite profiles (20x25 mm) are substantially (30-50%) better than that of the corresponding, conventionally (chemically) treated systems (if 2% Butanox M-50 (peroxy) catalyst, 2% dimethylaniline and 0.05% promoter are added and it is left at room temperature for 36 hours) that consisting of the same components. This indicates a better adhesion between the fiber and the matrix.
2. I have proven with measurements that the whole tensile failure process of the studied braided composite tubes (the internal diameter is 25.5 mm and average external diameter is 26.1 mm) can be divided into four, well-separable section of deformation:
 - I. *Range of engineering applications*, where the deformation is proportional to the stress and no cracks and breakage is experienced;
 - II. *Range of continuous neck-forming*, where neck-forming occurs as a result of further deformation and this neck expands along the whole length of the specimens as far as clamping;
 - III. *Range of the impregnated bundle tension*, where bundles slip on each other and orientate into the direction of loading and the process continues as bundle tension;
 - IV. *Range of final failure*, where the fiber bundles start to break and then the final failure takes place.
3. I have proven that the fiber bundle cell model can be applied well to describe the tensile force of the braided composites.
 - 3.1. In Range I, where the tensile process of the braided composite is proportional to the force (F_C , Eqn. (T1)), the initial tensile stiffness in the studied braiding angle range (48-67°) can be estimated with the oblique bundle (ET-bundle) (simplest) model.

$$F_C = \varphi \cdot \frac{\overline{F_B}}{2n \cdot N} \cdot \frac{\overline{A_C}}{A_S} + (1 - \varphi) \cdot \overline{E_M} \cdot u \cdot \overline{A_C}, \quad (\text{T1})$$

where u is the strain, φ is the fiber content, $\overline{F_B}$ is the average tensile force of bundle, n is the number of carriers, N is the number of elementary fibers in a roving, $\overline{A_C}$ is the average cross-section area of the composite, A_S is that of elementary fibers and $\overline{E_M}$ is the average tensile modulus of elasticity of the matrix.

3.2 I have derived a hyperbolic contraction function ρ , ratio of external radii, Eqn. (T2), which is well applicable in Range I to describe the radial deformation of the composite tube (both the braid and the matrix) with the help of the contraction parameter (b) determined in the measurements.

$$\rho = \frac{1}{(1+u)^b}. \quad (\text{T2})$$

4. I have shown that the first maximum of the tensile force (neck-formation force) for the studied composite correlates well ($R=0.95$) with the modeled maximal value of tensile force in the function of the braiding angle.
 - 4.1. The first breakage peak of the real composite – due to neck-forming – appears at 44% of the modeled value (the real average square error was 11.9%) based on the minimization of the quadratic deviation of the measured and modeled values.
 - 4.2. The measurable peaks of stress at the beginning of neck-forming show a steep change, predicted by modeling, in the studied braiding angle range (48-67°). The deviation between the measured and transformed values was 2%.
5. I have proven that a small value of the standard deviation (3.52°) around the average value of the braiding angle (57.09°) has practically no effect on the initial tensile stiffness and on the neck-forming force of the studied composite tubes.
6. I have worked out the ETH-bundle model in which the preset bundle (EH) is a composite bundle that is the parallel combination of the oblique and preset bundles, hence the tensile force of triaxially braided composites (containing oblique and longitudinal bundles as well) can be described ($\overline{F_B^{ETH}}$, Eqn. (T3)) in Range I. This provides an opportunity to estimate the initial stiffness of braided tubes, furthermore it supplies an indirect method to determine loosening and its standard deviation of axial tows.

$$F_C = \varphi \cdot \frac{\overline{F_B^{ETH}}}{(2n + n_a) \cdot N} \cdot \frac{\overline{A_C}}{\overline{A_S}} + (1 - \varphi) \cdot \overline{E_M} \cdot u \cdot \overline{A_C}, \quad (T3)$$

where n_a is the number of axial tows.

Summary

In my dissertation the mechanical properties of carbon fiber reinforced, braided, epoxy-acrylate matrix composites crosslinked with electron beam have been investigated then the tensile properties of circular cross-sectional composites have been modeled.

At the beginning of my work the correspondent literature has been reviewed, on the basis of which it can be stated that the fiber reinforced new type textile structures, e.g. braiding as a textile technology, and electron beam crosslinking has been unexploited, in composite profiles and tubes manufacturing yet, hitherto. Although the textile mechanical properties of braided structures are known, there is no model available to describe the mechanical properties and failure mechanism of such composites where braiding is used as reinforcing structure of composites. I have found that the fiber bundle cell modeling method is adaptable to not only unidirectional but also to other multiaxial reinforced layers with different bundle orientation, thus the mechanical properties of braided composites can be predicted.

In the first part of my dissertation the advantage of the applicability of electron beam curing has been studied in case of braided composite profiles. I have experienced that the carbon fiber reinforced, braided, epoxy-acrylate matrix composites have been advantageously crosslinked with EB and this improvement is revealed by the better mechanical properties. Conventional mechanical analysis methods and “drop-weight” crash tests have been carried out on the composite profiles to compare the properties. The results have showed that the mechanical properties of the EB treated composite profiles are 30-50% better than that of the corresponding, conventionally (chemically) treated systems. It has been revealed that not only the high modulus but also an advantageous impact (crash) behavior characterizes the new carbon fiber reinforced braided composite.

The further parts of my dissertation involve the modeling and examination of the effect of different braiding parameters on braided circular cross-sectional composite tubes. The fiber bundle cell modeling method, developed by Vas, has been used and extended to the mathematical description of the mechanical behavior of the braided composite tubes. Then impact of the parameters on the normalized tensile stress has been investigated.

The tensile failure process of the studied braided composite tubes can be divided into four, well-separable sections of deformation: *I. Range of engineering applications*, where the load-uptake is quasi-linear (it is to be noted that this is the range that can be modeled so far). It is visible that after neck-forming takes place along the whole clamping distance (*II. Range of continuous neck-forming*) a significant tensile force reserve evolves since the initial diameter has already dropped and the wall thickness increased (the cross-section area remained quasi constant), additionally the fiber bundles are oriented in the direction of load (slipping on one another), and this way the process ended in impregnated bundle tension (*III. Range of the impregnated bundle tension*). This resulted in a three times higher tensile force compared to the initial, local maximum. It can be mentioned that the fiber content changed only to a small extent (<0.5%) meanwhile. Finally, the rovings started to break continuously after the maximal load and the final failure took place (*IV. Range of final failure*).

I have proven that the fiber bundle cell models can be applied well to describe the tensile force of the braided composites. In Range I the tensile force of the braided composite, and hence the initial tensile stiffness in the studied braiding angle range (48-67°) can be described with the oblique bundle (ET-bundle) (simplest) model. I have derived, based on the theoretical considerations, a hyperbolic contraction function which is well applicable in Range I to describe the radial deformation of the composite tube and its constituents (both the braid and the matrix) with the help of the contraction parameter ($b=0.32$) defined in the measurements. A small standard deviation (3.52°) around the average value of the braiding angle (57.09°) has no effect on the initial tensile stiffness and on the force of neck-forming of the studied composite tubes based on the theoretical and experimental analyses.

The first maximum of the tensile force (neck-formation force) of the studied composite against neck-forming as the force that belongs to first local maximum correlates well ($R=0.95$) with the modeled maximal value of tensile force in the function of the braiding angle. The first breakage peak of the real composite – due to neck-forming – appeared at 44% of the modeled value (the real average square error was 11.9%) based on the minimization of the quadratic deviation of the measured and modeled values. The measurable peaks of stress at the beginning of neck-forming show the steep change predicted by modeling in the studied braiding angle range (48-67°). The difference between the measured and transformed values was 2%.

The modeling of the introduction of axial fibers into the composite, only with the ET-bundle is not suitable to describe the properties of triaxially braided composites, therefore the

model was amplified. The ETH-bundle model in which the preset bundle (EH) is extended and is the parallel combination of the oblique and preset bundles has been worked out, hence the tensile force of triaxially braided composites (containing oblique and longitudinal bundles, as well) can be described (Eqn. (T3)). This provides an opportunity to estimate the initial tensile stiffness of braided tubes, furthermore it supplies an indirect method to determine the loosening and its standard deviation of axial tows. In the studied cases the parameter values turned out to be $\overline{\varepsilon_0} = -0.02$, $\sigma_{\varepsilon_0} = 0.0125$, and these are only technology-dependent according to the measurements.

Finally I have discussed the results and I have revealed a possible solution for the continuous operation, furthermore the applicability of my theoretical and experimental results have also been mentioned and I also dealt with my own questions that point out the direction of my further research.

References

1. Gay, D., Hoa, S.V., Tsai, S.W.: Composite Materials: Design and Applications, CRC Press LLC, USA, 2003.
2. Czvikovszky, T., Nagy, P., Gaál, J.: A polimertechnika alapjai (Fundamentals of Polymer Engineering), Műegyetemi Kiadó, Hungary, 2000.
3. Chou, T-W., Ko, F.K.: Textile Structural Composites, Elsevier, Netherland, 1989.
4. Cox, B.N., Flanagan, G.: Handbook of Analytical Methods for Textile Composites, Prepared for Langley Research Center under Contract NAS1-19243, March 1997.
5. Jederán M., Tárnoky, F.: Textilipari Kézikönyv (Handbook of Textile Technology), Műszaki Könyvkiadó, Budapest, 1979.
6. <http://www.herzog-online.com>, 2004.
7. Vas, L.M.: Textiltermékek Tervezése (Design of Textile Products), Textbook, Manuscript, BME Department of Polymer Engineering, Hungary, 2000.
8. Mouritz, A.P., Bannister, M.K., Falzon, P.J., Leong, K.H.: Review of applications for advanced three-dimensional fibre textile composites, Composites: Part A, **30**, 1445–1461, 1999.
9. Kamiya, R., Cheeseman, B.A., Popper, P., Chou, T.-W.: Some recent advances in the fabrication and design of three-dimensional textile preforms: a review, Composites Science and Technology, **60**, 33-47, 2000.
10. Tong, L., Mouritz, A.P., Bannister M.K.: 3D Fibre Reinforced Polymer Composites, Elsevier, Netherland, 2002.
11. Venkatappa Rao, G., Sampath Kumar, J.P., Banerjee, P.K.: Characterization of a braided strip drain with coir and jute yarns, Geotextiles and Geomembranes, **18**, 367-384, 2000.
12. de Oliveira Simões, J.A., Marques, A.T.: Determination of stiffness properties of braided composites for the design of a hip prosthesis, Composites: Part A, **32**, 655–662, 2001.
13. Eurocarbon Ltd.: <http://www.eurocarbon.com>, 2004.
14. Murata Machinery Ltd.: <http://www.muratec.co.jp>, 2004.
15. A&P Technology Co.: <http://www.braider.com>, 2004.
16. Hamada, H., Kameo, K., Sakaguchi, M., Saito, H., Iwamoto, M.: Energy-absorption properties of braided composite rods, Composites Science and Technology, **60**, 723-729, 2000.

17. Chiu, C.H., Tsai, K.-H., Huang, W.J.: Crash-failure modes of 2D triaxially braided hybrid composite tubes, *Composites Science and Technology*, **59**, 1713-1723, 1999.
18. Thornton, P.H.: Energy absorption in composite structures, *Journal of Composites Materials*, **13**, 247-62, 1979.
19. Hull, D.: A unified approach to progressive crushing of fibre-reinforced composite tubes, *Composites Science and Technology*, **40**, 377-421, 1991.
20. Farley, G.L.: Energy absorption of composite materials, *Journal of Composite Materials*, **17**, 26-79, 1983.
21. Thornton, P.H.: The crash behavior of glass fiber reinforced plastic sections, *Composites Science and Technology*, **27**, 199-223, 1986.
22. Mamalis, A.G., Manolakas, D.E., Viegela, G.C.: Crashworthy behavior of thin-walled tubes of fiberglass composite materials subjected to axial loading, *Journal of Composite Materials*, **24**, 72-91, 1990.
23. Hull, D.: Axial crushing of fibre reinforced composite tubes, In the *Structural Crashworthiness*, London, Butterworths, 118-135, 1983.
24. Thornton, P.H., Harwood, J.J., Beardmore, P.: Fiber-reinforced plastic composites for energy absorption purposes, *Composites Science and Technology*, **24**, 275-298, 1985.
25. Farley, G.L., Jones, R.M.: Crashing characteristics of continuous fiber-reinforced composite tubes, *Journal of Composite Materials*, **26**, 37-50, 1992.
26. Hamada, H., Ramakrishna, S., Nakamura, M., Maekawa, Z.: Energy absorption behavior of hybrid composite tubes, In the *Proceeding of the 10th Annual ASM/ESD Advanced Composites Conference*, Dearborn, Michigan, 511-522, 7-10 November, 1994.
27. Peijs, A.A.J.M., Vanklinken, E.J.: Hybrid composites based on polyethylene and carbon fibers, Part V. energy absorption under quasistatic crash conditions, *Journal of Materials Science Letters*, **11**, 520-522, 1992.
28. Karbhari, V.M., Falzon, P.J., Herzberg, I.: Energy absorption characteristics of hybrid braided composite tubes, *Journal of Composite Materials*, **31**, 1164-1186, 1997.
29. Chiu, C.H., Tsai, K.-H., Huang, W.J.: Effects of braiding parameters on energy absorption capability of triaxially braided composite tubes, *Journal of Composite Materials*, **32**, 1964-1983, 1998.
30. Chiu, C.H., Lu, C.K., Wu, C.M.: Energy absorption characteristics of 3-D braided composite square tubes. *Journal of Composite Materials*, **31**, 2309-2327, 1997.

31. Saito, H., Chirwa, E.C., Inai, R., Hamada, H.: Energy absorption of braiding pultrusion process composite rods, *Composite Structures*, **55**, 407–417, 2002.
32. Mouritz, A.P., Bains, C., Herszberg, I.: Mode I interlaminar fracture toughness properties of advanced textile fibreglass composites, *Composites: Part A*, **30**, 859–870, 1999.
33. Karbhari, V.M., Haller, J.E., Falzon, P.K., Herszberg, I.: Post-impact crash of hybrid braided composite tubes, *International Journal of Impact Engineering*, **22**, 419–433, 1999.
34. Karbhari, V.M., Haller, J.E.: Rate and architecture effects on progressive crush of braided tubes, *Composite Structures*, **43**, 93-108, 1998.
35. Hamada, H., Nakatani, T., Nakai, A., Kameo, K.: The crashing performance of a braided I-beam, *Composites Science and Technology*, **59**, 1881-1890, 1999.
36. Goodman, D.L., Palmese, G.R.: Curing and Bonding of Composites using Electron Beam Processing, In the *Handbook of Polymer Blends and Composites*, Rapra Technology, UK, 2002.
37. Korenev, S.: Electron beam curing of composites, *Vacuum*, **62**, 233-236, 2001.
38. Saunders, C., Lopata, V., Kremers, W.: *Electron Curing of Composite Structures for Space Applications*, Executive summary, Canada, 1997.
39. Lopata, V.J., Saunders, C.B., Singh, A., Janke, C.J., Wrenn, G.E., Havens, S.J.: Electron-beam-curable epoxy resins for the manufacture of high-performance composites, *Radiation Physics and Chemistry*, **56**, 405-415, 1999.
40. Chappas, W.J., Devney, B.G., Olding, R.P., McLaughlin, W.L.: EB curing of maritime composite structures, *Radiation Physics and Chemistry*, **56**, 417-427, 1999.
41. Berejka, A.J., Eberle, C.: Electron beam curing of composites in North America *Radiation Physics and Chemistry*, **63**, 551–556, 2002.
42. Singh, A.: Radiation processing of carbon fibre-reinforced advanced composites, *Nuclear Instruments and Methods in Physics Research B*, **185**, 50-54, 2001.
43. Lopata, V.J., Barnard, J.W., Saunders, C.B., Stepanik, T.M.: New electron beam facility for R&D and production at Acsion industries, *Nuclear Instruments and Methods in Physics Research B*, **208**, 102–105, 2003.
44. Sui, G., Zhang, Z.-G., Chen, C.-Q., Zhong, W.-H.: Analyses on curing process of electron beam radiation in epoxy resins, *Materials Chemistry and Physics*, **78**, 349–357, 2002.

45. Turgis, J-D., Vergé, C., Coqueret, X.: Composition effects on the EB-induced cross-linking of some acrylate and methacrylate copolymers, *Radiation Physics and Chemistry*, **67**, 409-413, 2003.
46. Degrand, H., Cazaux, F., Coqueret, X., Defoort, B., Boursereau, F., Larnac, G.: Thermal effects on the network structure of diglycidylether of bisphenol-A polymerized by electron-beam in the presence of an iodonium salt, *Radiation Physics and Chemistry*, **68**, 885-891, 2003.
47. Salleh, N.G., Gläsel, H.J., Mehnert, R.: Development of hard materials by radiation curing technology, *Radiation Physics and Chemistry*, **63**, 475–479, 2002.
48. Czvikovszky, T., Hargitai, H., Rácz, I., Csukat, G.: Reactive compatibilization in polymer alloys, recyclates and composites, *Nuclear Instruments and Methods in Physics Research B*, **151**, 190-195, 1999.
49. Lawrence, C.B., McKeown, J., Svendsen, E.B.: Real-time confirmation of electron-beam dose, *Radiation Physics and Chemistry*, **52**, 543-547, 1998.
50. Woods, R.J., Pikaev, A.K.: *Applied Radiation Chemistry: Radiation Processing*, Wiley-Interscience Publication, Inc., USA, 1994.
51. Czajlik, I., Takács, E., Alpár, T., Czvikovszky, T.: *Advanced Materials Made by Radiation Processing*, *Radiation Physics and Chemistry*, **31**, 639-645, 1988.
52. Crivello, J.V.: *Advanced curing technologies using photo-and electron beam*, *Radiation Physics and Chemistry*, **63**, 21–27, 2002.
53. Janke, J. J., Norris, R.E., Yarborough, K., Havens, S. J., Lopata, V. J.: *Critical Parameters for Electron Beam Curing of Cationic Epoxies and Property Comparison of Electron Beam Cured Cationic Epoxies Versus Thermal Cured Resins and Composites*, EB curing Composites Workshop, Oak Ridge, Tennessee, USA, 1996.
54. Czajlik, I., Takács, E., Czvikovszky, T.: *The Effect of Monomer Functionality in EB-Curable Coatings*, *Radiation Physics and Chemistry*, **35**, 76-80, 1990.
55. Zuorong, C., Dechao, Z., Lu, M., Ye, L.: *A homogenisation scheme and its application to evaluation of elastic properties of three-dimensional braided composites*, *Composites: Part B*, **32**, 67–86, 2001.
56. Nemat-Nasser, S., Hori, M.: *Micromechanics: overall properties of heterogeneous materials*, North-Holland Series in Applied Mathematics and Mechanics, Netherland, 1993.
57. Aboudi, J.: *Mechanics of composite materials - a unified micromechanical approach*, Elsevier, Netherland, 1991.

58. Willis, J.R.: Variational and related methods for the overall properties of composites, *Advanced Applied Mechanics*, **21**, 1–78, 1981.
59. Hill, R.: Theory of mechanical properties of fibre-reinforced materials: I. Elastic behaviour, *Journal of Mechanics and Physics of Solids*, **12**, 199–212, 1964.
60. Budiansky, B.: On the elastic moduli of some heterogeneous materials, *Journal of Mechanics and Physics of Solids*, **13**, 223–227, 1965.
61. Chou, T.W.: *Microstructural design of fiber composites*, Cambridge University Press, UK, 1992.
62. Ko, F.K., Pastore, C.M.: Structure and properties of an integrated 3-D fabric for structural composites. In: Vinson JR, Taya M, editors. *Recent advances in composites in the United States and Japan*, ASTM STP 864. Philadelphia: American Society for Testing and Materials, 1985.
63. Cox, B.N., Davis, J.B.: Knitted composites for energy absorption under tensile loading, *Composites: Part A*, **32**, 91–105, 2001.
64. Kuo, W.-S., Chen, H.I.: Fabrication and microgeometry of two-step braided composites incorporating pultruded rods, *Composites Science and Technology*, **57**, 1457-1467, 1997.
65. Kuo, W.S., Chen, H.I.: Elastic moduli and damage mechanisms in 3D braided composites incorporating pultruded rods, *Composites: Part A*, **29A**, 681-692, 1998.
66. Chen, L., Tao, X.M., Choy, C.L.: On the microstructure of three-dimensional braided preforms, *Composites Science and Technology*, **59**, 391-404, 1999.
67. Kuznetsov, E. N.: Geometric analysis of woven or braided reinforcement for use in composite shells, *Composites: Part B*, **28B**, 565-572, 1997.
68. Wang, Y.Q., Wang, A.S.D.: Microstructure/property relationships in three-dimensionally braided fiber composites, *Composites Science and Technology*, **53**, 213-222, 1995.
69. Wang, Y.Q., Wang, A.S.D.: Geometric mapping of yarn structures due to shape change in 3-D braided composites, *Composites Science and Technology*, **54**, 359-370, 1995.
70. Zhang, Y.C., Harding, J.: A numerical micromechanics analysis of the mechanical properties of a plain weave composites, *Computers & Structures*, **36**, 839–844, 1990.
71. Li, W., Hammad, M.: Structural analysis of 3-d braided preforms for composites, Part I: the four-step preforms, *Journal of Textile Institute*, **81**, 491–514, 1990.
72. Cox, B.N., Carter, W.C., Fleck, N.A.: A binary model of textile composites - I. Formulation, *Acta Metallurgica*, **42**, 3463–3479, 1994.

73. Gaessegen, E.H., Pastore, C.M., Griffin OH, Birger, A.: Geometrical and finite element modeling of textile composites, *Composites Part B*, **27**, 43–50, 1996.
74. Wang, Y., Sun, X.: Digital-element simulation of textile processes, *Composites Science and Technology*, **61**, 311-319, 2001.
75. Zhou, G., Sun, X., Wang, Y.: Multi-chain digital element analysis in textile mechanics, *Composites Science and Technology*, **64**, 239-244, 2004.
76. D'Amato, E.: Finite element modelling of textile composites, *Composite Structures*, **54**, 467-475, 2001.
77. Tang, Z.X., Postle, R.: Mechanics of three-dimensional braided structures for composite materials - Part I: fabric structure and fibre volume fraction, *Composite Structures*, **49**, 451-459, 2000.
78. Tang, Z.X., Postle, R.: Mechanics of three-dimensional braided structures for composite materials - Part II: prediction of the elastic moduli, *Composite Structures*, **51**, 451-457, 2001.
79. Hashin, Z., Rosen, R.W.: The elastic moduli of fiber-reinforced materials, *Journal of Applied Mechanics*, **31**, 223–232, 1994.
80. Hashin, Z., Shtrikman, S.: A variational approach to the theory of the elastic behaviour of multiphase materials, *Journal of Mechanics and Physics of Solids*, **11**, 127–140, 1963.
81. Hashin, Z.: Analysis of properties of fiber composites with anisotropic constituents, *Journal of Applied Mechanics*, **46**, 543–550, 1979.
82. Aboudi, J.: Micromechanical analysis of composites by the method of cells, *Applied Mechanics Review*, **42**, 103–128, 1989.
83. Hull, D.: An introduction to composite materials, Cambridge University Press, UK, 1981.
84. Pastore, C.M., Gowayed, Y.A.: A self-consistent fabric geometry model: modification and application of a fabric geometry model to predict elastic properties of textile composites, *Journal of Composites Technology and Research*, **16**, 32–36, 1994.
85. Yang, J.M., Ma, C.L., Chou, T.W.: Fiber inclination model of three-dimensional textile structural composites, *Journal of Composite Materials*, **20**, 472–484, 1986.
86. Raju I, Wang JT. Classical laminate theory models for woven fabric composites, *Journal of Composites Technology and Research*, **16**, 289–303, 1994.
87. Ishikawa, T., Chou, T.W.: In-plane thermal expansion and thermal bending coefficients of fabric, *Journal of Material Science*, **17**, 3211–3220, 1993.

88. Ishikawa, T., Chou, T.W.: Elastic behavior of woven hybrid composites, *Journal of Composite Materials*, **16**, 2–19, 1982.
89. Ishikawa, T., Chou, T.W.: One-dimensional micromechanical analysis of woven fabric composites, *Journal of American Institute of Aeronautics and Astronautics*, **21**, 1714–1721, 1983.
90. Naik, N.K., Shembekar, P.S.: Elastic behaviour of woven fabric composites: I – lamina analysis, *Journal of Composite Materials*, **26**, 2197–2225, 1992.
91. Shembekar PS, Naik NK. Elastic behaviour of woven fabric composites: II – laminate analysis, *Journal of Composite Materials*, **26**, 2226–2246, 1992.
92. Naik NK, Shembekar PS. Elastic behaviour of woven fabric composites: III – laminate design, *Journal of Composite Materials*, **26**, 2523–2541, 1992.
93. Halpin, J.C., Jerine, K., Whitney, J.M.: The laminate analogy for 2 and 3 dimensional composite materials, *Journal of Composite Materials*, **5**, 36–49, 1951.
94. Dasgupta, A., Agarwal, R.K., Bhandarkar, S.M.: Three-dimensional modeling of woven-fabric composites for effective thermo-mechanical and thermal properties, *Composites Science and Technology*, **56**, 209–223, 1996.
95. Vas, L.M., Rácz, Zs.: Modeling and Testing The Fracture Process of Impregnated Carbon Fiber Roving Specimens During Bending – Part I: Fiber Bundle Model, *Journal of Composite Materials*, **38**, 1757-1786, 2004.
96. Vas, L.M., Rácz, Zs., Nagy, P.: Modeling and Testing The Fracture Process of Impregnated Carbon Fiber Roving Specimens During Bending – Part II: Experimental Studies, *Journal of Composite Materials*, **38**, 1787-1802, 2004.
97. Weibull, W.: A Statistical Distribution Function of Wide Applicability, *Journal of Applied Mechanics*, **18**, 293-297, 1951.
98. Bolotin, V.V.: *Statisztikai módszerek a szerkezetmechanikában (Statistical Methods in the Structural Mechanics)*, Műszaki Könyvkiadó, Hungary, 1970.
99. Williams, J.G.: *Stress Analysis of Polymers*, Lowe & Brydone Ltd., Norfolk, 1973.
100. Wisnom, M.R.: Relationship Between Strength Variability and Size Effect in Unidirectional Carbon Fibre/epoxy, *Composites*, **22**, 47-52, 1991.
101. Gibson, R.F.: *Principles of Composite Material Mechanics*, McGraw Hill, USA, 1994.
102. Sutherland, L.S., Guedes Soares, C.: Review of Probabilistic Models of the Strength of Composite Materials, *Reliability Engineering and System Safety*, **56**, 183-196, 1997.
103. Cotterell, B.: The Past, Present, and Future of Fracture Mechanics, *Engineering Fracture Mechanics*, **69**, 533-553, 2002.

104. Morton, W.E., Hearle, J.W.S.: Physical Properties of Textile Fibers, The Textile Institute Butterworths, Manchester & London, 1962.
105. Hearle, J.W.S., Grosberg, P., and Backer S.: Structural Mechanics of Fibers, Yarns, and Fabrics, Volume 1., Wiley-Interscience, 1969.
106. Hearle, J.W.S., Thwaites, J.J., Amirbayat J.: Mechanics of Flexible Fibre Assemblies, Sijthoff & Nordhoff, Alpen an der Rijn, The Netherlands, USA, 1980.
107. Zurek W.: The Structure of Yarn, Published for the U.S. Department of Agriculture and the National Science Foundation, Washington, D.C., by the Foreign Scientific Publications, Department of the National Center for Scientific, Technical and Economic Information, Warsaw, Poland, 1975.
108. Phoenix, S.L.: Probabilistic Concept in Modeling the Tensile Test Behavior of Fiber Bundles and Unidirectional Fiber/matrix Composites, ASTM Conference, 130-151, 1974.
109. Phoenix, S.L.: Statistical Theory for Strength of Twisted Fibre Bundles with Applications to Yarns and Cables, Textile Research Journal, **49**, 407-423, 1979.
110. Phoenix, S.L.: Statistical Aspect of Failure of Fibrous Materials, ASTM Conference, 455-483, 1979.
111. Phoenix, S.L.: Modeling the Statistical Lifetime of Glass Fiber/Polymer Matrix Composites in Tension, Composite Structures, **48**, 19-29, 2000.
112. Harlow, D.G. and Phoenix, S.L.: The Chain-of-Bundles Probability Model For the Strength of Fibrous Materials I: Analysis and Conjectures, Journal of Composite Materials, **12**, 195-214, 1978.
113. Harlow, D.G., Phoenix, S.L.: The Chain-of-Bundles Probability Model for the Strength of Fibrous Materials II: A Numerical Study of Convergence, Journal of Composite Materials, **12**, 314-334, 1978.
114. Grishanov, S.A., Harwood, R.J., Bradshaw, M.S., A Model of Fibre Migration in Staple-fibre Yarn, Journal of the Textile Institute, **90**, 298-321, 1999.
115. Vas, L.M.: A statisztikus kötegszilárdság és alkalmazása a szál- és fonalvizsgálatokban (The Statistical Fiber Bundle Strength and its Application in Testing Fibers and Yarns), Magyar Textiltechnika (Hungarian Textile Technique), **43**, 165-185, 1990.
116. Vas, L.M.: Újabb eredmények a síkban rendezett szál- és fonalkötegek szakítási elméletében (Latest Results in the Tensile Test Theory of Fiber and Yarn Bundles Ordered into Plane), Magyar Textiltechnika (Hungarian Textile Technique), **45**, 71-75, 137-142, 187-191, 1992.

117. Vas, L.M. and Császi, F.: Use of Composite-Bundle Theory to Predict Tensile Properties of Yarns, *Journal of the Textile Institute*, **84**, 448-463, 1993.
118. Vas, L.M., Halász, G.: Modelling the Breaking Process of Twisted Fiber Bundles and Yarns, *Periodica Polytechnica*, **38**, 325-350, 1994.
119. Czvikovszky, T.: Application of Low-Energy Electron-Beam Curing in Plastics Processing and Coating Technologies, *Radiation Physics Chemistry*, **26**, 547-553, 1985.
120. Farmer, C. J. D., Janke, C. J., Lopata, V. J.: The Electron Beam Cure of Epoxy Paste Adhesives, *EB curing Composites Workshop*, Oak Ridge, Tennessee, USA, 1996.
121. Singh, A.: Radiation processing of carbon fiber-reinforced advanced composites, *Nuclear Instruments and Methods in Physics Research B*, **185**, 50–54, 2001.
122. Fengmei, L., Jianwen, B., Xiangbao, C., Huaying, B., Huiliang, W.: The Influencing Factors EB Curing of Epoxi Matrix, *Radiation Physics and Chemistry*, **63**, 557-561, 2002.
123. Zoltek Ltd.: <http://www.zoltek.hu>, 2004.
124. Tenax Ltd.: <http://www.tenax-fibers.com>, 2004.
125. *Zsigmond, B.*: Műanyagok kisenergiájú elektronkezelése (Low energy electron treatment of plastics), *Anyagvizsgálók lapja (Journal of Material Testers)*, **12**, 94-98, 2002.
126. EB-Tech Ltd.: <http://www.eb-tech.com>, 2004.
127. ISO 14125:1998 standard: Fibre-reinforced plastic composites. Determination of flexural properties.
128. MSZ EN ISO 178:2001 standard: Plastics. Determination of flexural properties.
129. MSZ EN ISO 527-4:1999 standard: Plastics. Determination of tensile properties. Part 4: Test conditions for isotropic and orthotropic fibre-reinforced plastic composites.
130. MSZ EN ISO 527-5:1999 standard: Plastics. Determination of tensile properties. Part 5: Test conditions for unidirectional fibre-reinforced plastic composites.
131. MSZ EN ISO 14130:1999 standard: Fibre-reinforced plastic composites. Determination of apparent interlaminar shear strength by short-beam method.
132. MSZ EN ISO 1393:1999 standard: Plastics piping system. Glass-reinforced thermosetting plastics (GRP) pipes. Determination of longitudinal tensile properties.
133. JIS R 7601:1986 standard: Testing methods for carbon fiber.
134. Nagy, V.: Testing Yarns Using Image Processing Systems, MSc Thesis, Hungary, 2002.
135. Vas, L.M., Halász, G., Takács, M., Eördögh, I., Szász, K.: Measurement of Yarn Diameter and Twist Angle with Image Processing System, *Periodica Polytechnica*, **38**, 277-296, 1994.

136. Halász, L., *Zsigmond, B.*, Czvikovszky, T.: Production and Analysis of Composites Reinforced with Braided Carbon Fiber Structure, Proceedings of the Third Conference on Mechanical Engineering, Budapest, Hungary, 715-719, 2002.
137. Halász, L., *Zsigmond, B.*, Czvikovszky, T.: Szénszálból készített fonatolt szálstruktúrával erősített kompozit szerkezet vizsgálata (Investigation of carbon fiber reinforced braided structural composite), Proceedings of Conference on Reinforced Plastics, Balatonfüred, Hungary, 2002.
138. *Zsigmond, B.*: Szénszálerősítésű, fonatolt kompozit profil gyártása (Manufacturing of carbon fiber reinforced braided composite), Proceedings of 11th International Conference in Mechanical Engineering, Kolozsvár, Romania, 2003.
139. *Zsigmond, B.*, Halász, L., Czvikovszky, T.: EB processing of braided carbon fiber composite profiles, Nuclear Instruments and Methods in Physics Research B, **208**, 247-251, 2003.
140. *Zsigmond, B.*, Halász, L., Czvikovszky, T.: Electron beam processing of carbon fiber reinforced braided composites, Radiation Physics and Chemistry, **67**, 441-445, 2003.
141. Kollár, L.P., Springer, G.S.: Mechanics of composite structures, Cambridge University Press, USA, 2003.
142. *Zsigmond, B.*, Czvikovszky, T.: A szénszálerősítésű, epoximátrixú kompozit mechanikai tulajdonságainak vizsgálata a gyantatartalom függvényében (Investigation of the mechanical properties of carbon fiber reinforced, epoxy matrix composite as function of the matrix content), Műanyag és gumi (Plastics and Rubbers), **39**, 91-94, 2002.
143. *Zsigmond, B.*, Vas, L.M.: Examination of the tensile state of fibers in braided fiber reinforced composite tubes, Periodica Polytechnika, under submission, 2005.
144. *Zsigmond, B.*, Vas, L.M.: Fonatolt, szénszálerősítésű kompozit csövek húzása (Tensile of braided carbon fiber reinforced composite tubes), Műanyag és Gumi (Plastics and Rubbers), under submission, 2005.
145. Póka, L.: Unidirekcionálisan erősített, szénszálalás kompozitok vizsgálata (Investigation of unidirectional, carbon fiber reinforced composites), MSc Thesis, Hungary, 2003.

Appendix

Appendix A – Properties of applied fibers

Applied tensile tester: ZWICK Z005

Test speed: 1 mm/min

Clamping length: 25 mm

Test temperature: RT

Applied image processing system: Projektina 4011-4016/MMA

Panex[®] 33

Number of valid measurements: 132

Results based on [145].

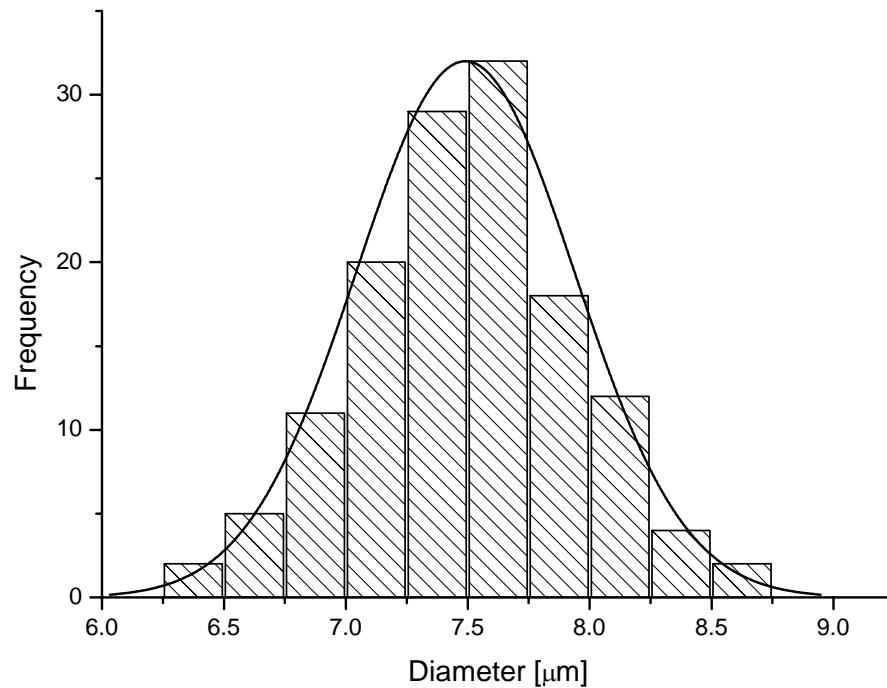


Figure A1 Histogram and density function of the diameter of Panex fibers ($\bar{d}=7.53$, $SD=0.52$)

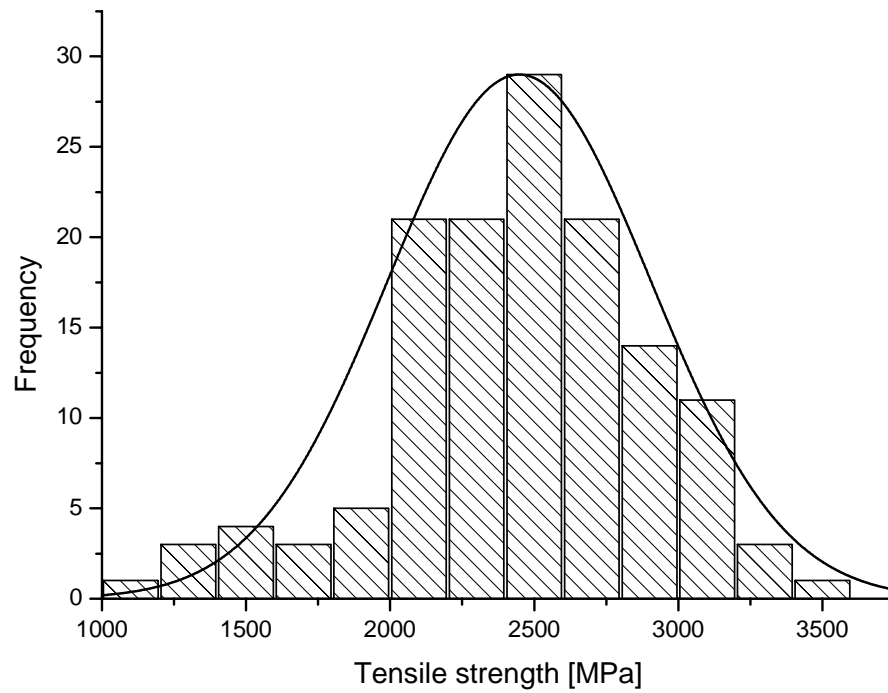


Figure A2 Histogram and density function of the tensile strength of Panex fibers ($\bar{\sigma}_s = 2460.3$, $SD = 478.15$)

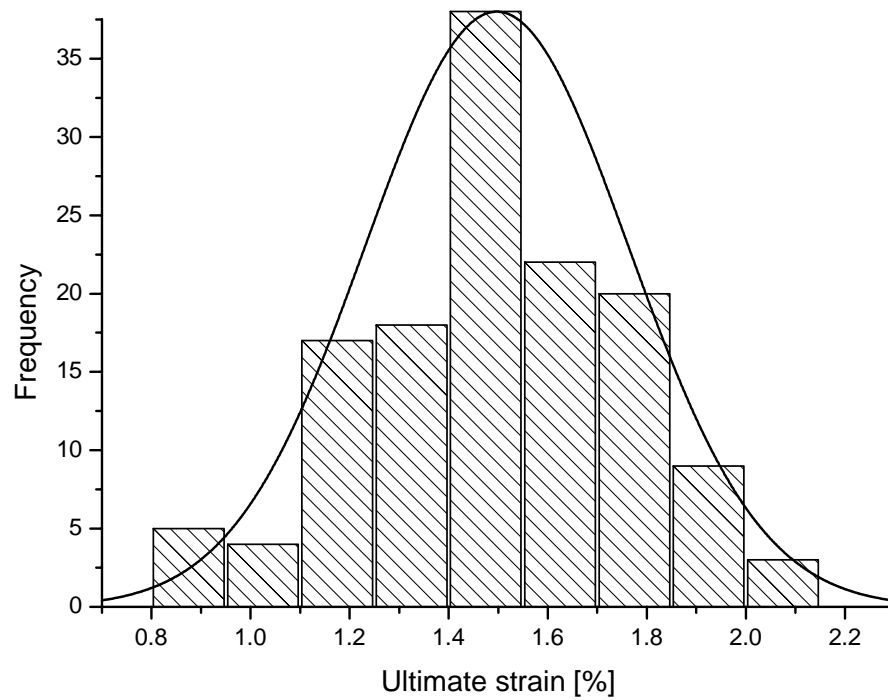


Figure A3 Histogram and density function of the ultimate strain of Panex fibers ($\bar{K} = 1.49$, $SD = 0.28$)

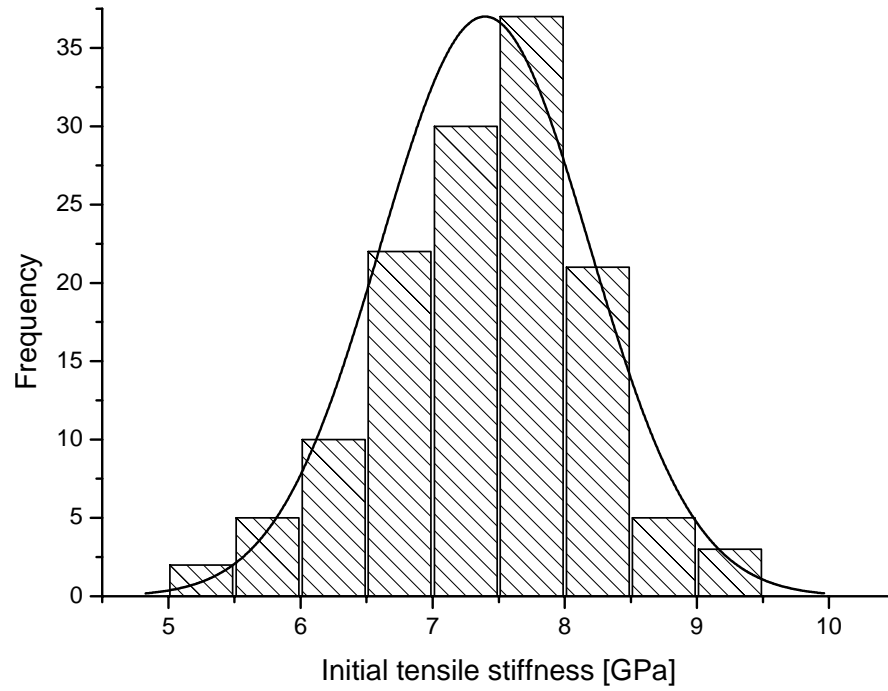


Figure A4 Histogram and density function of the initial tensile stiffness of Panex fibers ($\bar{\varepsilon}_s = 7.33$, $SD = 0.88$)

Tenax[®] STS 5631

Number of valid measurements: 52

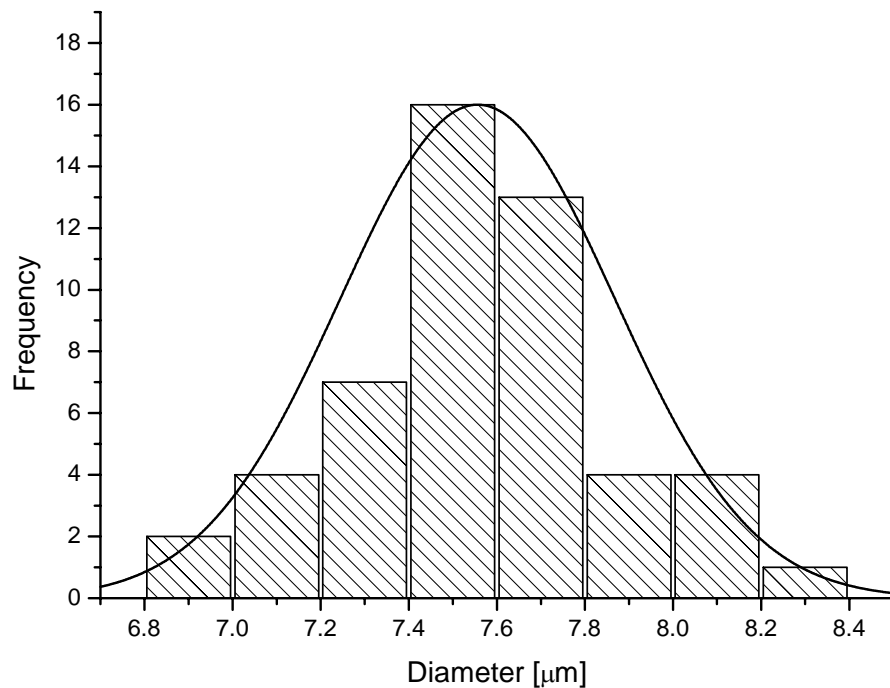


Figure A5 Histogram and density function of the diameter of Tenax fibers ($\bar{d} = 7.55$, $SD = 0.31$)

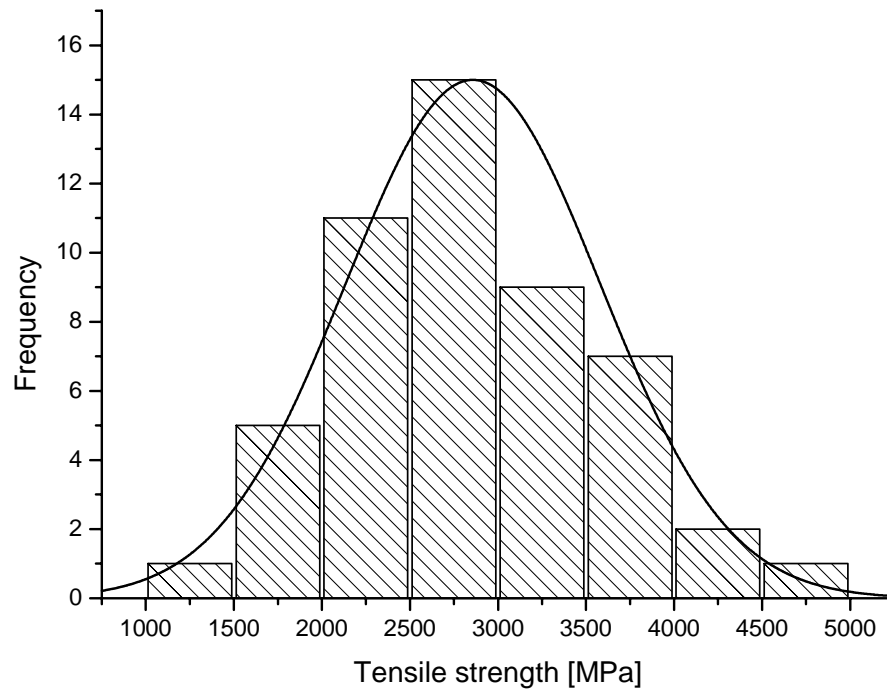


Figure A6 Histogram and density function of the tensile strength of Tenax fibers ($\bar{\sigma}_S = 2857.6$, $SD = 723.1$)

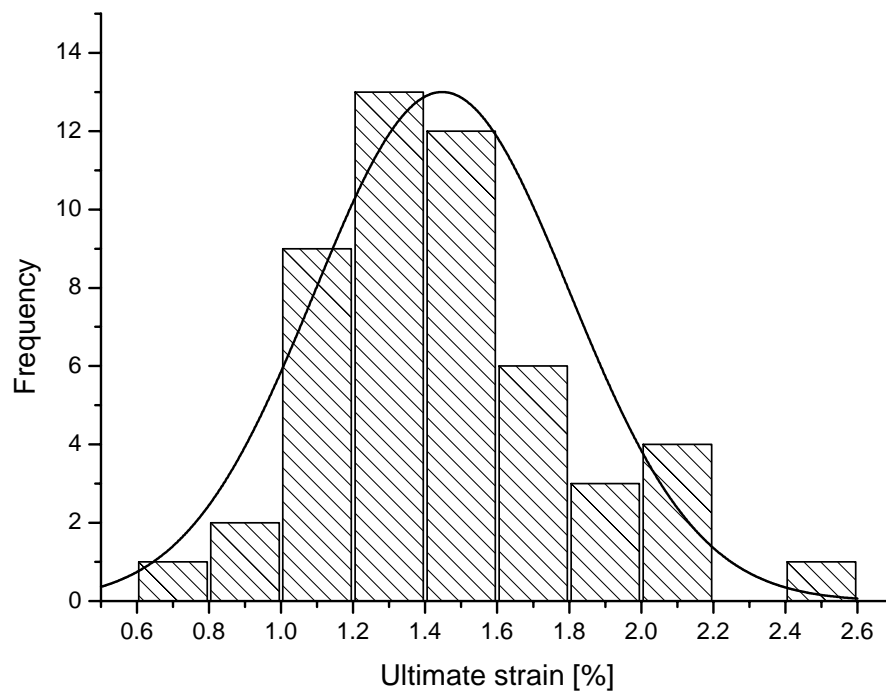


Figure A7 Histogram and density function of the ultimate strain of Tenax fibers ($\bar{\varepsilon}_S = 1.44$, $SD = 0.35$)

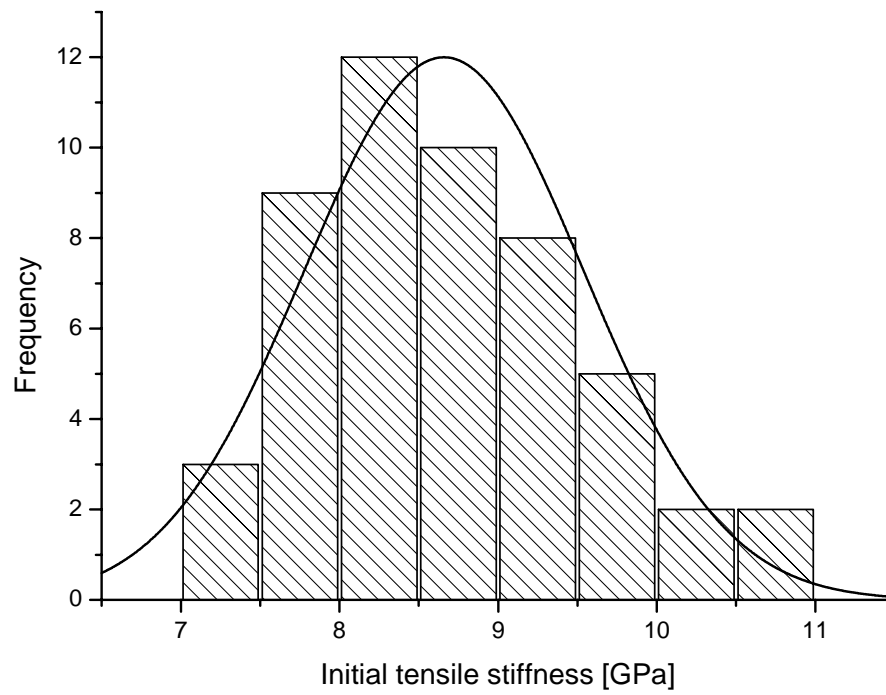


Figure A8 Histogram and density function of the initial tensile stiffness of Tenax fibers ($\bar{K}=8.66$, $SD=0.88$)

Appendix B – Properties of applied matrices

Applied tensile tester: ZWICK Z050

Test speed: 5 mm/min

Support distance: 50 mm

Test temperature: RT

Number of valid measurements in each case: 5

D411	Physically initiated						Chemically initiated	
	Dose [kGy]							
	98		123		156			
Thermal post-treatment	$E_{init,b}$	SD	$E_{init,b}$	SD	$E_{init,b}$	SD	$E_{init,b}$	SD
80 °C/min	[GPa]	[GPa]	[GPa]	[GPa]	[GPa]	[GPa]	[GPa]	[GPa]
0	0.97	0.03	1.36	0.02	1.48	0.04	1.05	0.05
10	1.15	0.05	1.39	0.02	1.53	0.04	1.11	0.03
20	1.19	0.07	1.39	0.03	1.55	0.02	1.15	0.03
30	1.20	0.10	1.40	0.01	1.56	0.03	1.22	0.02
60	1.21	0.09	1.40	0.02	1.56	0.05	1.22	0.04

Table T1 Initial bending modulus ($E_{init,b}$) and its standard deviation (SD) of D411 type resin (gray: graphed in Figure 34)

Average diameter of specimens: 14.07 mm, its standard deviation: 0.06 mm

D470	Physically initiated						Chemically initiated	
	Dose [kGy]							
	65		98		123			
Thermal post-treatment	$E_{init,b}$	SD	$E_{init,b}$	SD	$E_{init,b}$	SD	$E_{init,b}$	SD
80 °C/min	[GPa]	[GPa]	[GPa]	[GPa]	[GPa]	[GPa]	[GPa]	[GPa]
0	1.66	0.01	1.74	0.09	1.71	0.02	1.51	0.02
10	1.69	0.03	1.76	0.06	1.74	0.04	1.55	0.02
20	1.69	0.13	1.77	0.03	1.75	0.03	1.58	0.06
30	1.70	0.04	1.78	0.03	1.75	0.06	1.67	0.04
60	1.71	0.10	1.78	0.06	1.75	0.05	1.69	0.03

Table T2 Initial bending modulus ($E_{init,b}$) and its standard deviation (SD) of D470 type resin (gray: graphed in Figure 34)

Average diameter of specimens: 14.13 mm, its standard deviation: 0.06 mm

Appendix C – Properties of asymmetric composite profiles

Applied tensile tester: ZWICK Z050

Test temperature: RT

Number of valid measurements in each case: 5

Determined properties	Support distance	Test speed
	[mm]	[mm/min]
Interlaminar shear strength of composite walls	10	5
Initial bending modulus and strength of composite walls	50	10
Initial bending modulus of composite profiles	250	10

Table T3 Support distance and test speed at different measurements

	Dose [kGy]	Initial bending modulus [GPa]			
		Along width		Along height	
		$E_{init,b}$	SD	$E_{init,b}$	SD
Physically initiated	80	2.28	0.34	3.73	0.12
	115	4.52	0.40	5.41	0.47
	172	4.98	0.24	5.78	0.61
	229	5.21	0.53	6.02	0.20
	287	6.11	0.81	5.39	0.38
	401	6.15	0.19	5.41	0.28
Chemically initiated		2.57	0.51	4.18	0.98

Table T4 Initial bending modulus ($E_{init,b}$) and its standard deviation (SD) of composite profiles
Average geometry: D1: 20 mm – SD: 0.28 mm; D2: 25 mm – SD: 0.57 mm; w^* : 2.2 mm – SD: 0.1 mm

	Dose [kGy]	Initial bending modulus		Bending strength		Interlaminar shear strength	
		$E_{init,b}$	SD	σ_{bd}	SD	τ	SD
		[GPa]	[GPa]	[MPa]	[MPa]	[MPa]	[MPa]
Physically initiated	80	1.93	0.38	30.31	7.28	7.02	0.90
	115	2.40	0.62	36.85	14.09	7.41	0.51
	172	3.84	0.65	55.64	5.94	9.67	1.20
Chemically initiated		1.60	0.27	22.04	4.24	6.40	0.39

Table T5 Initial bending modulus ($E_{init,b}$), bending strength (σ_{bd}), interlaminar shear strength (τ) and their standard deviation (SD) of composite walls

Average geometry: w^* : 2.2 mm – SD: 0.1 mm; width: 13.2 mm – SD: 0.82 mm

Appendix D – Properties of composite tubes

Applied tensile tester: ZWICK Z020

Tensile speed: 10 mm/min

Clamping length: 150-200 mm

Test temperature: RT

Number of valid measurements in each case: 5

Determination of contraction parameter: Messphysik Videoextensometer ME-46

Distance of longitudinal markers: 50-75 mm

Determination of braiding angle: Projektina 4011-4016/MMA

Number of valid measurements in each case: 10-12

n	n_a	h₀	SD	α₀	SD	φ	b	F_{max}	SD
[-]	[-]	[mm]	[mm]	[°]	[°]	[v%]	[-]	[N]	[N]
8	0	1.12	0.02	55	0.9	23	0.32	4274.19	354.66
		1.12	0.03	61	0.4	23	0.32	1984.54	231.2
		1.14	0.02	67	0.7	23	0.32	1052.82	132.44
16	0	1.23	0.02	48	0.7	25	0.32	8794.50	675.98
		1.23	0.02	50	0.6	25	0.32	8048.11	814.16
		1.25	0.04	52	0.5	25	0.32	7040.81	649.42
		1.25	0.03	54	0.5	25	0.32	6072.00	711.23
		1.27	0.04	57	0.6	25	0.32	2982.87	357.81
16	0	1.26	0.04	57.09	3.52	25	0.32	2411.67	276.82
8	4	1.31	0.05	55	0.9	25	0.28	9940.83	1253.77
	8	1.35	0.04	55	0.8	25	0.25	18791.31	1782.43

Table T6 Properties of circular cross-sectional composites
Internal diameter in all cases was 25.5 mm.

Modeling of Braided Fiber Reinforced Composites Crosslinked by Electron Beam (Fonatolt, szélerősítésű, elektronkezeléssel térhálósított kompozitok modellezése)

Zsigmond Balázs

PhD értekezés

ÖSSZEFOGLALÁS

Disszertációmban fonatolt, szénszálerősítésű, epoxi-akrilát mátrixú, elektronkezeléssel térhálósított kompozitok mechanikai tulajdonságait vizsgáltam, majd modelleztem a kompozit csövek húzási jellemzőit.

Dolgozatom elején áttekintettem a szakirodalmat, amelyből megállapítottam, hogy az új típusú szálerősítéses struktúrák, pl. a fonatolás, mint textilipari technológia, továbbá az elektronkezeléssel történő térhálósítás a kompozit profil és cső gyártásában mindezidáig kihasználatlan maradt. A fonatolt előtermék kompozit erősítő struktúráként való alkalmazása során magának a kompozitnak a mechanikai tulajdonságára, tönkremenetelére vonatkozóan nincs kifejlesztett modell a kezünkben. A szálköteg cella modell alkalmasnak tűnik a fonatolt kompozitok mechanikai tulajdonságainak az előrejelzésére.

Munkám első részében bemutattam az elektronkezelés alkalmazhatóságának előnyeit fonatolt kompozit profil esetén. Azt tapasztaltam, hogy a fonatolt kompozit előnyösen elektronkezelhető, ami a mechanikai tulajdonságok javulásán követhető nyomon. Az eredmények azt mutatták, hogy az elektronkezelt kompozit profilok lényegesen (30-50%-al) jobb mechanikai tulajdonságokkal rendelkeznek, mint a hagyományos úton térhálósított rendszerek. Bemutattam, hogy nem csak a magas rugalmassági modulusz jellemzi a fonatolt terméket, de előnyös törési tulajdonságokkal is rendelkezik.

Disszertációm további részeiben fonatolt kör keresztmetszetű csöveket modelleztem, majd vizsgáltam különböző fonatolási paraméterek mellett. A Vas-féle szálkötegcella modellezési módszert felhasználva beágyazott szálköteg modellt dolgoztam ki a fonatolt kompozit csövek matematikai leírására, majd vizsgáltam a paraméterek normált húzó-feszültségre gyakorolt hatását.

Ezután feltártam a fonatolt kompozit teljes tönkremeneteli folyamatát, amely a deformáció négy jól elkülöníthető részére bontható: I. Mérnöki alkalmazás tartománya; II. Folyamatos nyakképződés tartománya, III. Impregnált kötegszakítás tartománya, valamint IV. Kötegszakadások, teljes tönkremenetel tartománya.

Ezt követően értékeltem a modell alkalmazhatóságát. Megállapítható, hogy a modell paraméterérzékenységét a mérési eredmények is alátámasztják, továbbá hogy a kidolgozott, ET köteget tartalmazó (legegyszerűbb) modellel az I. tartományban jól lehet becsülni a fonatolt kompozit kezdeti húzóerevségét az általam vizsgált fonatolási szögtartományban (48-67°). Az elméleti megfontolások alapján kialakított hiperbolikus kontrakciós függvény az I. tartományban jól alkalmazható a vizsgált kompozit cső radiális irányú deformációjának modellezésére. Az elméleti és a gyakorlati elemzések szerint a vizsgált kompozit csövek esetén a fonatolási szög átlagérték körüli (57,09°) kismértékű szórásának (3,52°) lényegében nincs hatása a húzóerevségre és a nyakképződési erőre.

A csak ET köteggel modellezett axiális szálbevezetés nem alkalmas megfelelően leírni az triaxiális fonatolt kompozit tulajdonságait, ezért a modellt továbbfejlesztettem. Az EH-köteggel kibővített ETH-köteg modell már alkalmas az axiális szálbevezetésű kompozitok kezdeti húzóerevségének a becslésére is, továbbá indirekt módszert szolgáltat az axiális szálak belazulásának és annak szórásának közvetett meghatározására, amelyek a mérések alapján lényegében csak technológiafüggőek.

Végül megvitattam az eredményeket, amelyben vázoltam az esetleges folytonos gyártás egy lehetséges megoldását, továbbá a dolgozatomban megfogalmazott gyakorlati és elméleti munkám hasznosulásának lehetőségeit, majd a még bennem megfogalmazódott nyitott kérdésekre is kitértem, amelyek irányt mutathatnak jövőbeni kutatásaimhoz.

Modeling of Braided Fiber Reinforced Composites Crosslinked by Electron Beam

Balázs Zsigmond

PhD Thesis

S U M M A R Y

In my dissertation the mechanical properties of carbon fiber reinforced, braided, epoxy-acrylate matrix composites crosslinked by electron beam have been investigated then the tensile properties of composite tubes have been modeled.

At the beginning of my work the correspondent literature has been reviewed, on the basis of which it can be stated that the fiber reinforced new type textile structures, e.g. braiding as a textile technology, and electron beam crosslinking has been unexploited, in composite profiles and tubes manufacturing yet, hitherto. There is no model available to describe the mechanical properties and failure mechanism of such composites where braiding is used as reinforcing structure of composites. I have found that the fiber bundle cell modeling method is adaptable to predict the mechanical properties of braided composites.

In the first part of my dissertation the advantage of the applicability of electron beam curing has been studied in case of braided composite profiles. I have experienced that the braided composites have been advantageously crosslinked with EB and this improvement is revealed by the better mechanical properties. The results have showed that the mechanical properties of the EB treated composite profiles are substantially (30-50%) better than that of the corresponding, conventionally (chemically) treated systems. It has been revealed that not only the high modulus but also an advantageous impact (crash) behavior characterizes the new carbon fiber reinforced braided composite.

The further parts of my dissertation involve the modeling and examination of the effect of different braiding parameters on braided circular cross-sectional composite tubes. The fiber bundle cell modeling method, developed by Vas, has been used and extended to the mathematical description of the mechanical behavior of the braided composite tubes. Then impact of the parameters on the normalized tensile stress has been investigated.

The tensile failure process of the studied braided composite tubes can be divided into four, well-separable sections of deformation: I. Range of engineering applications, II. Range of continuous neck-forming, III. Range of the impregnated bundle tension and IV. Range of final failure.

I have proven that the fiber bundle cell models can be applied well to describe the tensile force of the braided composites. In Range I the tensile force of the braided composite, and hence the initial tensile stiffness in the studied braiding angle range ($48-67^\circ$) can be described with the ET-bundle (simplest) model. I have derived, based on the theoretical considerations, a hyperbolic contraction function which is well applicable in Range I to describe the radial deformation of the composite tube. A small standard deviation (3.52°) around the average value of the braiding angle (57.09°) has no effect on the initial tensile stiffness and on the neck-formation force of the studied composite tubes based on the theoretical and experimental analyses.

The modeling of the introduction of axial fibers into the composite, only with the ET-bundle is not suitable to describe the properties of triaxially braided composites, therefore the model was amplified. The ETH-bundle model in which the preset bundle (EH) is extended, hence the tensile force of triaxially braided composites. This provides an opportunity to estimate the initial tensile stiffness of braided tubes, furthermore it supplies an indirect method to determine the loosening and its standard deviation of axial tows, which are only technology-dependent according to the measurements.

Finally I have discussed the results and I have revealed a possible solution for the continuous operation, furthermore the applicability of my theoretical and experimental results have also been mentioned and I also dealt with my own questions that point out the direction of my further research.

Modeling of Braided Fiber Reinforced Composites Crosslinked by Electron Beam

Balázs Zsigmond

PhD Thesis

A B S T R A C T

In my dissertation the mechanical properties of carbon fiber reinforced, braided, epoxy-acrylate matrix composites crosslinked by electron beam have been investigated then the tensile properties of composite tubes have been modeled. The tensile failure process of the studied braided composite tubes can be divided into four, well-separable sections of deformation. The fiber bundle cell models can be applied to describe the tensile force of the braided composites. The impact of the parameters of the model has been investigated. The amplified model provides an opportunity to estimate the initial tensile stiffness of triaxially braided tubes, furthermore it supplies an indirect method to determine the loosening and its standard deviation of axial tows. The measured and calculated values show good correlation.